Monte Carlo tests of renormalization-group predictions for critical phenomena in Ising models

Kurt Binder*, Erik Luijten

Institut für Physik, Johannes-Gutenberg-Universität, Staudinger Weg 7, D-55099 Mainz, Germany

Contents

Abstract

A critical review is given of status and perspectives of Monte Carlo simulations that address bulk and interfacial phase transitions of ferromagnetic Ising models. First, some basic methodological aspects of these simulations are briefly summarized (single-spin flip vs. cluster algorithms, finite-size scaling concepts), and

---

* Corresponding author. Tel.: + 49-6131-3923348; fax: + 49-6131-3925441.
E-mail address: kurt.binder@uni-mainz.de (K. Binder).

then the application of these techniques to the nearest-neighbor Ising model in $d = 3$ and 5 dimensions is described, and a detailed comparison to theoretical predictions is made. In addition, the case of Ising models with a large but finite range of interaction and the crossover scaling from mean-field behavior to the Ising universality class are treated. If one considers instead a long-range interaction described by a power-law decay, new classes of critical behavior depending on the exponent of this power law become accessible, and a stringent test of the ε-expansion becomes possible. As a final type of crossover from mean-field type behavior to two-dimensional Ising behavior, the interface localization–delocalization transition of Ising films confined between "competing" walls is considered. This problem is still hampered by questions regarding the appropriate coarse-grained model for the fluctuating interface near a wall, which is the starting point for both this problem and the theory of critical wetting.

1. Introduction

The Ising model [1–3] is one of the workhorses of statistical mechanics, playing a role similar to that of the fruitfly in genetics: techniques such as transfer-matrix methods [2,3] and high-temperature series expansions [4] have initially been formulated for the Ising model and were then generalized and applied to many other problems. Similarly, the Ising model has played a pivotal role in the development of concepts about critical phenomena, from scaling [5,6] and universality [7–9] to the renormalization group [10–22]. In addition, critical phenomena in Ising models have been under study by Monte Carlo (MC) simulations since about thirty years [23–37], and recently these studies have reached an accuracy [36–51] that is competitive with the most accurate renormalization-group estimates [52–55]. As far as the critical properties of the nearest-neighbor ferromagnetic Ising model are concerned, there is also fair agreement with estimates drawn from recent series-expansion analyses [56–59], the Monte Carlo renormalization-group (MCRG) approach [60–63], and the coherent-anomaly method [64].

Despite this impressive progress, there are still many problems left that are less well understood, and hence in the focus of the present article. Monte Carlo simulations of critical phenomena almost always rely on the use of finite-size scaling theory [24–37,65–97], but certain aspects of this theory still appear to be under discussion even for short-range Ising models [93–97], particularly if the system dimensionality d exceeds the marginal dimension d^* ($d^* = 4$ here; for $d > d^*$ the critical behavior is described by the simple Landau theory [5–22]). There has been a longstanding discrepancy between the simple predictions by Brézin and Zinn-Justin [74] and Monte Carlo results for the five-dimensional Ising model [72,73,98], and although this discrepancy has been resolved now [99–104], there are still controversial issues regarding the form of finite-size scaling functions above the upper critical dimension [93–96]. The question how to extend finite-size-scaling analyses to mean-field like systems is not a purely academic one, since classical mean-field critical behavior can also arise in two- and three-dimensional systems if the interaction is of sufficiently long range [5,14,45–51,87,92,105–108]. If there is an interaction $J(r)$ of infinite range that decays with distance r like an inverse power law, $J(r) \propto r^{-(d+\sigma)}$, the marginal dimension for $\sigma < 2$ gets lowered to $d^* = 2\sigma$, and consequently the critical behavior is classical for $0 < \sigma < d/2$. However, a very interesting situation also arises if the interaction range R is finite but large [45,46,48–50,87,92]: then the asymptotic critical behavior for very small temperature distances $t = (T - T_c)/T_c$ from the critical temperature T_c is the same as that of the short-range Ising model, but somewhat further away from T_c (although still in the region where $|t| \ll 1$) a crossover to classical critical behavior occurs. While qualitatively the understanding of such a crossover is already provided by the Ginzburg criterion [109], its quantitative description by renormalization-group theory has been a longstanding problem [110–124]. Since a related crossover occurs near the unmixing critical point in polymer blends as well (the larger the chain length N of the macromolecules, the more the system behaves mean-field like [125–133]), this crossover between Ising-like and mean-field critical behavior can be observed experimentally rather directly [134–141]. Various other systems (polymer solutions [142], micellar solutions [143] and ionic systems [144–147] that undergo phase separation) are also candidates for the observation of such crossover phenomena. Therefore, the theoretical understanding of this crossover is relevant to a broad variety of physical systems, and hence the Monte Carlo investigation of these crossover phenomena is one of the main topics of this article.

A final topic that we shall consider here is the statistical mechanics of fluctuating interfaces near walls and the related interface localization–delocalization transitions that occur in Ising films with competing boundary fields of the walls [148–159]. Ising lattices with nearest-neighbor ferromagnetic interactions are expected to exhibit rather complex phase diagrams [150,159]: phase transitions of either second order [148,149,152,154–157] or first order [150,158,159] are possible, and in the second-order case one again encounters a problem where crossover between two-dimensional Ising criticality and mean-field behavior occurs [157]. At the same time, the problem is intimately connected to the problem of critical wetting in the presence of short-range forces [160–177] and the appropriate choice of effective interface Hamiltonians [167,178–186], which are the starting point of analytic theories for these phenomena, is still a matter of discussion.

The outline of this review is as follows: In Section 2, we briefly recall the basic methodological aspects of Monte Carlo simulations, as far as they are essential for the reader to easily appreciate their use as a tool for the analysis of critical phenomena, but also for better understanding of the intrinsic limitations of such simulations. In Section 3, we then consider the analysis of critical behavior for the short-range Ising model in $d = 3$ dimensions, while Section 4 is devoted to the case of $d = 5$ dimensions. Section 5 deals with the case of large but finite interaction ranges, and the problem of crossover scaling between the Ising and mean-field universality classes, both in $d = 2$ and in $d = 3$ dimensions. Section 6 summarizes results for Ising models with interactions that decay as a power law. Finally, Section 7 deals with the interface delocalization problem, while Section 8 gives a summary and an outlook to related problems that have not been dealt with in this article.

2. Methodological tools

2.1. General aspects

As is well known [29–37], Monte Carlo simulations numerically evaluate canonical thermal averages of some observable A,

$$\langle A \rangle_T = \frac{1}{Z} \mathrm{Tr}\{A(\mathbf{x})\exp[-\mathcal{H}(\mathbf{x})/k_B T]\} \,, \tag{2.1}$$

where $Z = \mathrm{Tr}\{\exp[-\mathcal{H}(\mathbf{x})/k_B T]\}$ is the partition function, k_B is Boltzmann's constant, T is the absolute temperature and the Hamiltonian in our case is that of the Ising model, where N spins $S_i = \pm 1$ are placed on lattice sites labeled by the index i

$$\mathcal{H}_{\mathrm{Ising}}(\{S_i\}) = -\sum_{i \neq j} J_{ij}S_iS_j - H\sum_i S_i \,. \tag{2.2}$$

Here J_{ij} are the exchange constants, and we have also included a magnetic field H. The points $\mathbf{x}$ of the (quasiclassical) phase space are the configurations that can be taken by the N spins and the trace operation in Eq. (2.1) is a summation over all the 2^N states. Monte Carlo simulations replace this exact average by an approximate one, where M states $\{\mathbf{x}_\mu\}$ are selected by an

importance-sampling process,

$$\bar{A} = M^{-1} \sum_{\mu=1}^{M} A(\boldsymbol{x}_\mu) \ . \tag{2.3}$$

The importance-sampling process consists of the construction of a Markov chain of states $(\boldsymbol{x}_1 \to \boldsymbol{x}_2 \to \cdots \to \boldsymbol{x}_\mu \to \boldsymbol{x}_{\mu+1} \to \cdots)$, where a suitable choice of the transition probability $W(\boldsymbol{x}_\mu \to \boldsymbol{x}_{\mu+1})$ ensures that, for large enough μ, states $\boldsymbol{x}_\mu$ are selected according to the canonical equilibrium probabilities, $P_{\text{eq}}(\boldsymbol{x}_\mu) \propto \exp[-\mathcal{H}(\boldsymbol{x}_\mu)/k_{\text{B}}T]$.

From this brief description, we can already recognize the main limitations:

(i) Only in the limit $M \to \infty$ we can expect to obtain an exact result, while for finite M a "statistical error" is expected. The estimation of this error is a very nontrivial matter, since – depending on the precise choice of W – subsequently generated states are more or less correlated. In fact, if the Monte Carlo sampling process is interpreted dynamically (associating a (pseudo)time with the label μ of subsequent configurations, one can interpret the Monte Carlo procedure as the numerical implementation of a master equation describing a kinetic Ising model [187]), one recognizes that the "correlation time" is expected to diverge in the thermodynamic limit at a second-order phase transition ("critical slowing down" [188]).

(ii) While the importance sampling method guarantees that, for $\mu \to \infty$, the states are selected according to $P_{\text{eq}}(\boldsymbol{x}_\mu)$, for choices of μ that are not large enough there is still some "memory" of the (arbitrary!) initial state with which the Markov chain was started. In practice, one may start with a completely random spin configuration, or a state where all spins are up, or an (equilibrated) spin configuration of a previous Monte Carlo run (which, e.g., was carried out at some other temperature T). Invoking once more the above dynamic interpretation of Monte Carlo sampling, it is clear that one must "wait" until the system has "relaxed" from the initial state toward the correct thermal equilibrium. Also this "nonequilibrium relaxation time" [189–191] is divergent at a second-order phase transition in the thermodynamic limit. Due to finite-size effects, both the critical divergence of the above correlation time and the critical divergence of this nonequilibrium relaxation time will be rounded off to large but finite values. However, if one does not omit sufficiently many states generated at the beginning of the Markov chain before the averaging in Eq. (2.3) is started, systematic errors will still be generated.

(iii) For the realization of the Markov chain, (pseudo)random numbers are used both for constructing a trial state $\boldsymbol{x}'_\mu$ from a given state $\boldsymbol{x}_\mu$ and for the decision whether or not to accept the trial configuration as a new configuration (in the Metropolis algorithm this is done if the transition probability W exceeds a random number η that is uniformly distributed in the interval from zero to one [29–37]). The Monte Carlo method clearly requires random numbers, however, that are not only uniformly distributed in a given interval, but also uncorrelated, and in practice this absence of correlations is fulfilled only approximately [192–202]. Thus, it is necessary to carefully test the "quality" of the random numbers for each new application of the Monte Carlo method, and this is again a nontrivial matter, since there is no unique way of testing random-number generators [192–202], and there is no absolute guarantee that a random-number generator that has passed all the standard tests does not yield random numbers that lead, due to some subtle correlations among them, to systematic errors in a particular application. These remarks are not entirely academic – even in studies of the nearest-neighbor Ising model results are documented in the literature

[203–208] where "bad" random numbers have caused systematic errors. Thus for Monte Carlo studies which aim at a high precision it is clearly mandatory to check the results using different high-quality random-number generators and to verify that no systematic discrepancies are found.

(iv) Last, but certainly not least, the finite size of the simulated lattice (typically one chooses a (hyper)cubic lattice of linear dimension L with periodic boundary conditions in all lattice directions) causes a systematic rounding and shifting of the critical singularities one wishes to investigate: singularities of the free energy can only develop in the thermodynamic limit $L \to \infty$. This remark is particularly obvious for the correlation length ξ, which cannot diverge toward infinity in a finite simulation box, so that serious finite-size effects must be expected when ξ has grown to a size comparable to L. On the one hand, these finite-size effects constitute a serious limitation, hampering the possibility to extract critical properties from simulations in a direct manner, like it is done in experiments on real systems [209–213]. On the other hand, these finite-size effects offer a powerful tool, via finite-size scaling analyses [70,79,80,83,84], for the study of critical phenomena. While the key ideas of finite-size scaling are quite old [65,66] and their application in the context of simulations is standard [26–37], the optimal use of these concepts remains under discussion [214–223].

In the present article we do not attempt to give a full account of all these problems (i)–(iv), but shall restrict ourselves to a brief discussion of critical slowing down and statistical errors (Section 2.2) and how this problem is eased by the use of cluster algorithms (Section 2.3); in Section 2.4 we then recall those aspects of finite-size scaling analyses which are most relevant for the simulations described in the later sections. A complete discussion of finite-size scaling, of course, should also address aspects other than the critical behavior of the Ising model, but this is beyond the scope of our discussion. Other technical aspects, such as histogram extrapolations [224,225], multicanonical Monte Carlo methods [226–230], etc., will not be discussed here either.

2.2. The Metropolis algorithms and the problem of statistical errors

In the standard Metropolis algorithm [29–37,231], the Markov chain of states $x_1 \to x_2 \to \cdots \to x_\mu \to \cdots$ mentioned above is realized by attempting single-spin flips, $S_i \to S_j$. The procedure consists of the selection of a lattice site i that is considered for a flip (one may either choose the sites at random or go through the lattice in a regular fashion) and the calculation of the energy change $\delta\mathcal{H}$ in the Hamiltonian (2.2), that would be caused by this flip. From this energy change one computes the transition probability W,

$$W(x \to x') = \text{Min}[1, \exp(-\delta\mathcal{H}/k_B T)] . \tag{2.4}$$

If $W = 1$ the spin flip is always accepted. If $W < 1$, one draws a random number η uniformly distributed between zero and unity: if $\eta < W$ the spin is flipped, while otherwise this trial move is rejected and the old configuration is counted once more for the averaging, Eq. (2.3).

The quantities that are most straightforward to average are the energy per spin, $E = \langle\mathcal{H}\rangle_T/N$, and the magnetization per spin $\langle m \rangle$, or (in the absence of the symmetry-breaking field H) its

absolute value, or higher-order moments

$$\langle |m| \rangle = \frac{1}{N} \left\langle \left| \sum_{i=1}^{N} S_i \right| \right\rangle_T , \quad \langle m^k \rangle = \left\langle \left(\frac{1}{N} \sum_{i=1}^{N} S_i \right)^k \right\rangle_T , \quad k = 1, 2, \ldots . \tag{2.5}$$

For a discussion of critical behavior, one is also interested in the susceptibility χ and the specific heat C. These are typically calculated from fluctuation relations, which read (again all quantities are normalized per spin to allow for a straightforward thermodynamic limit)

$$C/k_{\mathrm{B}} = [\langle \mathscr{H}^2 \rangle - \langle \mathscr{H} \rangle^2]/(Nk_{\mathrm{B}}^2 T^2) , \tag{2.6}$$

$$\chi = [\langle m^2 \rangle - \langle m \rangle^2]N/(k_{\mathrm{B}} T) , \tag{2.7}$$

$$\chi' = [\langle m^2 \rangle - \langle |m| \rangle^2]N/(k_{\mathrm{B}} T) . \tag{2.8}$$

Note that (for $H = 0$) one needs to use the standard expression for χ [Eq. (2.7)] while for $T > T_{\mathrm{c}}$ the expression χ' [Eq. (2.8)] should be used for $T < T_{\mathrm{c}}$ [32,36]. The reason for the need of these two different expressions is the spontaneous symmetry breaking that occurs at T_{c}, due to the appearance of a spontaneous magnetization m_{sp}: In statistical mechanics, the proper definition of the spontaneous magnetization would be

$$m_{\mathrm{sp}} = \lim_{H \to 0} \lim_{N \to \infty} \langle m \rangle_{T,H} , \tag{2.9}$$

while at all nonzero temperatures one obtains a trivial result if the limits are interchanged, since

$$\lim_{H \to 0} \langle m \rangle_{T,H} = 0 \quad \forall N . \tag{2.9a}$$

Thus, for any finite N and $H = 0$, Eq. (2.7) is equivalent to $k_{\mathrm{B}} T \chi = N \langle m^2 \rangle_{T,H=0}$, which for large but finite N converges to $k_{\mathrm{B}} T \chi \approx N m_{\mathrm{sp}}^2 \to N$ as $T \to 0$. It follows that χ as defined in Eq. (2.7) is a monotonically increasing function when T decreases through T_{c} which does not show a maximum at any nonzero temperature under equilibrium conditions (if one uses a single-spin flip algorithm, full equilibrium is actually often not obtained for $T < T_{\mathrm{c}}$, due to the exponential divergence of the "ergodic time" τ_{e} with N for $T < T_{\mathrm{c}}$, and a spurious, observation-time-dependent maximum may occur for χ as well, as is discussed elsewhere in the literature [32,36]). On the other hand, we have

$$m_{\mathrm{sp}} = \lim_{N \to \infty} \langle |m| \rangle_{T,H=0} \tag{2.10}$$

and therefore χ' as defined in Eq. (2.8) converges to the correct expression for the susceptibility below T_{c}. Above T_{c}, however, χ and χ' differ by a trivial factor in the thermodynamic limit. This is realized by noting that the probability distribution of m, for sufficiently large $N = L^d$, is a simple Gaussian [31]

$$p_L(m) = L^{d/2}(2\pi k_{\mathrm{B}} T \chi^{(L)})^{1/2} \exp[-m^2 L^d/(2k_{\mathrm{B}} T \chi^{(L)})], \quad T > T_{\mathrm{c}}, \ H = 0 , \tag{2.11}$$

where the notation $\chi^{(L)}$ indicates that for large but finite L there still may be some residual finite-size effect in the susceptibility although in fact we do expect a smooth convergence toward

the susceptibility $\chi^{(\infty)}$ in the thermodynamic limit. From Eq. (2.11), it can easily be shown that [32]

$$\chi'^{(L)} = \chi^{(L)}(1 - 2/\pi) . \tag{2.12}$$

For T sufficiently far below T_c, the distribution function $p_L(m)$ can, near its peaks (which occur at $\pm m_{sp}$ as $L \to \infty$), be approximated by a sum of two Gaussians [31]

$$p_L(m) = \frac{1}{2} L^{d/2} (2\pi k_B T \chi'^{(L)})^{1/2} \{\exp[-(m - m_{max}^{(L)})^2 L^d/(2k_B T \chi'^{(L)})]$$

$$+ \exp[-(m + m_{max}^{(L)})^2 L^d/(2k_B T \chi'^{(L)})]\} \quad T < T_c, \quad H = 0 ; \tag{2.13}$$

again, the positions $\pm m_{max}^{(L)}$ of these peaks may differ from $\pm m_{sp}$ by some residual finite-size effects, but a smooth convergence of $m_{max}^{(L)}$ toward m_{sp} is expected as $L \to \infty$. Note that it is χ' (2.8) that is appropriate for the widths of the Gaussians in Eq. (2.13).

Thus the phase transition of the Ising model in zero field shows up via a change of the order-parameter distribution $p_L(m)$ from a single-peak shape to a double-peak shape. A convenient measure of this change in behavior is the fourth-order cumulant [31]

$$U_L = 1 - \langle m^4 \rangle / [3 \langle m^2 \rangle^2] , \tag{2.14}$$

which converges to zero for $T > T_c$, as one easily derives from Eq. (2.11), while it converges to $U_\infty = 2/3$ for $T < T_c$. At $T = T_c$, U_L converges to a nontrivial *universal* constant, as will be discussed below in the context of finite-size scaling. We also note that U_L appears in the literature in several variants and under a number of different names. For example, $g_L = -3U_L$ is confusingly referred to as the "renormalized coupling constant" [72] – we want to stress here that the use of this nomenclature is to be deprecated! Later this name was correctly used for the related quantity $g_L(L/\xi_L)^d$ where ξ_L is the finite-lattice correlation length [219]. In this article we shall also employ the simplified notation $Q_L = \langle m^2 \rangle^2 / \langle m^4 \rangle$. Other authors use still different normalizations and names, such as the "Binder parameter".

A crucial point of any Monte Carlo simulation is the estimation of the statistical errors of the various observables A that are recorded. Suppose we record M "measurements" $A(X_\mu)$ that are perfectly uncorrelated. Then the statistical error δA of the estimate $\bar{A}$ in Eq. (2.3) can be estimated as [232]

$$\overline{\delta A^2} = [\langle A^2 \rangle - \langle A \rangle^2]/M , \tag{2.15}$$

while the variance $\langle \sigma_A^2 \rangle = \langle A^2 \rangle - \langle A \rangle^2$ can be estimated from

$$\langle \sigma_A^2 \rangle \approx \sum_{\mu=1}^{M} [A(X_\mu) - \bar{A}]^2/(M - 1) . \tag{2.16}$$

Note the denominator $M - 1$ rather than M in Eq. (2.16): this denominator accounts for the fact that $\bar{A}$ in Eq. (2.16) is estimated from the same M "measurements" $A(X_\mu)$ already, and hence there remain only $M - 1$ rather than M statistically independent "measurements" of $[A(X_\mu) - \bar{A}]^2$. In practice, however, if observables such as the specific heat or susceptibilities are sampled from fluctuation relations, this point is sometimes ignored and the same formula Eq. (2.3) is used for the

estimation of variances as well,

$$\overline{\sigma_A^2} = \sum_{\mu=1}^{M} [A(\mathbf{X}_\mu) - \bar{A}]^2/M \ . \tag{2.17}$$

The replacement of $M-1$ [Eq. (2.16)] in favor of M [Eq. (2.17)] obviously leads to a systematic underestimation of quantities such as C or χ. While this bias is negligible in the limit of very large M, it does become a problem if the "measurements" $A(\mathbf{X}_\mu)$ are correlated: both the statistical error and the bias then get strongly enhanced.

Let us first consider the expectation value of the square of the statistical error, based on M successive observations $A_\mu \equiv A(\mathbf{X}_\mu)$ [187]:

$$\langle (\delta A)^2 \rangle = \left\langle \left[\frac{1}{M} \sum_{\mu=1}^{M} (A_\mu - \langle A \rangle) \right]^2 \right\rangle$$

$$= \frac{1}{M^2} \sum_{\mu=1}^{M} \langle (A_\mu - \langle A \rangle)^2 \rangle + \frac{2}{M^2} \sum_{\mu_1=1}^{M} \sum_{\mu_2=\mu_1+1}^{M} (\langle A_{\mu_1} A_{\mu_2} \rangle - \langle A \rangle^2) \ . \tag{2.18}$$

Changing the summation index μ_2 to $\mu_1 + \mu$, Eq. (2.18) can be rewritten as

$$\langle (\delta A)^2 \rangle = \frac{1}{M}[\langle A^2 \rangle - \langle A \rangle^2]\left\{ 1 + 2 \sum_{\mu=1}^{M} \left(1 - \frac{\mu}{M} \right) \phi_A^{(\mu)} \right\}, \tag{2.19}$$

where $\phi_A^{(\mu)}$ is an autocorrelation function

$$\phi_A^{(\mu)} = \frac{\langle A_{\mu_1} A_{\mu_1+\mu} \rangle - \langle A \rangle^2}{\langle A^2 \rangle - \langle A \rangle^2} \ . \tag{2.20}$$

This result can be interpreted associating a "time" $t_\mu = \delta t\, \mu$ with the Monte Carlo process, δt being the "time interval" between two successive "measurements" A_μ and $A_{\mu+1}$. It is possible to take $\delta t = 1/N$, i.e., every Monte Carlo move (e.g., every attempted spin flip in a single-spin-flip Metropolis algorithm) is included in the calculation, but then it is clear that subsequent states $\mathbf{X}_\mu$ are highly correlated for large N, since they differ by at most one out of N spin orientations. Thus it is more common to choose $\delta t = 1$ (corresponding to a "time" unit of 1 Monte Carlo step per spin), although near T_c it often is more efficient to take even less "measurements", e.g., $\delta t = 10$. Thus, we replace $\phi_A^{(\mu)}$ by $\phi_A(t)$ (noting also that in equilibrium there is an invariance with respect to the choice of the time origin),

$$\phi_A(t) = [\langle A(0)A(t) \rangle - \langle A \rangle^2]/[\langle A^2 \rangle - \langle A \rangle^2] \ , \tag{2.21}$$

and, by treating t as a continuous rather than a discrete variable, replace the sum in Eq. (2.19) by an integral, where $\tau_M = M\,\delta t$ is the observation time over which the averaging is extended,

$$\langle (\delta A)^2 \rangle = \frac{1}{M}[\langle A^2 \rangle - \langle A \rangle^2]\left[1 + 2 \int_0^{\tau_M} \frac{dt}{\delta t}\left(1 - \frac{t}{\tau_M} \right) \phi_A(t) \right]. \tag{2.22}$$

Defining a correlation time as

$$\tau_A = \int_0^{\infty} \phi_A(t)\,dt \tag{2.23}$$

and assuming that the observation time $\tau_M \gg \tau_A$, one can rewrite Eq. (2.22) as

$$\langle(\delta A)^2\rangle = \frac{1}{M}[\langle A^2\rangle - \langle A\rangle^2](1 + 2\tau_A/\delta t) \ . \tag{2.24}$$

If τ_A diverges near a critical point and δt is kept of order unity, as anticipated above, we have $\tau_A/\delta t \gg 1$ and Eq. (2.24) becomes

$$\langle(\delta A)^2\rangle = 2\frac{\tau_A}{\tau_M}[\langle A^2\rangle - \langle A\rangle^2] \ . \tag{2.25}$$

This result shows that the statistical error is independent of the choice of the time interval δt and only depends on the number $n = \tau_M/(2\tau_A)$ of statistically independent "measurements": although for a given observation time τ_M a choice of a smaller value δt results in a correspondingly larger value of the number of observations, it does not decrease the statistical error. It is only the ratio between the relaxation time τ_A and the observation time τ_M that matters. Thus, the estimation of these relaxation times is indispensable for a correct estimation of statistical errors. From these considerations it is already evident how useful it has been to develop algorithms that reduce the critical slowing down near phase transitions or even remove it completely.

These correlation times also have a significant effect on the problem of biased estimates mentioned above: unbiased estimates of variances are obtained if we take only n measurements $A(X_{\mu'})$ at time intervals $2\tau_A$ apart,

$$\langle\sigma_A^2\rangle \approx \sum_{\mu'=1}^{n} [A(X_{\mu'}) - \bar{A}]^2/(n-1) \ . \tag{2.26}$$

Often n is not very much larger than unity, and then Eq. (2.26) is significantly different from Eq. (2.17). This has been demonstrated by Ferrenberg et al. [233] for the three-dimensional Ising model at T_c, cf. Fig. 1. One can see that due to the systematic underestimation of both C and χ (by a factor $1 - 1/n$ for large n) the data approach their asymptotic values always from below with increasing number of measurements M (denoted as N in the figure). For C the saturation is reached somewhat faster than for χ, since the correlation time τ_E of the energy is smaller than the correlation time τ_m for the magnetization. Note also that the time needed to reach the correct saturation values increases with increasing L. This is due to the finite-size rounding of the relaxation time in the single-spin-flip kinetic Ising model:

$$\tau_E \propto \tau_m \propto L^z \quad T = T_c \ , \tag{2.27}$$

with a dynamical critical exponent $z \approx 2$ [234]. Therefore, there is a strong decrease of the number n of statistically independent "measurements" with increasing L, and it becomes very difficult to carry out, with single-spin-flip algorithms, meaningful simulations for values of L distinctly larger than those included in Fig. 1.

Another important aspect of statistical errors is the question how these scale with the linear dimension of the simulated systems. If we wish to record the energy or the magnetization, we conclude from Eqs. (2.6)–(2.8) and (2.25) that the squared errors are expected to scale inversely
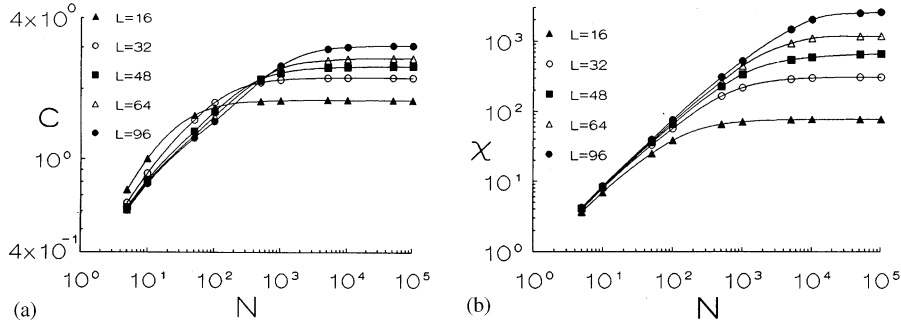
Fig. 1. Specific heat (a) and susceptibility (b) plotted vs. the number of measurements N in a bin, for $\delta t = 10$ MCS and the simple cubic nearest-neighbor Ising model at T_c [$J/k_B T_c = 0.221654$ was used here]. For each linear lattice dimension L, a total effort of at least 3×10^6 MCS/spin was invested, using a single-spin-flip algorithm. The "measurements" of energy and magnetization were grouped into bins containing N entries each, and then C and χ were calculated using Eq. (2.17). Finally, the results were averaged over all the available bins to reduce the statistical error compared to the systematic error resulting from the bias. From Ferrenberg et al. [233].

with the system volume $N = L^d$,

$$\langle (\delta E)^2 \rangle = \frac{2\tau_E}{\tau_M} \frac{k_B T^2 C}{L^d}, \quad \langle (\delta m)^2 \rangle = \frac{2\tau_m}{\tau_M} [\langle m^2 \rangle - \langle m \rangle^2] = \frac{2\tau_m}{\tau_M} \frac{k_B T \chi}{L^d} . \tag{2.28}$$

The property that squared errors scale inversely with the volume is called "strong self-averaging" [235] and only holds away from T_c, whereas at T_c it is replaced by so-called "weak self-averaging": Since, at T_c, in a finite system χ and C scale like powers of L [for $d \leq 4$ we have $\chi(T = T_c) \propto L^{\gamma/\nu}$, $C(T = T_c) \propto L^{\alpha/\nu}$, where α, γ and ν are the standard critical exponents of the specific heat, the susceptibility and the correlation length, respectively, see below], we have

$$\langle (\delta m)^2 \rangle \propto \frac{1}{n} L^{\gamma/\nu - d}, \quad \langle (\delta E)^2 \rangle \propto \frac{1}{n} L^{\alpha/\nu - d}, \quad T = T_c . \tag{2.29}$$

However, the situation is very different if we consider the errors of quantities that are derived from fluctuation relations, such as χ and C themselves [Eqs. (2.6)–(2.8)]: Now the quantity A in Eq. (2.25) has to be replaced by $L^d(\delta m)^2$ or $L^d(\delta E)^2$, respectively, with $\delta m = m - \langle m \rangle$ and $\delta E = E - \langle E \rangle$, and hence [235]

$$(k_B T \Delta \chi)^2 = \frac{1}{n} L^{2d}[\langle (\delta m)^4 \rangle - \langle (\delta m)^2 \rangle^2], \quad (k_B T^2 \Delta C)^2 = \frac{1}{n} L^{2d}[\langle (\delta E)^4 \rangle - \langle (\delta E)^2 \rangle^2] . \tag{2.30}$$

Using the fact that away from T_c both δm and δE are Gaussian distributed for large enough L, $\langle (\delta m)^4 \rangle = 3\langle (\delta m)^2 \rangle^2$, $\langle (\delta E)^4 \rangle = 3\langle (\delta E)^2 \rangle^2$ can be used to reduce Eq. (2.30) to

$$\sqrt{(k_B T \Delta \chi)^2} = \sqrt{\frac{2}{n}} L^d \langle (\delta m)^2 \rangle = \sqrt{\frac{2}{n}} k_B T \chi, \quad \text{i.e.} \ \sqrt{(\Delta \chi)^2}/\chi = \sqrt{2/n} , \tag{2.31}$$

$$\sqrt{(k_B T^2 \Delta C)^2} = \sqrt{\frac{2}{n}} L^d \langle (\delta E)^2 \rangle = \sqrt{\frac{2}{n}} k_B T^2 C, \quad \text{i.e.} \ \sqrt{(\Delta C)^2}/C = \sqrt{2/n} . \tag{2.32}$$

Thus we see that the relative error of quantities sampled from fluctuation relations does not decrease at all with increasing L, but gets small only when the number n of statistically independent samples becomes large. This property is called "lack of self-averaging" [235].

2.3. Cluster algorithms

From the discussion of statistical errors in the previous section it will be evident that critical slowing down makes it very difficult to obtain precise estimates for the observables of interest in the critical region, using the Metropolis algorithm and sufficiently large lattices. Only by use of highly efficient vectorizing algorithms on supercomputers with vector architecture and a massive invest-ment of CPU resources it has been possible to obtain very good results in this way [33,39,233]. Given this situation, the invention of cluster algorithms [225,236–251] that offer a dramatic reduction of critical slowing down has been crucial for allowing more widespread studies.

Here, we first discuss the original cluster algorithm for the nearest-neighbor Ising model in zero external field. The starting point is the Fortuin–Kasteleyn representation [252] of the partition function, writing $K = J/k_\mathrm{B}T$,

$$Z = \sum_{\{S_i\}} \exp\left(K \sum_{\langle ij \rangle} S_i S_j \right) = \sum_{\{S_i\}} \prod_{\langle ij \rangle} \mathrm{e}^K [(1 - p) + p\delta_{S_i S_j}] \tag{2.33}$$

or

$$Z = \sum_{\{S_i\}} \sum_{\{n_{ij}\}} \prod_{\langle ij \rangle} \mathrm{e}^K [(1 - p)\delta_{n_{ij},0} + p\delta_{S_i S_j}\delta_{n_{ij},1}] \,, \tag{2.34}$$

where the n_{ij} are auxiliary bond variables that can take the values 0 and 1. Only if the two spins S_i and S_j are equal, the bond n_{ij} is "occupied" or "active" ($n_{ij} = 1$) with probability p,

$$p = 1 - \exp(-2K) \,, \tag{2.35}$$

while otherwise $n_{ij} = 0$. In Eq. (2.33) we used the fact that the product $S_i S_j$ can only be $+1$ if both spins are equal and -1 if they are not, so $\exp(KS_i S_j) = x + y\delta_{S_i S_j}$ is easily solved for x and y. For Eq. (2.34) the simple identity

$$a + b = \sum_{n=0}^{1} (a\delta_{n,0} + b\delta_{n,1}) \tag{2.36}$$

has been used. Now the Swendsen–Wang algorithm [236] makes use of the joint probability distribution for the spin and bond variables implicit in Eq. (2.34). A "cluster update sweep" [35,251] then consists of alternating updates of the bond variables n_{ij} for a given spin configuration $\{S_i\}$ and updates of the spins S_i for the given bond configuration. Thus the algorithm consists of the following steps:

(i) If $S_i \neq S_j$, set $n_{ij} = 0$. If $S_i = S_j$, assign values $n_{ij} = 1$ and $n_{ij} = 0$ with probability p [Eq. (2.35)] or $1 - p$, respectively.

(ii) Identify clusters of spins that are connected by "active" bonds ($n_{ij} = 1$). Clearly, this step is relatively time-consuming, but in the context of the bond-percolation problem [253,254] rather efficient cluster-counting routines have been developed. In any case, this somewhat "technical" issue is out of consideration here.

Table 1
The critical exponent z of the integrated relaxation time τ_A of various observables (A = energy E, magnetization m, or susceptibility χ) in $d = 2$ and $d = 3$ dimensions ($\tau_A \propto L^z$). The typical error is of the order of 0.02

Algorithm	$d = 2$	$d = 3$	Observable	Reference
Metropolis	2.16	2.03	E and m	[234,256]
Swendsen–Wang	0.27	0.50	E	[238]
	0.20	0.50	χ	[238]
Wolff	0.26	0.28	E	[238]
	0.13	0.14	χ	[238]

(iii) Draw a random value ± 1 independently for each cluster (including clusters containing a single spin only), which then is assigned as the spin value for all spins in this cluster.

Note that the clusters defined in this way are "stochastic" clusters that differ from clusters that one could define on a purely geometric basis as contours around groups of identical spins [255]. In the present clusters, some bonds between identical spins are deleted with probability $p_{\text{del}} = 1 - p = \exp(-2K)$: Thus, in the high-temperature limit, $K \to 0$, large clusters cannot occur, unlike the "geometric clusters" where even for $K \to 0$ arbitrary large clusters occur with nonzero probability. Obviously the present "stochastic" clusters are on average smaller than the "geometric clusters": Only at $T \to 0$ ($K \to \infty$) p_{del} vanishes and the present clusters become identical to the geometric clusters.

It turns out that this Swendsen–Wang algorithm spends too much time identifying and handling small clusters, which are present at the critical point, too, although the important physics (such as the diverging correlation length) is embodied in the very large clusters only. For this reason, it is more efficient to consider a single cluster at a time, instead of making a full decomposition of the whole lattice into clusters. In this "single-cluster algorithm" due to Wolff [237–239] one chooses a lattice site at random, constructs only the "stochastic" cluster connected to this site, using the same probability p of setting active bonds as discussed above, and then flips all the spins of this cluster. If $\langle c \rangle$ denotes the average cluster size, a "sweep" through the lattice is defined by the number $L^d/\langle c \rangle$ of such single-cluster steps, while in the Metropolis single-spin-flip algorithm a "sweep" is defined when (on average) every of the L^d lattice sites has been considered once for a spin-flip. With these definitions of "sweeps", a sensible comparison of the correlation times of various quantities for the different algorithms is possible (Table 1) [35,256].

An important generalization of cluster algorithms is the extension to long-range interactions due to Luijten and Blöte [250]. It has the remarkable property that the efficiency is *independent* of the number of interactions per spin, and can be applied to any O(n) and Potts model without frustration. Furthermore, it is applicable to any interaction profile and dimensionality. Obviously, this implies an enormous improvement compared to conventional single-spin-flip and cluster algorithms alike, with a typical speed-up of several orders of magnitude. The essential ingredient of this method is that one does not consider every single interacting neighbor of a spin for inclusion into the cluster being built, but instead calculates which spin is the next one to be considered for inclusion. For the technical details, the reader is referred to the original literature [250], while also Ref. [257] contains a pedagogical introduction.

2.4. Finite-size scaling

As already mentioned in the introduction, the literature on finite-size scaling is rich and in some aspects still controversial [24–37,65–97], so that we cannot give an exhaustive review here; instead we focus on those aspects which are most pertinent to the Monte Carlo studies that are reviewed in the following sections.

The key idea (at least for systems that obey the hyperscaling relation [12–22] between critical exponents, $d\nu = \gamma + 2\beta$) is that the linear dimension L "scales with the correlation length ξ", $\xi \propto t^{-\nu}$, $t = T/T_c - 1$. For the probability distribution of observing a magnetization m in a cubic box of size L (with periodic boundary conditions) this idea implies [31]

$$P_L(m,t) = \xi^{\beta/\nu} P(L/\xi, m\xi^{\beta/\nu}) = L^{\beta/\nu} \tilde{P}(L/\xi, mL^{\beta/\nu}) \quad L \to \infty, \ \xi \to \infty, \quad L/\xi \text{ fixed} . \tag{2.37}$$

Here the function $P_L(m,t)$, a function of three variables L, m and t, is, via the scaling assumption, reduced to a "scaling function" (P or $\tilde{P}$, respectively) that depends on two arguments only (L/ξ and $m\xi^{\beta/\nu}$ or $mL^{\beta/\nu}$, respectively). For the sake of a transparent formulation, we have replaced the variable t by the related variable $\xi^{-1/\nu}$ in Eq. (2.37). We note from the outset that finite-size scaling holds in the limit where both $L \to \infty$ and $t \to 0$ (and consequently $m \to 0$), as is the case for all scaling descriptions near critical points. At fixed L and/or fixed ξ, corrections to the asymptotic critical behavior embodied in Eq. (2.37) must be considered, as is discussed below.

The scale factors $\xi^{\beta/\nu}$ or $L^{\beta/\nu}$ in Eq. (2.37) trivially follow from the condition that $P_L(m,t)$ is normalized to unity:

$$\int_{-1}^{+1} P_L(m,t)\,dm = 1 \quad \forall t, \quad \forall L . \tag{2.38}$$

In the limit considered, $P_L(m,t)$ is nonzero only near $m = 0$ and hence the integration limits ± 1 can be replaced by $\pm \infty$ with negligible error. Naturally, the scaling forms with P and $\tilde{P}$ in Eq. (2.37) are fully equivalent, since with the arguments $X = L/\xi$, $Y = m\xi^{\beta/\nu}$ we can form new variables $X = L/\xi$, $Z = YX^{\beta/\nu} = mL^{\beta/\nu}$.

The moments $\langle m^k \rangle$ considered in Eq. (2.5) can be found straightforwardly from Eq. (2.37) as

$$\langle m^k \rangle = \int_{-\infty}^{+\infty} m^k P_L(m,t)\,dm = L^{-k\beta/\nu} \tilde{M}_k^{\pm}(L/\xi) = L^{-k\beta/\nu} M_k(L^{1/\nu}t) , \tag{2.39}$$

where $\tilde{M}_k^{\pm}(X)$ is the resulting scaling function, with the symbol $\pm$ referring to the sign of t. It is more convenient to work with the single function M_k which may have both positive and negative arguments and in fact is analytic near $t = 0$, while $\tilde{M}_k^{\pm}$ would be singular near $X \to 0$. Eqs. (2.7), (2.8) and (2.14) then yield (using $\langle m \rangle \equiv 0$ in zero external field)

$$\langle |m| \rangle = L^{-\beta/\nu} M_1(L^{1/\nu}t) , \tag{2.40}$$

$$\chi = (L^d/k_B T) L^{-2\beta/\nu} M_2(L^{1/\nu}t) , \tag{2.41}$$

$$\chi' = (L^d/k_B T) L^{-2\beta/\nu} \{M_2(L^{1/\nu}t) - [M_1(L^{1/\nu}t)]^2\} \tag{2.42}$$

and

$$U_L = 1 - M_4(L^{1/\nu}t)/\{3[M_2(L^{1/\nu}t)]^2\} \equiv \tilde{U}(L^{1/\nu}t) . \tag{2.43}$$

Analogously, the quantity $Q_L = \langle m^2 \rangle^2 / \langle m^4 \rangle$ can be written as $Q_L = \tilde{Q}(L^{1/\nu}t)$ in this limit.

From Eqs. (2.40)–(2.42) we recover simple power laws in the limit $L/\xi \to \infty$ or $L^{1/\nu}t \to \infty$, requiring that powers of L must cancel to obtain a sensible thermodynamic limit. Hence (taking $X' \equiv L^{1/\nu}t$),

$$M_k(X' \to -\infty) \propto (-X')^{k\beta}, \quad \langle|m|\rangle \propto \xi^{-\beta/\nu} \propto (-t)^\beta, \quad t < 0 , \tag{2.44}$$

$$M_k(X' \to \infty) \propto (X')^{-k\gamma/2}, \quad k_{\mathrm{B}}T\chi \propto k_{\mathrm{B}}T\chi' \propto L^{d-2\beta/\nu-\gamma/\nu}t^\gamma, \quad t > 0 . \tag{2.45}$$

We recognize from this result that hyperscaling is built into the description (2.37), since the power of L in Eq. (2.45) only cancels if $d\nu = 2\beta + \gamma$ [31].

Just like Eqs. (2.40)–(2.42) imply simple power laws in t and hence in ξ if $L \to \infty$, one finds simple power laws in L in the limit $\xi \to \infty$, i.e., when considering the behavior right at T_c: $\tilde{M}_k^+(0) = \tilde{M}_k^-(0)$ are simple constants, and hence

$$\langle|m|\rangle_{T_c} \propto L^{-\beta/\nu}, \quad U_{L,T_c} = \tilde{U}(0) . \tag{2.46}$$

While the power laws for $\langle|m|\rangle$ and χ (or χ', respectively) involve nonuniversal prefactors (the critical amplitudes), both in the t dependence [Eqs. (2.44) and (2.45)] and in the L dependence [Eq. (2.46)], these amplitudes cancel out in the ratio $\tilde{U}(0)$ [or $\tilde{Q}(0)$], which therefore is a universal constant that has proven very useful for the identification of the corresponding universality class.

For completeness, we mention that the finite-size scaling description can be extended to the energy per spin E and the specific heat C [Eq. (2.6)],

$$E = E_c + L^{-(1-\alpha)/\nu}\tilde{E}(L^{1/\nu}t) , \tag{2.47}$$

$$C/k_{\mathrm{B}} = L^{\alpha/\nu}\tilde{C}(L^{1/\nu}t) . \tag{2.48}$$

Imposing once more that powers of L must cancel in the thermodynamic limit, one finds

$$\tilde{E}(X' \to \pm\infty) \propto |X'|^{1-\alpha}, \quad \tilde{C}(X' \to \pm\infty) \propto |X'|^{-\alpha}, \quad C \propto |t|^{-\alpha} , \tag{2.49}$$

while for $t = 0$ we have the power laws in L (we assume $\alpha > 0$ here)

$$E - E_c \propto L^{-(1-\alpha)/\nu}, \quad C \propto L^{\alpha/\nu} . \tag{2.50}$$

Clearly, we have only considered the leading critical behavior in this description, and neither nonanalytic corrections to scaling nor analytic background terms (which are, e.g., expected for quantities such as the specific heat C) have been taken into account yet.

It is also of interest to estimate the correlation length itself from the simulations. One can either sample the spin pair correlation function

$$G(\mathbf{r}) = \langle S(\mathbf{r}_i)S(\mathbf{r}_i + \mathbf{r})\rangle \tag{2.51}$$

and study its asymptotic decay for large r in order to obtain the true correlation range [$G(r) \propto \exp(-r/\xi)$ for $r \gg \xi$; note that ξ defined in this way in general depends on the direction of the lattice [6]], or one can obtain the second-moment correlation length. This quantity is defined from the behavior of the structure factor $S(\mathbf{k})$ at small k,

$$\xi^2 = [S(0)/S(\mathbf{k}) - 1]/k^2 , \tag{2.52}$$
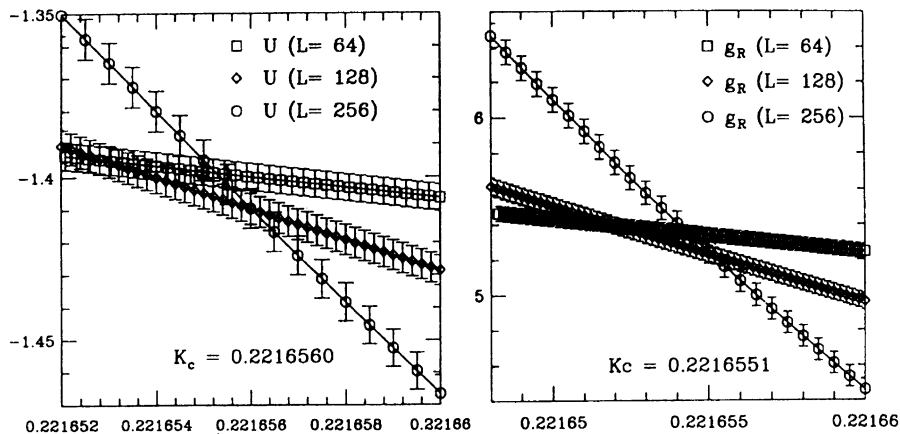
Fig. 2. Plot of $-3U = \langle m^4 \rangle / \langle m^2 \rangle^2 - 3$ (left) and $g_{\mathrm{R}} = 3(L/\xi)^3 U$ (right) vs. $K = J/k_{\mathrm{B}}T$ for the nearest-neighbor Ising model on the simple cubic lattice. The data were obtained from histogram reweighting of data taken at $K_{\mathrm{sim}} = 0.221655$; thus the values of U and g_{R} shown as different points are not based on independent runs, but are highly correlated, and the plotted error bars are just the statistical error observed at K_{sim}. Three choices of L are shown, data being obtained with the Swendsen–Wang cluster algorithm at the Thinking Machine CM-5 computers, based on about 500 000 measurements per size. The estimates for K_{c} are taken from the crossing points of data for $L = 128$ and $L = 256$. From Gupta and Tamayo [62].

where

$$S(\boldsymbol{k}) = \frac{1}{L^d} \left\langle \left| \sum_i S(\boldsymbol{r}_i) \exp(\mathrm{i}\boldsymbol{k} \cdot \boldsymbol{r}_i) \right|^2 \right\rangle . \tag{2.53}$$

We now briefly discuss how these finite-size scaling relations can be utilized to investigate critical phenomena. The first task is to locate the critical temperature T_{c}. A method that does not need any a priori knowledge of critical exponents is based on the observation [31] that at T_{c} the cumulant U_L should take a universal value $\tilde{U}(0)$, Eq. (2.46). On the other hand, we know that for $T < T_{\mathrm{c}}$, U_L converges to $U_\infty = 2/3$ for $L \to \infty$, while for $T > T_{\mathrm{c}}$, $U_L \to 0$ in this limit, and $\mathrm{d}U_L/\mathrm{d}T|_{T_{\mathrm{c}}} \propto \tilde{U}'(0)L^{1/\nu}$ [cf. Eq. (2.43)]. These results imply that $U_L(T)$ for different L should be a family of curves which all merge at $U_L = 2/3$ at low temperatures, splay out and intersect in a unique intersection point $\tilde{U}(0)$ at T_{c}, and then spread out again, since the slope at this intersection point scales as $L^{1/\nu}$.

If one is satisfied with a modest accuracy, this is indeed a very useful and simple method, and it therefore has been of widespread use for a variety of systems [32–37]. However, if a very high precision in the location of T_{c} is desired, deviations from this intersection property will be found, due to the residual effect of corrections to finite-size scaling. These corrections to the leading finite-size scaling behavior are only small if sufficiently large lattice sizes are available. As an example, Fig. 2 presents a plot of $-3U$ and the renormalized coupling constant $g_{\mathrm{R}} = (L/\xi)^d [3 - \langle m^4 \rangle / \langle m^2 \rangle^2]$ vs. $K \equiv J/k_{\mathrm{B}}T$ for the nearest-neighbor Ising model [62]. Three rather large values of L are included: $L = 64$, $L = 128$ and $L = 256$. Due to the very fine resolution

of both abscissa and ordinate scale, one clearly finds three distinct intersection points in the range from $K = 0.221652$ to $K = 0.221656$, and there is a corresponding uncertainty in $-3U$ (the intersection is in the range between -1.39 and -1.41, corresponding to $\tilde{Q}(0) = 0.625 \pm 0.004$). The relative inaccuracy of K_c in this determination is only 10^{-5} or perhaps even less [since other criteria can be derived from the same simulation, the authors suggest $K_c = 0.221655\,(1)$ [62]].

Now an alternative way to find T_c is to locate the positions $K_c(L)$ where quantities such as C and χ' have a peak, and to extrapolate these peak positions toward $L \to \infty$ (we recall that χ itself does not have a peak, but is monotonically increasing toward $L^d/k_B T$ as $T \to 0$). Actually, in practice the peak of C is not well suited, since the specific-heat exponent α is rather small and the position t_{max} where the function $\tilde{C}(X')$ takes its maximum is strongly affected both by singular corrections to scaling and by regular background terms, unless L is exceedingly large. Only when the singular contribution written in Eq. (2.48) is actually dominant, we can conclude that the maximum of C occurs at a value $X'^{(C)}_{max} = L^{1/\nu} t^{(C)}_{max}$ where the function $\tilde{C}(X')$ has its maximum

$$t^{(C)}_{max} = X'^{(C)}_{max} L^{-1/\nu} \,. \tag{2.54}$$

We emphasize that there is no reason to expect that the maximum of C and the maximum of χ' [Eq. (2.42)], with

$$\chi' = (L^{\gamma/\nu}/k_B T_c)\tilde{\chi}'(L^{1/\nu} t) \,, \tag{2.55}$$

will coincide: Actually one finds a maximum at a different value $X'^{(\chi')}_{max}$ of the scaling variable, and hence

$$t^{(\chi')}_{max} = X'^{(\chi)}_{max} L^{-1/\nu} \,. \tag{2.55}$$

Similar behavior occurs for other quantities which exhibit a maximum, such as the temperature derivative of moments, $d\langle |m| \rangle/dT$, $d\langle m^2 \rangle/dT$, etc. These temperature derivatives (or corresponding derivatives $d\langle |m| \rangle/dK, \ldots$) can be obtained from suitable fluctuation relations

$$d\langle A \rangle/dK = (\langle AE \rangle - \langle A \rangle\langle E \rangle)L^d \,. \tag{2.56}$$

Histogram reweighting [224,225] is a convenient technique to record these correlation functions $\langle AE \rangle - \langle A \rangle\langle E \rangle$ for a range of values around a suitably chosen value K_{sim} and to find their maxima. The recipe is then to extrapolate all the resulting "pseudocritical" couplings $K_c^{(A)}(L)$ vs. $L^{-1/\nu}$ and to attempt to locate a unique critical point $K_c = K_c^{(A)}(\infty)$, cf. Fig. 3. Here, we have included data from both Gupta and Tamayo [62] (using the Swendsen–Wang algorithm, for sizes $L = 64, 128, 256$) and Ferrenberg and Landau [39] (using the Metropolis algorithm for sizes in the range $24 \leq L \leq 96$) to show that reasonably consistent results are obtained. To take into account the leading singular correction to scaling in the extrapolation shown in Fig. 3, one should use a formula [39]

$$K_c^{(A)}(L) = K_c + a^{(A)} L^{-1/\nu}[1 + b^{(A)} L^{-\omega} + \cdots] \,, \tag{2.57}$$

involving a (universal) correction-to-scaling exponent ω and a (nonuniversal) amplitude factor $b^{(A)}$. The data in Fig. 3 do not give a clear indication whether or not such corrections to scaling are important in this range of system sizes, although the fluctuation in the cumulant intersection points suggests that such corrections are still present.
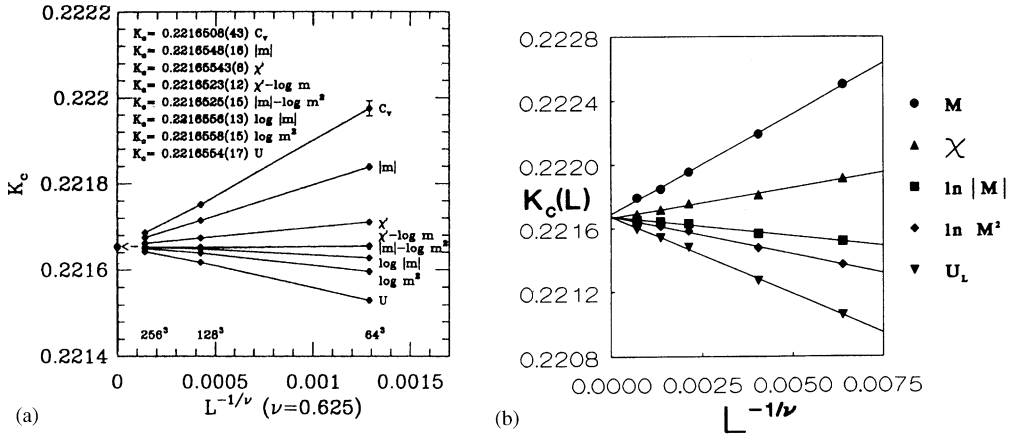
Fig. 3. (a) Estimate of K_c by extrapolation of data for $K_c^{(A)}(L)$ for different observables A, as shown in the figure, plotting $K_c^{(A)}(L)$ vs. $L^{-1/\nu}$ assuming $\nu = 0.625$. The data are for $K_{\mathrm{sim}} = 0.221655$. The resulting best estimate for K_c is $K_c = 0.221654\,(2)$. From Gupta and Tamayo [62]. (b) Same as in Fig. 3(a), but using data for much smaller sizes ($24 \leq L \leq 96$) on more expanded scales. A rather good linear fit is obtained, using $\nu = 0.629$, and the resulting estimate for K_c then is $K_c = 0.2216595\,(26)$, which is nowadays believed to be somewhat too high (cf. Table 2). From Ferrenberg and Landau [39].

In principle, corrections to scaling could be safely ignored if still much larger sizes could be simulated reliably. While calculations of Ising models have been performed up to lattice sizes of 4800^3 [258] (as well as short runs for 5888^3 [259] and [in $d = 2$] 496640^2 [259] and [in $d = 5$] 112^5 [258] spins), these calculations could not produce well-equilibrated configurations at T_c, thus prohibiting a meaningful finite-size analysis. Also it may well be doubted that an appreciable statistical accuracy can be reached for these systems.

An alternative strategy is not to strive for as large lattices as possible but on the contrary work with relatively small lattices (or, at best, lattices of intermediate size) and to obtain results of very high statistical quality, so that the problem of various corrections to the leading asymptotic behavior can be addressed in a serious way [39–51,214]. This will be the strategy emphasized in the following sections. For this purpose, it is helpful not to proceed simply on an entirely phenomenological level [as done in Eqs. (2.37)–(2.57)], but to take some guidance from the renormalization-group description of finite-size scaling [67,83,260]. Denoting the normalized free-energy density by $f = F/(k_B T L^d)$, where the free energy F is related to the partition function Z as $F = -k_B T \ln Z$, we obtain the following behavior under a renormalization transformation with a scaling factor b (see, e.g., Ref. [42]):

$$f(t, h, u, L^{-1}) = b^{-d} f_{\mathrm{sing}}(b^{y_t} t, b^{y_h} h, \{b^{y_i} u_i\}, b/L) + g(t, h, \{u_i\}) \quad i = 1, 2, \ldots \ . \tag{2.58}$$

Here t and h are the temperature-like and magnetic-field-like scaling fields, which are "relevant" in the renormalization-group sense, while $\{u_i\}$ is the set of all other scaling fields, which are "irrelevant variables" [14–22]. The pertinent exponents are denoted as y_t, y_h (which are both positive) and $\{y_i\}$ (< 0) respectively. The function $g(t, h, \{u_i\})$ is the regular (analytic) part resulting from the scale transformation, and f_{sing} the singular part. The key aspect of the renormalization-group theory of finite-size scaling is that the inverse linear dimension L^{-1} simply scales with b; no

other scaling power appears here. For our purposes, it will be sufficient to keep one irrelevant variable (the one with the largest exponent $y_1 \equiv - \omega$), which we shall simply denote as u. Note also the relation with the standard critical exponents [14–22]

$$y_t = 1/v, \quad y_h = d - \beta/v \ . \tag{2.59}$$

By differentiating k times with respect to h, and setting $b = L$ and $h = 0$, one obtains

$$f^{(k)}(t,0,u,L^{-1}) = L^{ky_h - d}f_{\text{sing}}^{(k)}(L^{y_t}t,0,L^{-\omega}u,1) + g^{(k)}(t,0,u) \ . \tag{2.60}$$

We now first concentrate on the moments $\langle m^2 \rangle$ and $\langle m^4 \rangle$, which follow from differentiations of the free energy with respect to the physical magnetic field H,

$$\langle m^2 \rangle = - L^{-d}(\partial^2 f/\partial H^2)_{H=0}, \quad \langle m^4 \rangle = - L^{-3d}(\partial^4 f/\partial H^4)_{H=0} + 3L^{-2d}(\partial^2 f/\partial H^2)^2_{H=0} \ . \tag{2.61}$$

The Ising spin up–spin down symmetry ensures that the scaling field h is an odd function of H. However, it does not need to be simply proportional to it, but can contain higher odd powers of H as well. Similarly, the scaling field t has a power-series expansion in $K_{\text{nn}} - K_c$ [we write $J_{\text{nn}}/k_B T = K_{\text{nn}}$ for the nearest-neighbor coupling here to emphasize that one may allow for further-neighbor interactions as well [42]], where both even and odd powers can occur. Thus

$$\frac{\partial^2 f}{\partial H^2} = f^{(2)}\left(\frac{\partial h}{\partial H}\right)^2, \quad \frac{\partial^4 f}{\partial H^4} = f^{(4)}\left(\frac{\partial h}{\partial H}\right)^4 + 4f^{(2)}\left(\frac{\partial h}{\partial H}\right)\left(\frac{\partial^3 h}{\partial H^3}\right) \ . \tag{2.62}$$

Both the analytic term in Eq. (2.60) and the second term on the right-hand side of the above expression for $\partial^4 f/\partial H^4$ give rise to corrections to scaling. We now use Eqs. (2.59)–(2.62) to derive a systematic expansion of $Q_L = \langle m^2 \rangle^2/\langle m^4 \rangle$ in powers of t and u (or $K_{\text{nn}} - K_c$ and u, respectively). After some algebra, the result is, for the limit where t is small and L large but finite [42],

$$Q_L(K_{\text{nn}}) = Q + a_1(K_{\text{nn}} - K_c)L^{1/v} + a_2(K_{\text{nn}} - K_c)^2L^{2/v} + a_3(K_{\text{nn}} - K_c)^3L^{3/v} + \cdots$$
$$+ b_1L^{-\omega} + b_2L^{-d+2\beta/v} + \cdots \ , \tag{2.63}$$

where Q is a universal constant, whereas the expansion coefficients $a_1, a_2, a_3, \ldots$ and $b_1, b_2, \ldots$ are nonuniversal. The powers of the geometric factor $\partial h/\partial H$ have canceled in the first term on the right-hand side of Eq. (2.63) and the last term results from the analytic background term in Eq. (2.60). The corrections resulting from Eq. (2.62) are decaying even more rapidly with L and have been omitted.

The magnetic susceptibility $\chi = L^d\langle m^2 \rangle/k_B T$ becomes [42]

$$k_B T\chi = g^{(2)}(t) + L^{2y_h - d}f_{\text{sing}}^{(2)}(L^{y_t}t,0,L^{-\omega}u,1) \ , \tag{2.64}$$

which yields upon expansion in t and u

$$k_B T\chi = c_0 + c_1(K_{\text{nn}} - K_c) + \cdots$$
$$+ L^{\gamma/v}[a_0 + a_1(K_{\text{nn}} - K_c)L^{1/v} + a_2(K_{\text{nn}} - K_c)^2L^{2/v} + \cdots + b_1L^{-\omega} + \cdots] \ , \tag{2.65}$$

where the a_i, b_i and c_i are nonuniversal coefficients, different from those used in (2.63). Similar expansions can be derived from Eq. (2.60) for $k = 0$ to obtain both the energy and the specific heat

[42]. Extending the treatment to include local fields H_0, H_r that couple to spins at positions 0 and **r**, the spin–spin correlation function $G(r)$ [Eq. (2.51)] can be included in this treatment as well, and also expansions for the temperature derivatives of χ and Q can be derived in the same way [42]. The strategy is then to obtain very precise data for a broad range of sizes ($3 \leq L \leq 40$ was studied by Blöte et al. [42] for the short-range Ising model in $d = 3$ dimensions) and all these quantities. Each quantity is fitted independently, using K_c, the critical exponents and the nonuniversal constants as fit parameters. In order to avoid ambiguities with these fitting procedures, it is advisable to proceed in steps, using the values of the critical exponents from field-theoretic renormalization [20] as initial guesses to obtain a good first estimate of K_c. This result is then used as input in an analysis where one tries to obtain the critical exponents from the fit, and thus the fitting procedures can be iterated. In a final stage, one can also keep a subset of the exponents fixed to fit the remaining ones, etc., and apply many consistency checks. The outcome of such an analysis will be described in the next section. As emphasized above, we have assumed the validity of hyperscaling throughout, and thus hyperscaling is implicit in the expansions Eqs. (2.63) and (2.65) on which the analysis of the next section is based. However, we shall discuss the necessary modification of this treatment in Section 4, where we consider Ising models in more than four dimensions, where hyperscaling is violated. Also the extension of finite-size scaling to properly describe the crossover from one universality class to another one will be described only in the context where this is needed to understand the crossover between the Ising universality class and the mean-field universality class (Section 5).

Even for the short-range Ising model in $d = 3$ dimensions, our discussion of the use of finite-size scaling has been far from exhaustive: we have not discussed deviations from finite-size scaling predicted to occur in the limit $L \to \infty$ at fixed $\xi < \infty$ [97]. If one considers the relative difference between a quantity in the thermodynamic limit (such as the susceptibility χ) and its counterpart in the finite system, $\chi_L = L^d \langle m^2 \rangle_L / k_B T$,

$$\Delta \equiv (\chi - \chi_L)/\chi = \Delta(\xi, L) , \qquad (2.66)$$

it is argued that, in the limit $L \to \infty$ at fixed ξ, Δ is not in accord with finite-size scaling [which would imply that $\Delta(\xi, L)$ only depends on ξ/L]. However, since the scale for this deviation from finite-size scaling is very small [of the order of $\exp(-L/\xi)$ which is negligible in the considered limit], this problem is presumably not a practical limitation on finite-size scaling analyses of critical phenomena.

We also do not address the approach of numerically computing finite-size scaling functions [216–218,220], where one attempts to construct ratios such as χ_L/χ as function of L/ξ_L, ξ_L being derived from Eq. (2.52). It has been suggested that this type of finite-size scaling works already for small values of L and that no a priori information on the critical behavior of the system is required. This procedure would test finite-size scaling itself by means of the resulting data collapse. The extrapolated results for χ, ξ, etc. can be fitted straightforwardly to power laws in order to extract the critical exponents. Although the results of this approach so far look quite encouraging [220], we feel there is a need to worry about the effects of the various corrections to scaling, that are possibly masked in this approach, leading to systematic deviations in the estimates of critical properties. Thus, even for the short-range Ising model in $d = 3$ the finite-size scaling analysis of critical phenomena is still an active topic of research.

Table 2
The critical coupling of the nearest-neighbor simple cubic Ising lattice

K_c	0.221655 (5)	0.221620 (6)	0.221663 (9)	0.2216544 (3)	0.221660 (4)
Reference and year	[56] 1983	[58] 1989	[261] 1997	[262] 1998	[263] 1998
Method			High-temperature series extrapolation		
K_c	0.221654 (6)	0.221652 (6)	0.221652 (3)	0.221655 (1)	
Reference and year	[60] 184	[264] 1989	[61] 1992	[62] 1996	
Method			Monte Carlo renormalization group		
K_c	0.2216595 (26)	0.2216544 (10)	0.221657 (3)	0.221648 (4)	0.2216576 (22)
Reference and year	[39] 1991	[38] 1991	[265] 1991	[40] 1993	[41] 1994
Method			Monte Carlo (MC) and finite-size scaling		
K_c	0.2216546 (10)	0.2216544 (6)	0.221655 (15)	0.221655 (1)	0.2216546 (10)
Reference and year	[42] 1995	[43] 1996	[220] 1996	[62] 1996	[266] 1998
Method			Monte Carlo (MC) and finite-size scaling (FSS)		

3. Results for the critical behavior of the three-dimensional Ising model with short-range interactions

In this section we summarize the results that were obtained in the last decade for various critical properties of the Ising model. Table 2 quotes estimates for the critical coupling K_c of the nearest-neighbor model (some of the exponent estimates have also been obtained for models including next-nearest and 3rd nearest-neighbor interactions, in an attempt to reduce corrections to scaling [42,63]; these results are not included here). It now appears well established that the critical point occurs at

$$K_c = 0.221655\ (5) \tag{3.1}$$

which was already suggested from high-temperature series extrapolations as early as 1983 [56]. However, among the attempts to narrow down the error bar of this estimate, the method of high-temperature series extrapolation [58,261–263] seems to be rather inconclusive, as is shown by a comparison of the more recent estimates obtained by this technique. Thus, if we ignore this method and rely exclusively on MCRG [60–62,264] and MC [38–43,265,266] estimates, we see that it is rather certain that

$$K_c = 0.221655\ (2)\ . \tag{3.2}$$

This refined estimate still barely excludes the Rosengren conjecture [267]

$$\tanh(K_c) = (\sqrt{5} - 2)\cos(\pi/8), \quad \text{i.e., } K_c = 0.22165863 \dots\ . \tag{3.3}$$

On the other hand, there are strong theoretical arguments against Eq. (3.3) [268].
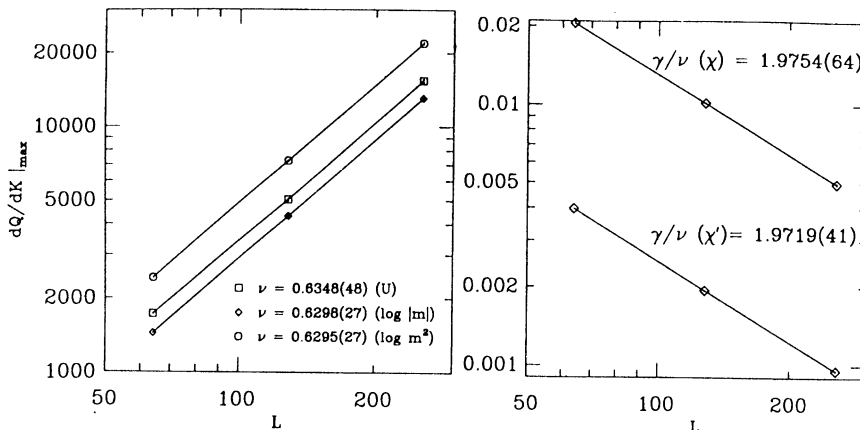
Fig. 4. Log–log plot of derivatives $dQ/dK|_{max}$ of several quantities Q, namely $Q = -3U$, $Q = \ln\langle|m|\rangle$ and $Q = \ln\langle m^2\rangle$, vs. L (Q is here not to be confused with the amplitude ratio it generally indicates). Corresponding estimates for ν are quoted in the figure (left). Log–log plot of $\langle m^2\rangle$ at $K = K_c = 0.221655$ vs. L (curve labeled χ (right), curve labeled χ' refers to $\langle m^2\rangle - \langle|m|\rangle^2$). From Gupta and Tamayo [62].

Having established the location of the critical point with a satisfactory accuracy, one can proceed to estimate the critical exponents. Often, fits are carried out where K_c is kept fixed. Different choices for K_c create different biases for the resulting exponent estimates; unfortunately the quoted uncertainties do not always reflect the effect of this bias.

As indicated in Section 2.3, different strategies can be applied with respect to the treatment of corrections to scaling: one, naive, strategy is to choose in a finite-size scaling analysis the range of linear dimensions L sufficiently large and simply fit the Monte Carlo data at T_c to the power laws in Eq. (2.46) that yield β/ν and γ/ν. Corresponding data for temperature derivatives at T_c

$$dU/dK|_{K=K_c} \propto d\ln\langle|m|\rangle/dK|_{K_c} \propto d\ln\langle m^2\rangle/dK|_{K_c} \propto L^{1/\nu}, \quad L \to \infty \,, \tag{3.4}$$

are fitted to obtain $1/\nu$. To avoid the bias from the choice of K_c one can also use the corresponding derivative at the value $K = K_m$ where the derivative is maximal (Fig. 4). The second strategy is to also include smaller values of L in the analysis and not just rely on the leading power laws [Eqs. (2.46) and (3.4)] but rather include corrections to finite-size scaling in the fit, applying expansions such as Eqs. (2.63) and (2.65). Table 3 summarizes the corresponding results, again comparing the outcome of different methods. We have put the results stemming from field-theoretic renormaliz-ation-group methods [53,55] at the top of the table: over the last twenty years, these results have not been questioned, and even in the light of all the additional work summarized in this table, there is no good reason to question the accuracy of the estimates obtained by Zinn-Justin et al. [53,55].

In contrast, the estimates obtained both from extrapolation of high-temperature series [56,57,261–263,269–271] and from Monte Carlo-based methods [39,42,60–63,220,222,223, 264,266,272] are more varying, although they now both appear to have reached a level that is comparable in accuracy. In some cases the table includes entries where the error has not been given(!), and in some cases extremely small error estimates are quoted – these estimates seem overly optimistic to us, however: We feel that both high-temperature series extrapolations and

Table 3
Estimates for the exponents $y_t = 1/\nu$, $y_h = 3 - \beta/\nu$ and ω

Method	Ref.	Year	y_t	y_h	ω
Field-theoretic	[53]	1980	1.587 (4)	2.485 (2)	0.79 (3)
renormalization group	[55]	1998	1.586 (3)	2.483 (2)	0.799 (11)
High-temperature	[333]	1981	1.585 (8)	2.482 (5)	
series extrapolation	[334]	1981	1.586 (4)	2.482 (3)	0.90 (11)
	[56]	1983	1.585 (10)	2.482 (6)	
	[269]	1985	1.5823 (25)	2.4806 (15)	0.85 (8)
	[270]	1987	1.582 (7)	2.480 (6)	
	[271]	1990	1.587 (4)	2.4821 (4)	0.83 (5)
	[57]	1991	1.587	2.4823	0.84
	[261]	1997	1.577 (5)	2.481 (5)	
	[262]	1998	1.5835 (20)	2.4808 (20)	
	[263]	1998	1.587 (12)	2.483 (6)	
CAM	[64]	1995	1.586 (4)	2.482 (4)	
MCRG	[60]	1984	1.590 (10)	2.485 (3)	
	[264]	1989	1.590 (8)	2.4865 (25)	
	[61]	1992	1.602 (5)	2.4870 (15)	0.825 (25)
	[62]	1996	1.600 (3)	2.488 (3)	0.7
	[63]	1996	1.585 (3)	2.481 (1)	
MC	[39]	1991	1.590 (2)	2.4914 (28)	
FSS	[41]	1994	1.590 (2)	2.482 (7)	
	[42]	1995	1.587 (2)	2.4815 (15)	0.82 (6)
	[62]	1996	1.585 (7)	2.487 (3)	
	[220]	1996	1.558	2.465	
	[44]	1997	1.585 (3)		
	[266]	1999	1.5865 (14)	2.4815 (4)	0.82
	[223]	1999	1.5883 (5)	2.4821 (2)	0.845 (10)
	[222]	1999	1.5878 (13)	2.4817 (4)	
	[272]	1999	1.5888 (12)	2.4821 (5)	0.87 (4)

Monte Carlo methods at this point have reached an accuracy that is competitive with the accuracy of field-theoretic renormalization-group results for the Ising model, but it would be premature to claim that the accuracy already is much better. Thus, in our opinion it is rather certain that the exponent estimates that follow from Monte Carlo analysis can be summarized as

$$y_t = 1.588\ (2), \quad y_h = 2.482\ (2), \quad \omega = 0.83\ (4) , \tag{3.5}$$

well consistent with the estimates of [53,55]. It remains to be seen whether the high accuracy claimed in very recent work [222,223,266,272] can be maintained. We also note that some rather recent estimates [220] fall well outside the range of Eq. (3.5), but these estimates were obtained from fits of extrapolated bulk data over a fairly extended range in the reduced temperature t, and no corrections to scaling terms were allowed for. Thus, these estimates (which deliberately did not quote any estimates for the error) really should be discarded, and we have included them in

Table 3 just for the sake of completeness of the historical record. Some other estimates included in Table 3 were not taken from simulations of the Ising model but rather from the ϕ^4 model on the simple cubic lattice [222,223]; at this point we rely on the hypothesis that the Ising model (with discrete spins $S_i = \pm 1$) and the ϕ^4 model (with continuous degrees of freedom $-\infty < \phi_i < \infty$) do belong to the same universality class.

Some of the studies mentioned above have attempted to extract more than two exponents (y_t and y_h or ν and η, respectively) from the finite-size scaling analysis (e.g., one can obtain γ/ν and β/ν independently, or one can try to estimate $(1-\alpha)/\nu$ from the critical part of the energy, etc.). By means of such analyses, both the hyperscaling relation ($\gamma/\nu + 2\beta/\nu = d$) and the thermodynamic scaling relation ($\gamma + 2\beta = 2 - \alpha$) can be tested. Within the quoted accuracy of the various studies, the scaling relations always were found to be fulfilled rather convincingly. For details of these studies we refer the interested reader to the original publications quoted in Table 3.

Other critical properties of the Ising model have also been estimated occasionally, such as the finite-size scaling invariant $Q = \langle m^2 \rangle^2 / \langle m^4 \rangle$ at $K = K_c$. While early estimates [39] only reached a relatively modest accuracy, $Q \approx 0.63$ (1), Blöte et al. [42] obtained the rather precise estimate $Q = 0.6233$ (4) and this result was even more refined by Blöte et al. [266], $Q = 0.62358$ (15), while Ballesteros et al. [272] obtained $Q = 0.6238$ (4) and Hasenbusch et al. [222] found $Q = 0.62393$ (13).

The related renormalized coupling constant g_R^∞, defined by

$$g_R^\infty = \lim_{K \to K_c} \lim_{L \to \infty} \left(\frac{L}{\xi}\right)^d [3 - \langle m^4 \rangle / \langle m^2 \rangle^2] \tag{3.6}$$

has also received considerable attention in the literature [219,221,262,273–275]. Estimates from field-theoretic calculations [275] yielded $g_R = 23.73$ (2), while series expansions gave $g_R = 23.69$ (10) [273] or $g_R = 23.55$ (15) [274]. While originally it was concluded [219] that Monte Carlo results strongly disagree with these estimates, Ballesteros et al. [221] have presented new data that are compatible with these estimates, though not really accurate! The problem is complicated, because $g_R(L,K)$ approaches its limiting behavior nonuniformly, i.e., g_R^∞ differs from the quantity $\tilde{g}_R$ obtained by taking the limits in Eq. (3.6) in the reverse order: $\tilde{g}_R = 5.25$ (3) [221].

There is also a considerable interest in precisely estimating the (nonuniversal) critical amplitudes of various quantities, in order to find results for the universal critical amplitude ratios [213]. While such critical amplitude ratios have been estimated both by field-theoretic renormalization-group methods [55] and by high-temperature series expansions [58,213], recent Monte Carlo estimates of these quantities are comparably scarce [276–278]. We define the critical amplitudes of the specific heat C, the correlation length ξ, the susceptibility χ, the order parameter $\langle |m| \rangle$, the singular part of the free energy f_{sing} and the surface tension σ as follows [213]:

$$C = (A^\pm/\alpha)|t|^{-\alpha}, \quad \langle |m| \rangle = B(-t)^\beta, \quad \chi = \Gamma^\pm |t|^{-\gamma}, \quad \xi = \xi_0^\pm |t|^{-\nu}, \tag{3.7}$$

$$f_{\text{sing}} = f_0^\pm |t|^{2-\alpha}, \quad \sigma = \sigma_0(-t)^{2-\alpha-\nu}. \tag{3.8}$$

Two-scale factor universality [279] implies that all of the following combinations of these amplitudes are universal

$$A^+/A^-, \quad \Gamma^+/\Gamma^-, \quad R_C = A^+\Gamma^+/B^2, \quad \xi_0^+/\xi_0^-, \quad R_\xi^+ = (A^+)^{1/d}\xi_0^+,$$

$$(\xi_0^+)^d f_0^+, \quad (\xi_0^-)^d f_0^-, \quad f_0^+/f_0^-, \quad r_{\sigma\xi} = \sigma_0(\xi_0^+)^{d-1} \quad \omega = [4\pi\sigma_0(\xi_0^-)^{d-1}]^{-1}. \tag{3.9}$$

Table 4
Selected critical amplitude values for the $d = 3$ Ising model

Quantity	ε-expansion	Field-theoretic RG in $d = 3$	High-T/Low-T series	Monte Carlo
A^+/A^-	$\begin{cases} 0.524 \pm 0.010 \text{ [280]} \\ 0.527 \pm 0.037 \text{ [55]} \end{cases}$	$\begin{cases} 0.541 \pm 0.014 \text{ [280]} \\ 0.537 \pm 0.019 \text{ [55]} \end{cases}$	0.523 ± 0.009 [58]	0.550 ± 0.012 [276]
Γ^+/Γ^-	$\begin{cases} 4.9 \text{ [280]} \\ 4.73 \pm 0.16 \text{ [55]} \end{cases}$	$\begin{cases} 4.77 \pm 0.30 \text{ [280]} \\ 4.79 \pm 0.10 \text{ [55]} \end{cases}$	4.95 ± 0.15 [58]	$\begin{cases} 4.75 \pm 0.03 \text{ [277]} \\ 5.18 \pm 0.33 \text{ [283]} \end{cases}$
ξ_0^+/ξ_0^-	1.91 [281]	2.013 ± 0.028 [282]	1.96 ± 0.01 [58]	$\begin{cases} 2.06 \pm 0.01 \text{ [283]} \\ 1.95 \pm 0.02 \text{ [277]} \end{cases}$
$3\Gamma^-/[(\xi_0^-)^3 B^2]$		14.4 ± 0.2 [282]	14.8 ± 1.0 [58]	$\begin{cases} 17.1 \pm 1.9 \text{ [283]} \\ 14.3 \pm 0.1 \text{ [277]} \end{cases}$
$\Gamma^+/[(\xi_0^+)^3 B^2]$		3.02 ± 0.08 [280]	3.09 ± 0.08 [58]	$\begin{cases} 3.36 \pm 0.23 \text{ [283]} \\ 3.05 \pm 0.05 \text{ [277]} \end{cases}$
R_ξ^+	0.27 [280]	0.2700 ± 0.0007	0.2659 ± 0.0007 [58]	
$f_0^+(\xi_0^+)^3$				0.0355 ± 0.0015 [277]
$R_{\sigma\xi}$	0.2 [284]	0.39 ± 0.03 [285]	0.36 ± 0.01 [286]	0.34 ± 0.02 [278]
ω	1.5 [284]		0.86 [288]	$\begin{cases} 1.2 \pm 0.3 \text{ [287]} \\ 0.88 \pm 0.04 \text{ [278]} \end{cases}$

Of course, not all of these ratios are independent: e.g., f_0^+/f_0^- and A^+/A^- are obviously related as the specific heat is the second temperature derivative of the free energy and from ξ_0^+/ξ_0^- and $R_{\sigma\xi}$ one can easily obtain ω (which should not be confused with the leading irrelevant exponent). Nevertheless, we want to mention these combinations, because they are commonly used in the literature. Many more universal amplitude ratios come into play if one considers the dependence of various quantities on the magnetic field at $t = 0$ [213]. However, we are not aware that this problem has found much attention from simulations recently – some more work in this direction would be desirable!

Table 4 summarizes some of the predictions on the ratios defined in Eq. (3.9) that can be found in the literature [55,58,276–288]. The accuracy of early estimates for these quantities was often overestimated, and even the most recent results for these ratios are much less accurate than these for the corresponding exponents. Also here, more work on these quantities would clearly be desirable.

4. The nearest-neighbor Ising model in $d=5$ dimensions

4.1. A brief review of the pertinent theory

One of the basic results of renormalization-group theory [10–22] is that, for systems with short-range interactions, nonclassical critical exponents only occur for $d < 4$ dimensions, while for

$d > 4$ the "classical" exponents of simple Landau theory apply. The case $d = 4$ itself is a borderline case, where logarithmic corrections to the classical power laws are present. A test of this case with Monte Carlo simulations is fairly involved [289] and will remain out of consideration here. However, the situation in $d = 5$ should be much simpler and Monte Carlo simulations for this case should provide a good testing ground to check whether our current theoretical understanding of systems above their upper critical dimensionality is in fact complete. While obviously no laboratory experiment can be carried out in $d = 5$ spatial dimensions, the study of such high (but integer[1]) [290] dimensions is in fact straightforward by means of simulational techniques.

We start by reviewing the adaption of the theory of finite-size scaling to this case [72–74]. Using the fact that for $d > d^* = 4$ we have the Landau values for the exponents y_t, y_h and the (leading) correction to scaling exponent ω,

$$y_t = 2, \quad y_h = 1 + d/2, \quad \omega = d - 4 , \tag{4.1}$$

the singular part of the free-energy density f_L of a finite system with linear dimensions L in a external field h is written as [cf. Eq. (2.58) for $b = L$] [71]

$$f_L(t, h, L) = L^{-d} \tilde{f} \left\{ t \left(\frac{L}{\xi_0^+} \right)^2, hL^{1+d/2}, uL^{4-d} \right\} . \tag{4.2}$$

Here we have used the mean-field result $\xi = \xi_0^+ t^{-1/2}$ (for $t > 0$) and scaled the length L with the length ξ_0^+ to make the first argument of $\tilde{f}$ dimensionless [and to remind the reader of the finite-size scaling principle that this term simply can be interpreted as $(L/\xi)^2$].

Now an important issue is that although $(-\omega) = 4 - d$ for $d > 4$ is negative and hence $uL^{4-d} \to 0$ for $L \to \infty$, one nevertheless may not omit the last term, because u is a "dangerous irrelevant variable" [291,292]. This statement means that the scaling function $\tilde{f}(x, x', y)$ is singular in the limit $y \to 0$ and cannot be simply replaced by $f(x, x', 0)$. Also the variable y is normalized such that it is dimensionless, and this is borne out by our notation by writing $u \propto \ell_0^{d-4}$, where ℓ_0 is another (microscopic) length, so that $y = (L/\ell_0)^{4-d}$. For brevity we will henceforth simply write ξ_0 instead of ξ_0^+.

Taking suitable derivatives of Eq. (4.2) with respect to the field h we can write for the order parameter $\langle |m| \rangle$, the (high-temperature) susceptibility χ and the ratio Q (in zero field)

$$\langle |m| \rangle = L^{-(d-2)/2} P_m \{ t(L/\xi_0)^2, (L/\ell_0)^{4-d} \} , \tag{4.3}$$

$$k_B T \chi = -(\partial^2 f_L/\partial h^2)_T = L^d \langle m^2 \rangle = L^2 P_\chi \{ t(L/\xi_0)^2, (L/\ell_0)^{4-d} \} \tag{4.4}$$

and

$$Q = \langle m^2 \rangle^2 / \langle m^4 \rangle = P_Q \{ t(L/\xi_0)^2, (L/\ell_0)^{4-d} \} , \tag{4.5}$$

where P_m, P_χ and P_Q are the (universal [293]) finite-size scaling functions of the quantities $\langle |m| \rangle$, χ and Q. The question how these functions behave in the limit $y \to 0$ was first addressed in [72],

---

[1] Preliminary data have also been obtained for the case $d = 6$.

where it was assumed that the dangerous irrelevant variable y enters in the form of multiplicative singular powers of y, e.g.,

$$f_L(x, x', y) \approx y^{p_3} \tilde{f}_L(xy^{p_1}, x'y^{p_2}) \quad \text{as } y \to 0 \;, \tag{4.6}$$

with p_1, p_2 and p_3 suitable exponents [72]. This assumption was in the first place motivated by the fact that this is the mechanism that operates for the scaling in the bulk for $d > 4$ [292]. In addition, Eq. (4.6) is supported by various phenomenological arguments. In particular, it was argued [72,73] that standard thermodynamic fluctuation theory requires, for $T < T_c$ and sufficiently large L, that the distribution function $P_L(m)$ of the magnetization per spin for m near the spontaneous magnetization $\pm m_{sp}$ can be written as a sum of two Gaussians [cf. Eq. (2.13)]. Using $m_{sp} = B(-t)^{1/2}$ and $\chi' = \Gamma^-(-t)^{-1}$ the arguments of the exponential functions in Eq. (2.13) have the form

$$-\frac{1}{2}[(m/B)(-t)^{-1/2} \mp 1]^2 (L/\ell_T)^d \;, \tag{4.7}$$

where the "thermodynamic length" ℓ_T is defined as

$$\ell_T = [m_{sp}^{-2} \chi']^{1/d} = (B^{-2} \Gamma^-)^{1/d}(-t)^{-2/d} \;. \tag{4.8}$$

Taking moments of $P_L(m)$ it was then concluded that the scaling functions P_m, P_χ and P_Q in Eqs. (4.3)–(4.5) should reduce to scaling functions of a single variable

$$(L/\ell_T)^{d/2} = tL^{d/2}\xi_0^{-2}\ell_0^{(4-d)/2} = x/\sqrt{y} \;, \tag{4.9}$$

$$\langle |m| \rangle = L^{-d/4} \tilde{P}_m(tL^{d/2}\xi_0^{-2}\ell_0^{(4-d)/2}) \;, \tag{4.10}$$

$$\chi = L^{d/2} \tilde{P}_\chi(tL^{d/2}\xi_0^{-2}\ell_0^{(4-d)/2}) \tag{4.11}$$

and

$$Q = \tilde{P}_Q(tL^{d/2}\xi_0^{-2}\ell_0^{(4-d)/2}) \;. \tag{4.12}$$

Scale factors for the magnetization and the susceptibility have been absorbed in P_m (or $\tilde{P}_m$) and P_χ (or $\tilde{P}_\chi$), respectively, while in ratios like Q (and hence in P_Q and $\tilde{P}_Q$) such scale factors cancel out and fully universal scaling functions remain.

   While these arguments did not yield explicit expressions for the scaling functions, Brézin and Zinn-Justin [74] did propose such an explicit form, suggesting that for $d > d^* = 4$ one could split the argument of the Boltzmann factor into a contribution due to the uniform magnetization (the "zero mode") and contributions of nonuniform magnetization fluctuations, which can be treated perturbatively. Thus

$$\exp\left[-\frac{\mathscr{H}\{S_i\}}{k_B T} \right] = \exp\left\{ -\frac{(m^2/m_{sp}^2 - 1)^2}{8k_B T \chi'/m_{sp}^2} L^d + \text{fluctuation contributions} \right\} \;. \tag{4.13}$$

The fluctuation contributions were argued to yield only a shift of T_c,

$$T_c(L)/T_c(\infty) - 1 \propto L^{2-d} \;, \tag{4.14}$$

which is of higher order than the rounding of the singularities [scaling like $L^{-d/2}$, cf. Eq. (4.10)–(4.12)] and hence negligible in the limit of large L, compared to the finite-size effects

included in Eqs. (4.10)–(4.12). If the fluctuation contributions in Eq. (4.13) are ignored completely, this so-called "zero-mode theory" yields an explicit result for the distribution function of the magnetization,

$$P_L(m) \propto L^{d/2} \exp\{ - [m^2/(B^2 t) - 1]^2 (L/\ell_T)^d/8 \} \,. \tag{4.15}$$

From this result it is straightforward to obtain $\tilde{P}_m$, $\tilde{P}_\chi$ and $\tilde{P}_Q$. In particular, one derives the universal constant at T_c [74]

$$Q|_{T_c} = \tilde{P}_Q(0) = 8\pi^2/\Gamma^4(1/4) \approx 0.456947 \,. \tag{4.16}$$

This treatment has recently been criticized by Chen and Dohm [93–95] who presented detailed arguments that for $d > d^*$ the standard treatment of the ϕ^4 field theory in continuous space yields a misleading description of the finite-size behavior, being different from the finite-size behavior of a ϕ^4 model on a lattice, which is believed to be equivalent to an Ising Model [10–22]. Chen and Dohm emphasized that therefore the justification given for the zero-mode theory is invalid and stated that the moment ratio mentioned above does not have the universal properties predicted previously [94]. Their analysis is based on the ϕ^4-model on a (hyper)cubic lattice,

$$\mathcal{H} = \sum_i \left[\frac{r_0}{2} \phi_i^2 + u_0 (\phi_i^2)^2 \right] + \sum_{i,j} \frac{J_{ij}}{2} (\phi_i - \phi_j)^2 \,, \tag{4.17}$$

where r_0, u_0 and the J_{ij} are constants, and ϕ_i is an n-component vector. Chen and Dohm have considered both the limit $n \to \infty$, which can be treated exactly, and the case $n = 1$ (which corresponds to the Ising model); the latter, however, is only treated to one-loop order in a perturbation expansion. In terms of the reduced moments

$$\theta_m(Y) = \int_0^\infty d\phi \, \phi^m \exp\left[-\frac{1}{2} Y\phi^2 - \phi^4 \right] \Big/ \int_0^\infty d\phi \exp\left[-\frac{1}{2} Y\phi^2 - \phi^4 \right] \,, \tag{4.18}$$

the scaling functions $P_\chi(x, y)$ and $P_Q(x, y)$ are written

$$P_\chi(x, y) = \frac{1}{J_0} \frac{\theta_2(Y(x, y))}{\sqrt{y + 36 I_2(\bar{r})y^2}} \,, \tag{4.19}$$

$$P_Q(x, y) = [\theta_2(Y(x, y))]^2/\theta_4(Y(x, y)) \,, \tag{4.20}$$

with $J_0 = \sum_{i,j} J_{ij} (\boldsymbol{r}_i - \boldsymbol{r}_j)/dL^d$ and

$$Y(x, y) = [x - 12y I_1(\bar{r}) - 144 \theta_2(x/\sqrt{y}) I_2(\bar{r}) y^{3/2}]/[\sqrt{y}(1 + 36 I_2(\bar{r})y)^{1/2}] \,. \tag{4.21}$$

Here further abbreviations $\bar{r} \equiv x + 12 \theta_2(x/\sqrt{y})\sqrt{y}$ and

$$I_m(x) = (2\pi)^{-2m} \int_0^\infty dy \, y^{m-1} \exp(-xy/4\pi^2) \left[\left(\frac{\pi}{y} \right)^{d/2} - \left(\sum_{p=-\infty}^{+\infty} e^{-yp^2} \right)^d + 1 \right] \tag{4.22}$$

were introduced.

Eqs. (4.18)–(4.22) are the first results for the scaling functions P_χ and P_Q that contain the dependence on both variables $x = tL^2\xi_0^{-2}$ and $y = (L/\ell_0)^{4-d}$ separately and explicitly. However, at the same time these results do confirm the validity of the "zero-mode" results, such as

Eqs. (4.10)–(4.12) and (4.16), in the limit of large enough L (when $y \to 0$). This is obvious from Eq. (4.21), since for $y \to 0$ we find

$$Y(x,y) \to x/\sqrt{y}, \quad P_\chi(x,y) = (J_0\sqrt{y})^{-1}\theta_2(x/\sqrt{y}), \quad P_Q = [\theta_2(x/\sqrt{y})]^2/\theta_4(x/\sqrt{y}), \qquad (4.23)$$

fully compatible with Eqs. (4.9)–(4.12) and the results proposed by Brézin and Zinn-Justin [74], including Eq. (4.16).

4.2. Comparison with Monte Carlo results

While already in early Monte Carlo work it was claimed from very small linear dimensions, $L = 3$ to 7 [72,73], that the data agree with the scaling structure of Eqs. (4.10)–(4.12), there seemed to occur a discrepancy with Eq. (4.16) and this discrepancy was confirmed in later work using somewhat larger sizes ($L \leq 15$) [98]. In contrast, it was then shown in Ref. [99] for a completely different class of models, which are however expected to be described by the same renormalization-group equations as high-dimensional Ising models, that Eq. (4.16) holds to a very high accuracy, for a wide range of distances to the upper critical dimension. It was also demonstrated how the findings of Ref. [98] could be traced back to the neglect of certain corrections to scaling and an insufficient statistical accuracy. Nevertheless, several additional attempt were undertaken to clarify matters by more extensive simulations of the five-dimensional Ising model itself [100–104] and it is fair to say that on the simulational side there no longer exists any discrepancy regarding the value of the parameter Q at criticality. On the analytical side, however, matters appear to be less clear, in particular regarding the shape of the finite-size scaling functions [93–95]. Here we shall describe the approach taken in the most recent analysis [104] where a comparison with both the "zero-mode" results [74] and the alternative expressions, Eqs. (4.18)–(4.22), was made.

Fig. 5 shows that if one studies the variation of Q over a wide range ($0.3 \lesssim Q \lesssim 1$) and uses a correspondingly wide range of the scaling variable $tL^{5/2}$, $-4 \leq tL^{5/2} \leq +4$, the data suggest that already for these relatively limited system sizes the scaling prediction, Eq. (4.12) is a reasonable approximation, although there are still slight deviations. The accuracy of the currently available data is such that statistical scatter and systematic deviations can be clearly distinguished. This allows a closer look at the behavior of the amplitude ratio in the neighborhood of T_c, revealing how the deviations found in Refs. [72,73] and also in Ref. [98] could come about. For this, we refer to Fig. 6, where only data for Q near $tL^2 = 0$ are included. If corrections to Eq. (4.12) were negligible, we would expect in this plot the three curves for the three values of L to intersect at $tL^2 = 0$ at the critical value of Q (4.16). On the other hand, if corrections to scaling are non-negligible, one would have expected that there is no longer an unique intersection point at all, but a different intersection for each pair of curves, i.e., a behavior qualitatively analogous to Fig. 2. However, what happens instead is that the three curves apparently still have a intersection point, but at a wrong value: this intersection occurs not at $t = 0$, but at a negative value of tL^2, and the value of Q is here correspondingly higher than in Eq. (4.16). Interestingly, the theory of Chen and Dohm [95] qualitatively predicts precisely such a behavior with a spurious "intersection point", although it is clearly not in quantitative agreement with the Monte Carlo data either.
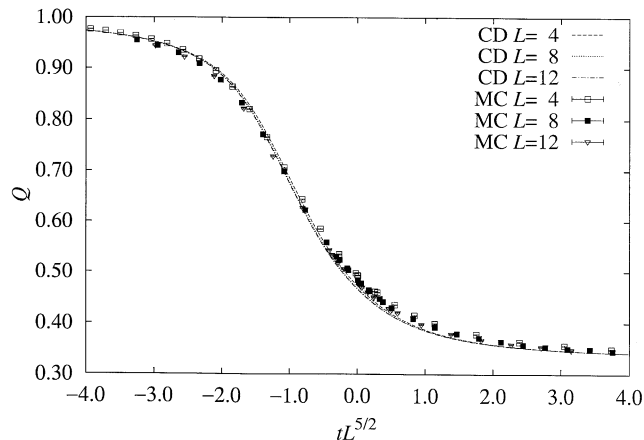
Fig. 5. Plot of $Q = \langle m^2 \rangle^2 / \langle m^4 \rangle$ for the nearest-neighbor Ising model in $d = 5$ dimensions vs. the scaling variable $tL^{5/2}$ [cf. Eq. (4.12)], including both Monte Carlo (MC) data for $L = 4$ [72], $L = 8, 12$ [103] and the results of Chen and Dohm (CD) [95], Eqs. (4.18)–(4.22). Note that the result of the zero-mode theory [74] results from setting $Y = x/\sqrt{y}$ in Eqs. (4.18)–(4.22). The critical temperature was estimated as $J/k_B T_c = 0.1139155$ (2), and the constants ξ_0, ℓ_0 were estimated as $\xi_0 = 0.549$ (2) and $\ell_0 = 0.603$ (13), see the text. From Luijten et al. [104].
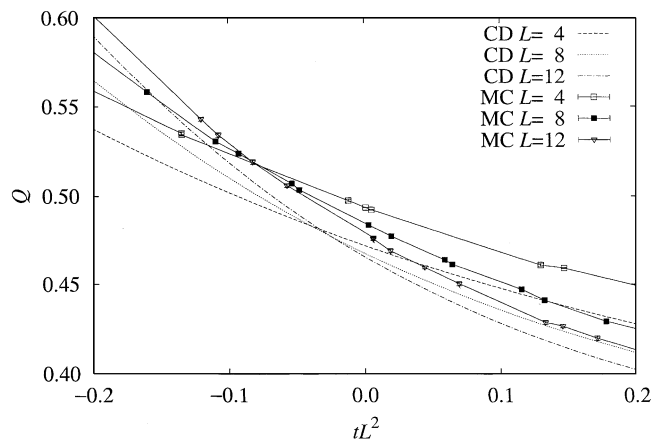
Fig. 6. Magnified plot of Q vs. tL^2 near $tL^2 = 0$, to demonstrate the occurrence of spurious cumulant intersections. Broken curves are again the predictions of Chen and Dohm (CD) [95], Eqs. (4.18)–(4.22), with the parameters as quoted in the caption of Fig. 5, while the symbols indicate the Monte Carlo data. From Luijten et al. [104].

For the comparison between the theory, Eqs. (4.18)–(4.22), and the simulation it is essential to determine the parameters T_c, ξ_0 and ℓ_0 correctly. Using data for χ in the range $5 \le L \le 22$, a finite-size scaling expansion similar to Eq. (2.65) was used [104],

$$\chi = L^{d/2}(c_0 + c_1 \hat{t} L^{y_t^*} + c_2 \hat{t}^2 L^{2y_t^*} + q_1 L^{4-d} + q_2 L^{2(4-d)}) , \qquad (4.24)$$

where $\hat{t}$ is a variable that includes a finite-size shift of T_c,

$$\hat{t} = t + \alpha L^{2-d} , \qquad (4.25)$$
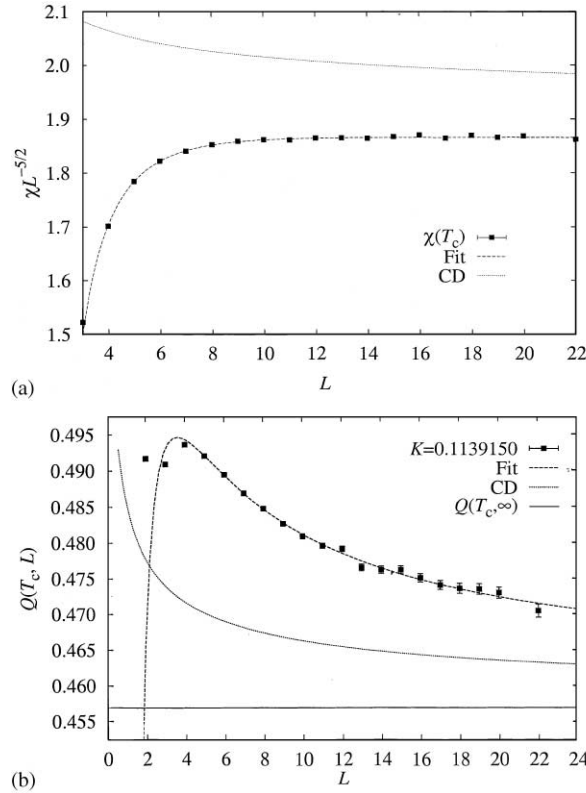
Fig. 7. Plot of (a) $\chi L^{-5/2}$ and (b) Q vs. L at $J/k_B T_c = 0.1139150$. The dashed curve in (a) is the fit according to Eq. (4.24), while the dotted curve is the result of Chen and Dohm [95], Eq. (4.19). In (b) the horizontal straight line highlights the asymptotic value, Eq. (4.16), while the broken curve is a fit of Q according to Eq. (5.28), and the dotted line represents again the result of Chen and Dohm [95], Eq. (4.20). From Luijten et al. [104].

and the parameters c_0, c_1, c_2, q_1, q_2 and α are adjustable constants. In a first step of the fitting procedure, y_t^* was also treated as an adjustable constant, which yielded $y_t^* = 2.53$ (4) and $J/k_B T_c = 0.1139152$ (4). Obviously this result does not indicate any serious problem with the prediction [cf. Eq. (4.9)] $y_t^* = y_t + \omega/2 = 2 + (d-4)/2 = 5/2$. In the second step of the fitting procedure, this exponent was also fixed at its theoretical value, yielding then, in particular, $J/k_B T_c = 0.1139155$ (2) and $c_0 = 1.91$ (2). Using now the asymptotic result following from Eq. (4.19), namely ($J_0 = 2J/k_B T$)

$$\chi = L^{d/2} P_\chi(0,0) = \frac{L^2 \theta_2(0)}{J_0 \sqrt{y}} = \frac{L^{d/2}}{\sqrt{\ell_0} J_0} \frac{\Gamma(3/4)}{\Gamma(1/4)} \ , \tag{4.26}$$

one recognizes that the constant c_0 is directly related to the length ℓ_0, for which one finds (in units of the lattice spacing) $\ell_0 = 0.603$ (13) [104].

The procedure of estimating ℓ_0 is reviewed here in such detail since it has been criticized by Chen and Dohm [95] in a note added to their paper. While we consider this criticism as unfounded, we leave it to the reader to form his own opinion on this apparently controversial issue.[2]

Also the parameter ξ_0 can be extracted from the Monte Carlo data, since in the limit $y \to 0$, at fixed small t, Eqs. (4.4), (4.19) imply

$$\chi t = \frac{\xi_0^2}{J_0} \frac{x}{\sqrt{y + 36 I_2(\bar{r}) y^2}} \theta_2(Y(x,y)) \overset{y \to 0}{\to} \xi_0^2 / J_0 \ . \tag{4.27}$$

Alternatively, in Ref. [104] it was found convenient to use the result from high-temperature series [294] for this purpose, $\chi = A/(1 - v/v_c)$ where $v = \tanh(J/k_B T)$ and $A = 1.311\,(9)$. Rewriting this in terms of t yields $\chi = 1.322 t^{-1}$ and Eq. (4.27) gives $\xi_0 = 0.549\,(2)$.

Having fixed all constants of the theories [Eqs. (4.9)–(4.12) or (4.18)–(4.22), respectively], we show in Fig. 7 the approach of both χ and Q at T_c to their limiting behaviors. For Q an expansion analogous to Eq. (4.24) was used [103]

$$Q(L,t) = \tilde{P}_Q(0) + c_1' \hat{t} L^{d/2} + c_2' \hat{t}^2 L^d + q_1' L^{4-d} + q_2' L^{2(4-d)} \ . \tag{4.28}$$

In addition, analyses have been performed where $Q(\infty, 0)$ was *not* fixed at its theoretical value $\tilde{P}_Q(0)$, Eq. (4.16), but also in this case the results were nicely compatible with Eq. (4.28) [289]. The data show that even for $L = 22$ the data are still far from their asymptotic values, due to strong corrections to the leading finite-size scaling behavior $Q(L,0) = \tilde{P}_Q(0)$ and $\chi L^{-5/2} = c_0$. The theory of Chen and Dohm [95], which is claimed to describe exactly the leading corrections (of order $L^{-1/2}$) to the asymptotic behavior, is not useful in this regime. In particular, for $\chi L^{-5/2}$ it predicts a monotonic decrease toward the asymptotic value, while the Monte Carlo data reach a shallow maximum first and then a decrease in a much less pronounced way (note that, by construction, both curves in Fig. 7b converge to the *same* constant c_0!).

Thus the present state of affairs concerning this model is somewhat disappointing: although one knows all the critical exponents exactly (including those of the correction terms), and even finite-size scaling functions are believed to be known exactly both in the limit $y \to 0$ (where the "zero-mode" results [74] hold) and also beyond it, where nonuniform terms in Eq. (4.13) were computed via perturbation theory in first-order loop expansion for the ϕ^4 model [Eq. (4.17)], there is no explicit understanding of the behavior found in the accessible range of L (Fig. 7). The simulation data are compatible with the approach to "zero-mode" results [74] for $L \to \infty$, but the approach is surprisingly slow, and for the accessible range of L other corrections than those derived by Chen and Dohm [95] are dominant. Luijten et al. [104] have speculated that this discrepancy could be due to the need of including second-order terms in the loop expansion, or that corrections might be present due to the fact that an Ising model only asymptotically agrees with a ϕ^4 model [Eq. (4.17)]. Thus the effects of statistical fluctuations on critical behavior are not even completely clear when ultimately the critical behavior is mean-field like.

---

[2] After submission of the present review, Chen and Dome [335] attempted a reanalysis allowing for an additional amplitude factor $A = 0.678$ (the present treatment means $A \equiv 1$). Thus fitting an additional parameter the discrepancy between their theory and the Monte Carlo results can be reduced.

Table 5
The cutoff distance R_m of the interaction function, the corresponding coordination number q, and the effective range of interaction R for the equivalent-neighbor Ising model in $d = 2$ and $d = 3$ dimensions

	$d = 2$			$d = 3$	
q	R_m^2	R^2	q	R_m^2	R^2
4	1	1	6	1	1
8	2	3/2	18	2	5/3
12	4	7/3	26	3	27/13
20	6	17/5	32	4	39/16
24	8	25/6	56	5	99/28
36	10	6	80	6	171/40
60	18	148/15	92	8	219/46
100	32	81/5	122	9	354/61
160	50	517/20	146	10	474/73
224	72	1007/28	170	11	606/85
316	100	4003/79	178	12	654/89
436	140	7594/109	202	13	810/101
			250	14	1146/125

5. Crossover scaling in Ising systems with large but finite interaction range in $d=2$ and $d=3$ dimensions

5.1. General theory

In this section we consider the Hamiltonian [45–51,92]

$$\mathscr{H}/k_{\mathrm{B}}T = -\sum_i \sum_{j>i} K(\boldsymbol{r}_i - \boldsymbol{r}_j)S_iS_j - h_0\sum_i S_i, \quad S_i = \pm 1 \tag{5.1}$$

with an interaction $K(r)$ defined as

$$K(\boldsymbol{r}) \equiv cR^{-d} \quad r = |\boldsymbol{r}_i - \boldsymbol{r}_j| \le R_m; \quad K(\boldsymbol{r}) = 0 \quad r > R_m \ . \tag{5.2}$$

Here c is a constant, R_m a cutoff distance and the range R of the interaction $K(\boldsymbol{r})$ is defined in terms of its second moment, as usual,

$$R^2 = \frac{\sum'_{j(\neq i)}(\boldsymbol{r}_i - \boldsymbol{r}_j)^2 K(\boldsymbol{r}_i - \boldsymbol{r}_j)}{\sum'_{j(\neq i)} K(\boldsymbol{r}_i - \boldsymbol{r}_j)} = \frac{1}{q}\sum'_{j(\neq i)}|\boldsymbol{r}_i - \boldsymbol{r}_j|^2 \ . \tag{5.3}$$

Here q is the coordination number of this "equivalent-neighbor Ising model" and $\sum'$ indicates that the summation is restricted to $r \le R_m$. For large R_m we have a simple proportionality between R and R_m, $R^2 = R_m^2/2$ ($d = 2$) or $3R_m^2/5$ ($d = 3$), whereas for small R_m there are lattice effects. In Table 5 we have listed the choices of R_m^2 that have been studied [49,92].

For $R \to \infty$ this model crosses over to the trivial mean-field model of a ferromagnet, in which every spin interacts equally with every other spin, and then the simple Weiss molecular field theory becomes exact [9]. However, when R is large but finite one expects that mean-field theory describes
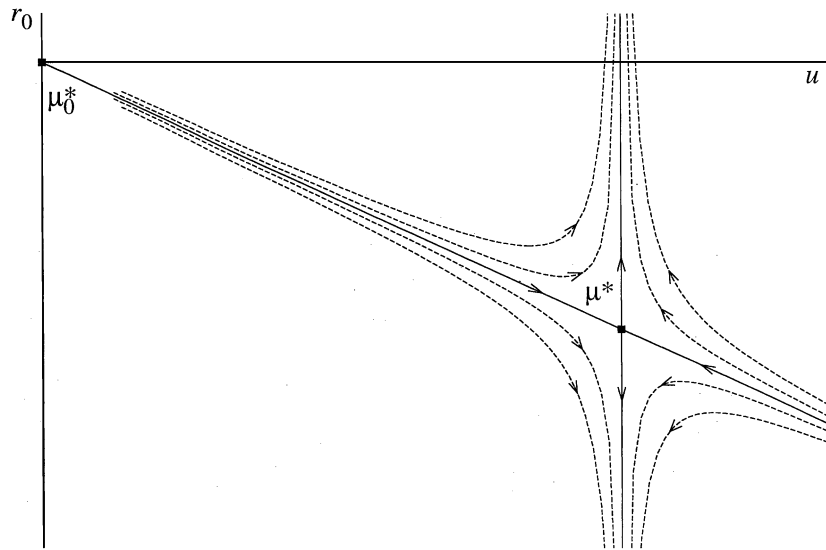
Fig. 8. Qualitative picture of the renormalization trajectory describing the crossover from the Gaussian fixed point $\mu_0^* = (r_0 = 0, u = 0)$ to the Ising fixed point $\mu^* = (r_0^*, u^*)$. From Luijten et al. [92].

the behavior of the model quite well, except in a very narrow neighborhood of the critical point: There ultimately mean-field theory must break down, and a crossover from mean-field critical behavior (critical exponents $\alpha = 0$ [finite jump in the specific heat], $\beta = 1/2$, $\gamma = 1$, $\nu = 1/2$, $\eta = 0$ [8,9,15,16]) to the critical behavior of the "Ising universality class" [13–21] occurs. The analysis of this crossover by means of Monte Carlo simulations is in the focus of the present section.

To analyze this crossover it is instructive to consider the associated Ginzburg–Landau field theory in continuous space [92]

$$\mathcal{H}(\phi)/k_B T = -\int_V d\mathbf{r}\left\{\frac{1}{2}\int_{|r-r'|<R_m} d\mathbf{r}'\left[\frac{c}{R^d}\phi(\mathbf{r})\phi(\mathbf{r}')\right] - \frac{1}{2}v\phi^2(\mathbf{r}) - u_0\phi^4(\mathbf{r}) + h_0\phi(\mathbf{r})\right\}, \quad (5.4)$$

where $\phi(\mathbf{r})$ is the single-component order-parameter field, v is a temperature-like variable, and u_0 is a constant. After Fourier transformation and suitable rescaling of ϕ, this can be rewritten as (remember that $N = L^d$ is the total number of lattice sites)

$$\bar{\mathcal{H}}(\psi_k)/k_B T = \frac{1}{2}\sum_k\left[k^2 + \frac{r_0}{R^2}\right]\psi_k\psi_{-k} + \frac{u}{4R^4N}\sum_{k_1}\sum_{k_2}\sum_{k_3}\psi_{k_1}\psi_{k_2}\psi_{k_3}\psi_{-k_1-k_2-k_3} - \frac{h}{R}\sqrt{\frac{N}{2}}\psi_{k=0}.$$
$$(5.5)$$

See Ref. [92] for a detailed derivation of the relation between the new parameters u, h and the old ones (u_0, h_0). The variable r_0 is proportional to the relative deviation of the temperature from its critical-point value in mean-field theory.

We are interested in identifying the crossover scaling variable associated with the crossover from the Gaussian fixed point $(u = 0, r_0 = 0)$ to the nontrivial fixed point (Fig. 8). Because of the trivial

character of the Gaussian fixed point and the fact that the crossover scaling description should hold all the way from the Ising fixed point to the Gaussian fixed point, one can infer the length scale ℓ_0 exactly,

$$\ell_0 = R^{4/(4-d)} \ . \tag{5.6}$$

This is done by considering a renormalization transformation by a length scale ℓ,

$$k = k\ell, \quad N' = N\ell^{-d}, \quad \psi'_{k'} = \ell^{-1}\psi_k \ . \tag{5.7}$$

Note that Eq. (5.7) was constructed such that the Hamiltonian is left invariant,

$$\bar{\mathscr{H}}'(\psi'_{k'})/k_{\mathrm{B}}T = \frac{1}{2}\sum_{k'}\left[k'^2 + \frac{r_0}{R^2}\ell^2\right]\psi'_{k'}\psi'_{-k'} + \frac{u}{4R^4N'}\ell^{4-d}\sum_{k'_1}\sum_{k'_2}\sum_{k'_3}\psi'_{k'_1}\psi'_{k'_2}\psi'_{k'_3}\psi'_{-k'_1-k'_2-k'_3}$$
$$- \frac{h}{R}\sqrt{\frac{N'}{2}}\ell^{1+d/2}\psi'_{k'=0} \ . \tag{5.8}$$

For $d < 4$, the ψ^4 term grows and the system moves away from the Gaussian fixed point μ_0^* toward the Ising fixed point. The crossover to Ising-like critical behavior occurs when the coefficient of the ψ^4 term is of the same order as the $k^2\psi^2$ term, which is unity: This happens when $\ell = \ell_0$ as given in Eq. (5.6). By comparing the coefficient of the ψ^4 term to that of the $r_0\psi^2$ term, one derives a criterion that states for which temperatures the critical behavior will be Ising-like and for which temperatures it will be classical: actually this is nothing but the well-known Ginzburg criterion [109]! One expects the Gaussian fixed point to dominate the renormalization flow if, irrespective of ℓ, the ψ^4 coefficient is small compared to the temperature coefficient. Thus, one requires the scaled combination $uR^{-4}\ell^{4-d}/(r_0R^{-2}\ell^2)^{(4-d)/2}$ to be small, or, equivalently (see also [87])

$$r_0^{(4-d)/2}R^d/u \gg 1 \ . \tag{5.9}$$

Since the total free energy is conserved along the renormalization trajectory, we can conclude that the singular part of the free-energy density resulting from Eqs. (5.4), (5.5) and (5.8) must satisfy the scaling relation

$$\tilde{f}_{\mathrm{s}}\left(\frac{r_0}{R^2}, \frac{u}{R^4}, \frac{h}{R}\right) = \ell^{-d}\tilde{f}_{\mathrm{s}}\left(\frac{r_0}{R^2}\ell^2, \frac{u}{R^4}\ell^{4-d}, \frac{h}{R}\ell^{1+d/2}\right) \ . \tag{5.10}$$

We see that a finite and nonzero value for the second argument of $\tilde{f}_{\mathrm{s}}$ is retained exactly when ℓ takes the value of the crossover scale ℓ_0. Thus, we conclude from Eq. (5.10) that the singular part of the free energy scales with R as follows:

$$\tilde{f}_{\mathrm{s}} = R^{-4d/(4-d)}\hat{f}_{\mathrm{s}}(\tilde{r}_0 R^{2d/(4-d)}, \tilde{u}, hR^{3d/(4-d)}) \ . \tag{5.11}$$

In Eq. (5.10) we have anticipated that a natural choice of coordinates (Fig. 8) is to measure $\tilde{r}_0$ and $\tilde{u}$ as distances from the Ising fixed point, unlike in the original Hamiltonian, where r_0 and u_0 are distances from the Gaussian fixed point. Eq. (5.11) describes how the temperature distance $\tilde{r}_0$ from criticality and the magnetic field h scale with the range of interaction R: Note that here the crossover exponent is known exactly, unlike for other cases of crossover, such as the crossover between the Ising and Heisenberg universality classes in isotropic magnets with varying uniaxial anisotropy [295]. Obviously, the same result for the crossover exponent follows from

simple-minded arguments using the Ginzburg criterion [87,109]. The location of the nontrivial fixed point μ^* (Fig. 8), the associated critical exponents y_t, y_h, ω and the explicit form of the scaling functions $\tilde{f}_s$ or $\hat{f}_s$, respectively, cannot be obtained exactly. The calculation of these scaling functions (as well as of corresponding scaling functions of free-energy derivatives, e.g. of the susceptibility) remains a nontrivial task for both renormalization-group approaches [110–124] and Monte Carlo calculations [45–50,87], as will be described below. If we carry out a rescaling transformation by a factor b in the neighborhood of the Ising fixed point, the nontrivial exponents y_t, y_h and ω must show up in the transformation as follows:

$$\hat{f}_s = b^{-d} R^{-4d/(4-d)} \hat{f}_s(tR^{2d/(4-d)}b^{y_t}, \tilde{u}b^{-\omega}, hR^{3d/(4-d)}b^{y_h}) , \qquad (5.12)$$

where for simplicity we have replaced the variable $\tilde{r}_0$ by the reduced temperature distance t from the true critical point, suppressing the prefactor in the relation $\tilde{r}_0 \propto t$. From Eq. (5.12), one can derive scaling relations for critical amplitude prefactors of the magnetization, the susceptibility, the specific heat, etc. [87,92], in powers of R. In addition, we can generalize Eq. (5.12) immediately to the case of finite-size scaling, by including ℓ/L in Eq. (5.10) or $\ell_0 b/L = bR^{4/(4-d)}/L$ in Eq. (5.12) as an additional scaling variable. The finite-size scaling behavior is then found by choosing b such that $\ell_0 b/L = 1$, i.e.,

$$b = LR^{-4/(4-d)} . \qquad (5.13)$$

The critical behavior of the magnetization m and the susceptibility χ are then obtained in terms of the first ($\hat{f}_s^{(1)}$) and second ($\hat{f}_2^{(2)}$) derivative of the scaling function $\hat{f}_s$ for the free energy as follows [92]:

$$m = L^{y_h-d} R^{(3d-4y_h)/(4-d)} \hat{f}_s^{(1)} \{tL^{y_t} R^{-2(2y_t-d)/(4-d)}, \tilde{u}L^{-\omega} R^{4\omega/(4-d)}, hL^{y_h} R^{(3d-4y_h)/(4-d)}\} , \qquad (5.14)$$

$$\chi = L^{2y_h-d} R^{2(3d-4y_h)/(4-d)} \hat{f}_s^{(2)} \{tL^{y_t} R^{-2(2y_t-d)/(4-d)}, \tilde{u}L^{-\omega} R^{4\omega/(4-d)}, hL^{y_h} R^{(3d-4y_h)/(4-d)}\} . \qquad (5.15)$$

The finite-size scaling right at T_c ($t=0, h=0$) can then be written as

$$\langle |m| \rangle = L^{y_h-d} R^{(3d-4y_h)/(4-d)} \tilde{m}(LR^{-4/(4-d)}) = L^{-d/4} \check{m}(LR^{-4/(4-d)}) , \qquad (5.16)$$

$$\chi = L^{2y_h-d} R^{2(3d-4y_h)/(4-d)} \tilde{\chi}(LR^{-4/(4-d)}) = L^{d/2} \check{\chi}(LR^{-4/(4-d)}) , \qquad (5.17)$$

and

$$Q = \check{Q}(LR^{-4/(4-d)}) , \qquad (5.18)$$

where $\tilde{m}, \check{m}, \tilde{\chi}, \check{\chi}$ and $\check{Q}$ are suitable scaling functions. Note that these functions have been defined such as to bring out a simple limiting behavior in the respective limits, namely $\tilde{m}$ ($\zeta \to \infty$) = const, $\tilde{\chi}$ ($\zeta \to \infty$) = const, while $\check{m}$ ($\zeta \to 0$) = const, $\check{\chi}$ ($\zeta \to 0$) = const. In the opposite limit the functions then must be simple power laws, which are easily extracted from Eqs. (5.16) and (5.17). On the other hand, the function $\check{Q}$ smoothly interpolates from the constant $\tilde{P}_Q(0)$ [Eq. (4.16)] that is reached for $\zeta \to 0$ to the constant $\check{Q}(\zeta \to \infty)$ which is the respective universal constant Q [Eq. (2.63)] for the corresponding universality class of the short-range Ising model at the respective dimensionality $d < 4$.

5.2. Numerical results for $d = 2$ dimensions

The first task is again the accurate numerical determination of the critical temperature. Note that the straightforward cumulant intersection method (Fig. 2) is not expected to work here, due to the
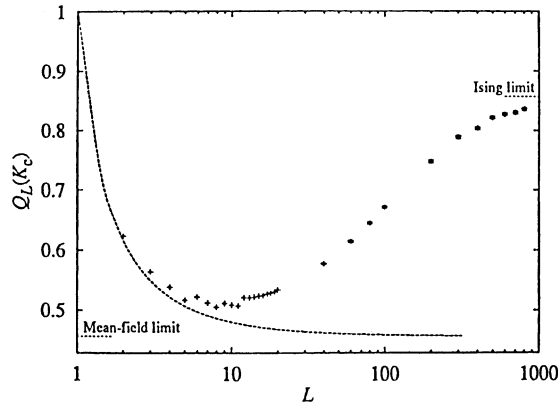
Fig. 9. The amplitude ratio $Q_L(K_c)$ at the critical point of the two-dimensional Ising model with interactions up to $R_m = \sqrt{140}$ as a function of linear system dimension L (discrete points). For large L, $Q_L(K_c)$ approaches the Ising limit $Q = 0.856216$ [296], dotted line. For decreasing L, $Q_L(K_c)$ approaches the mean-field limit $\tilde{P}_Q(0)$ [Eq. (4.16)], until the linear dimension becomes smaller than the range R_m and strong finite-size effects come into play. To illustrate that the system indeed behaves mean-field like for small sizes, Q was also plotted for finite systems in which all spins interact equally strongly (dashed curve). The points are seen to approach this curve for small L. From Luijten et al. [92].

presence of the argument $LR^{-4/(d-4)} = L/R^2$ in Eq. (5.18). As illustrated in Fig. 9, there is indeed a slow crossover that is spread out over several decades in L. Obviously, it is very difficult to cover the full crossover with a single choice of R. In order to reproduce the mean-field limit described in Eq. (4.16), one needs to choose R relatively large; at the same time, however, L must not become smaller than R, because otherwise every spin interacts with the same strength with every other spin and the character of finite-size effects is different in this limit: For such a finite mean-field system containing N spins, one easily derives $Q = \tilde{P}_Q(0) + 0.214002/\sqrt{N} + \mathcal{O}(1/N)$ [250] (dotted curved in Fig. 9). Fig. 9 shows that even for $R_m = \sqrt{140}$ one does not yet fully reach the mean-field result $Q = \tilde{P}_Q(0) \approx 0.456947$. On the other hand, in order to reach the Ising limit, values of $L/R^2 \approx 10^2$ are required (Fig. 10). The asymptotic value $Q = \check{Q}(\infty)$ for the Ising limit is known with very high precision, $Q = 0.856216(1)$ [296], and this number is used as an input for the analysis. Luijten et al. [46,92] used linear sizes up to $L = 500$ for $R_m^2 \leq 10$, and for larger ranges R_m system sizes up to $L = 700$ or even $L = 800$ ($R_m^2 = 100, 140$). For each run 10^6 Wolff clusters were generated after equilibration of the system, sampling the various thermodynamic quantities after every tenth Wolff cluster. $Q_L(K)$ was then fitted to Eq. (2.63), using the exponents appropriate to the $d = 2$ Ising case,

$$\nu = 1, \quad \beta = 1/8, \quad \omega = 2 . \tag{5.19}$$

The resulting estimates for the critical coupling K_c are plotted vs. R^{-2} in Fig. 11. Motivated by renormalization-group arguments [92], these data are fitted by a power law with a logarithmic correction,

$$qK_c = 1 + R^{-2}(a + b\ln R) + cR^{-4} , \tag{5.20}$$
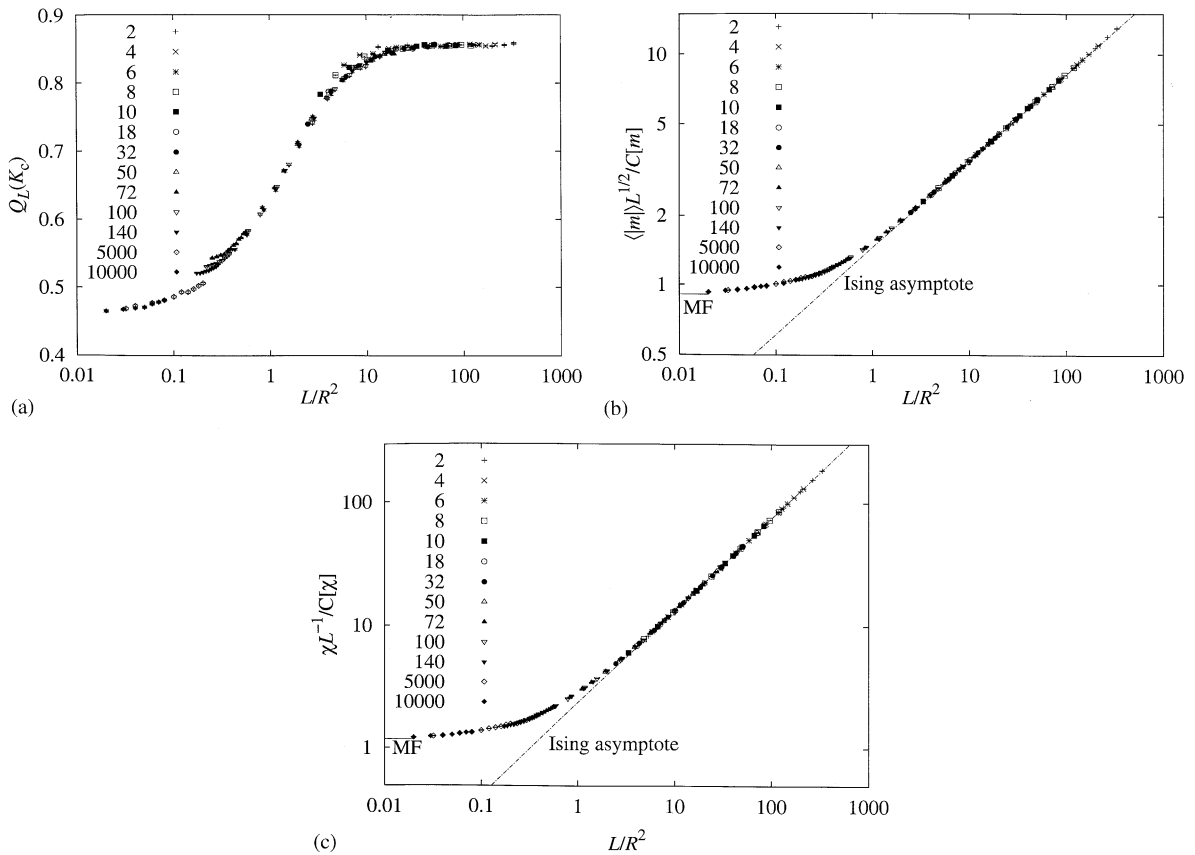
Fig. 10. Finite-size crossover scaling curves plotted in $d = 2$ dimensions at $T = T_c(R)$ vs. L/R^2 for (a) Q, (b) $\langle m \rangle L^{1/2}/C[m]$, and (c) $\chi L^{-1}/C[\chi]$. In order to remove some corrections to scaling, corrections $C[m] = 1 - R^{-2}(b_1 + b_2 \ln R^2)$ and $C[\chi] = 1 + R^{-2}(q_1 + q_2 \ln R^2) + q_3 R^{-4}$, with b_1, b_2, q_1, q_2 and q_3 adjustable constants, have been fitted to the data. (Note that the functional form of these finite-range corrections can be justified by renormalization-group arguments). Different symbols stand for the different choices of R_m^2, as indicated in the figure. Mean-field and Ising asymptotes are included in parts b and c. From Luijten et al. [46].

where $a = -0.267$ (6), $b = 1.14$ (6) and $c = -0.27$ (3). This relation (the curve drawn in Fig. 11) is useful for providing estimates for very large R (i.e., for $500 \leq R_m^2 \leq 10000$), where direct determinations of K_c from finite-size scaling would no longer be feasible.

Fig. 10 has already provided evidence that the crossover from mean-field behavior to short-range Ising behavior occurs in a smooth fashion and is spread out over several decades in the crossover scaling variable, which is L/R^2 for $d = 2$ [cf. Eqs. (5.16)–(5.18)]. Also the *thermal* crossover spans a comparatively wide regime but now the crossover scaling variable is tR^2 [cf. Eq. (5.12)]. Putting $b = 1$ in Eq. (5.12) one directly obtains

$$\langle |m| \rangle = t^{\beta} R^{(2d\beta - d)/(4-d)} \tilde{m}_t(tR^{2d/(4-d)}) = R^{-d/(4-d)} \check{m}_t(tR^{2d/(4-d)}) \tag{5.21}$$
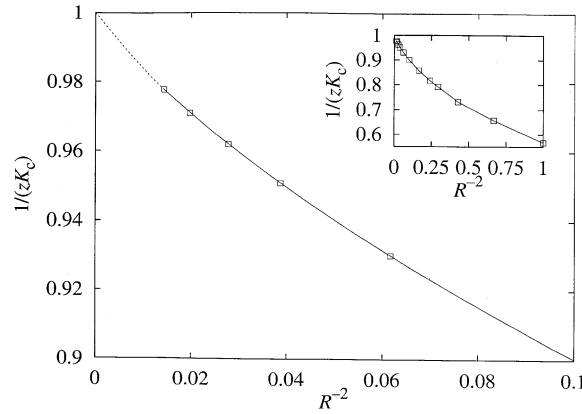
Fig. 11. Plot of $1/(zK_c)$ vs. R^{-2}, where z denotes the number of equivalent neighbors, for the $d = 2$ equivalent-neighbor Ising model. The dotted line denotes the extrapolation to the mean-field limit. The inset shows $1/(zK_c)$ over the full range of R^{-2} between the Ising and the mean-field limit. From Luijten et al. [92].

and

$$\chi = t^{-\gamma} R^{2d(1-\gamma)/(4-d)} \tilde{\chi}_t(tR^{2d/(4-d)}) = R^{2d/(4-d)} \breve{\chi}_t(tR^{2d/(4-d)}) , \qquad (5.22)$$

where we have attached the subscript t to the crossover scaling functions in order to distinguish them from those for the finite-size scaling crossover, Eqs. (5.16) and (5.17). Fig. 12 shows a corresponding plot for $\langle|m|\rangle$ and Fig. 13 for χ (at temperatures $T < T_c$). One sees that the "raw data" for $\langle|m|\rangle$ and χ only show a rough collapse and that there are various systematic deviations from a perfect match to a master curve. For example, for very small values of $|tR^2|$ the data start to deviate from the slope of the Ising asymptote and approximately cross over, for temperatures closer to T_c, to a constant value. This crossover to a horizontal slope occurs at an L-dependent location and is due to residual finite-size effects: Eqs. (5.21) and (5.22) only follow from Eqs. (5.16) and (5.17) in the limit $L \to \infty$ at fixed $tR^{2d(4-d)}$. The data which are affected by such finite-size effects were all omitted in part (b) of Figs. 12 and 13.

However, even in the remaining data one finds that, in the regime where $\langle|m|\rangle R$ is already proportional to $(-tR^2)^{1/8}$ for small $|tR^2|$, there is a systematic offset in the prefactor: One obtains a set of parallel straight lines rather than a collapse on a single line. It turns out that this effect results from a "finite-range" correction $C[m]$ to the critical amplitude. The same correction was already involved in the finite-size crossover scaling plot, Fig. 10. The presence of such corrections actually is no surprise at all – the treatment presented in the previous section applies for $R \to \infty$, $t \to 0$ and $tR^{2d/(4-d)}$ finite or $R \to \infty$, $L \to \infty$ and $LR^{-4/(4-d)}$ finite, whereas we have included rather small values of R in Figs. 10–13. If one would only include data lying in the appropriate scaling limit into the analysis, there would be no need for the present corrections: However, in order to reach, for large R, the scaling limit of the Ising universality class, one would have to simulate huge systems very close to $T_c(R)$. Presently, such simulations are not feasible, and therefore Luijten et al. [45–51,92] decided to include relatively small values of R in the analysis as well and to apply appropriate corrections. The functional form of this range-dependent corrections can be justified by renormalization-group arguments.
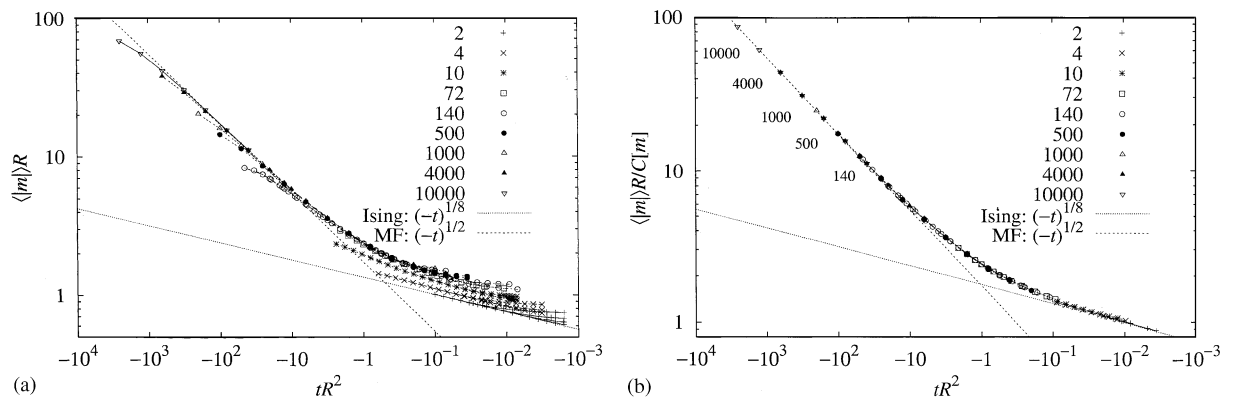
Fig. 12. Log–log plot of (a) $\langle|m|\rangle R$ and (b) $\langle|m|\rangle R/C[m]$ vs. tR^2, for the $d=2$ equivalent-neighbor Ising model, where the reduced temperature t is defined as $t=[T-T_c(R)]/T_c(R)$ and the symbols denote various choices of R_m^2 as indicated. In (a) no additional correction terms have been used, while in (b) the factor $C[m]$ has been divided out (see text), data points in the finite-size regime have been omitted, and data for $R_m^2 \geq 72$ have been corrected for saturation effects. The dotted straight lines show the asymptotic power laws in the Ising and mean-field regime, respectively. From Luijten et al. [46].
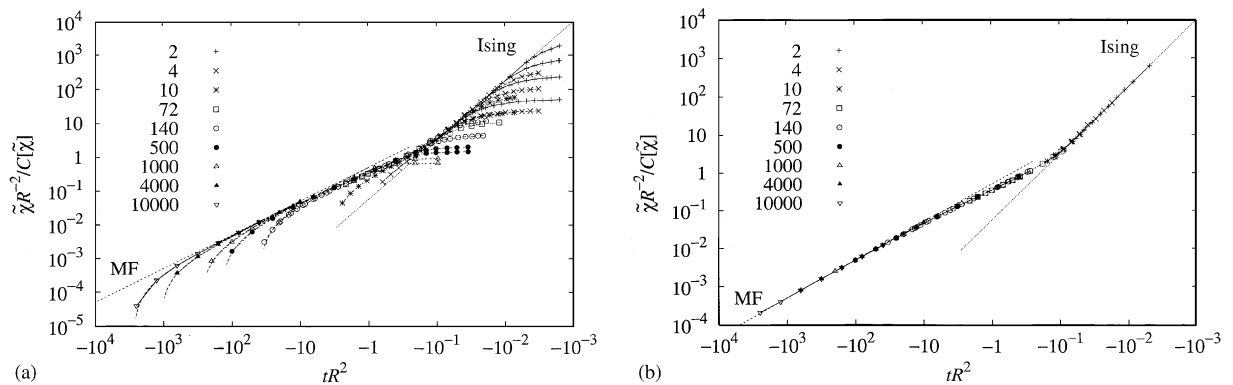
Fig. 13. Log–log plot for the susceptibility $\tilde{\chi} \equiv [\langle m^2 \rangle - \langle|m|\rangle^2]L^d/(k_{\mathrm{B}}T)$, normalized by a factor $R^2 C[\chi]$, see text, vs. the thermal crossover variable tR^2. Various choices of R_m^2 are included as indicated. In part (b) data points in the finite-size regime, which are included in (a), have been omitted, and data for $R_m^2 \geq 72$ were corrected for saturation effects. Dotted straight lines show the asymptotic power laws in the Ising and mean-field regime, respectively. From Luijten et al. [46].

A further systematic deviation from a data collapse for $\langle|m|\rangle$ is encountered for large values of $|tR^2|$: There the curves systematically bend away from the mean-field asymptote toward smaller values. This results from a saturation of the order parameter at low temperatures, as can be understood already within mean-field theory: the magnetization must fall below the power law $\langle|m|\rangle = \sqrt{3}(-t)^{1/2}$ as $T \to 0$ since then $\langle|m|\rangle \to 1$ rather than $\langle|m|\rangle \to \sqrt{3}$. In fact, from the self-consistent molecular-field equation $\langle|m|\rangle = \tanh(\langle|m|\rangle T_c/T)$ one can derive [46]

$$\langle|m|\rangle R \approx \sqrt{3}(-tR^2)^{1/2}\left[1 - \frac{2}{5R^2}(-tR^2) - \frac{12}{175R^4}(-tR^2)^2\right].$$

(5.23)

Using the term in square brackets to correct the numerical data for large $|tR^2|$, one obtains the almost perfect data collapse for the magnetization shown in Fig. 12b.

Similar effects occur in the susceptibility, Fig. 13: For small $|tR^2|$, the curves bend away from the Ising asymptote toward L-dependent plateau values because of finite-size effects and for large $|tR^2|$ the curves decrease more strongly than expected from the mean-field asymptote, which is again a saturation effect, since $\chi = (1 - m^2)/(t + m^2)$ in the molecular field approximation, and the numerator of this expression vanishes as $m \to 1$. In fact, it is straightforward to derive the expansion [46]

$$\chi^{\text{MF}}(T < T_c) \approx (-2t)^{-1}\left[1 + \frac{9}{5}t - \frac{36}{175}t^2 - \frac{36}{175}t^3 - \frac{13\,428}{67\,375}t^4\right] \qquad (5.24)$$

and using again the term in square brackets to correct the data for χ for these saturation effects, one obtains the perfect collapse on a master curve shown in part b of Fig. 13.

A very remarkable feature occurs in the central part of the crossover, for $-1 \leq tR^2 \leq -10^{-1}$, where the scaled data fall below the mean-field asymptote before reaching the Ising asymptote. This means that in the intermediate regime of the crossover scaling one finds an effective exponent $\gamma_{\text{eff}} < 1$! These effective exponents are traditionally defined as logarithmic derivatives [297],

$$\beta_{\text{eff}} \equiv \mathrm{d}\ln\langle|m|\rangle/\mathrm{d}\ln|t|, \quad \gamma_{\text{eff}} = -\mathrm{d}\ln\chi/\mathrm{d}\ln|t| = -t\,\mathrm{d}\ln\chi/\mathrm{d}t . \qquad (5.25)$$

While β_{eff} varies monotonically from the mean-field value $\beta_{\text{MF}} = 1/2$ for large $|tR^2|$ to the Ising value $\beta = 1/8$ for small $|tR^2|$ [46], the variation of γ_{eff} is monotonic above T_c but nonmonotonic below T_c (Fig. 14). The physical reason why γ_{eff}^+ varies monotonically while γ_{eff}^- shows this "underswing" is unclear, and there are presently no theoretical predictions for the crossover scaling functions shown in Figs. 13b and 14a! However, for $T > T_c$, γ_{eff} has been found by Pelissetto et al. [124] by means of a systematic perturbation around the mean-field limit, and the agreement with Fig. 14b is almost perfect, cf. Fig. 14c.

One question that has been left unanswered by the treatment of Section 5.1 is the universality of crossover scaling functions such as $\hat{f}_s$ [Eq. (5.12)] or the functions $\hat{f}_s^{(1)}$, $\hat{f}_s^{(2)}$, $\tilde{m}$, $\tilde{\chi}$, $\tilde{m}_t$, $\tilde{\chi}_t$ [Eqs. (5.14)–(5.17), (5.21), (5.22)] derived from it: Is there a single variable R that controls such crossover phenomena, or are there additional parameters on which these crossover scaling functions might depend? There is no complete consensus on this problem in the literature [110–124]. In the absence of clear theoretical guidance, and because of suggestions that the presence of an additional length scale might influence the nature of the crossover [121], it has been speculated that the shape of the interaction function $K(r)$ might play a role [50]. In order to check this conjecture, a function $K(r)$ was constructed that did not only involve a single length scale R, but rather two different scales R_1, R_2, by choosing $K(r) = K_1$ for $0 < r < R_1$ and $K(r) = K_2$ for $R_1 < r < R_2$. In order to create a strong asymmetry between the two domains, a large strength ratio was chosen, $K_1/K_2 = 16$. Now it is possible to choose very different combinations R_1, R_2 that yield the same effective range R, defined from Eq. (5.3) in the usual way. For example, choosing $R_1^2 = 93$, $R_2^2 = 140$ yields $R^2 = 48.8$ while the very different choice $R_1^2 = 4$, $R_2^2 = 140$ yields the quite similar value $R^2 = 49.99$. Indeed, one finds that both choices yield appreciably different results for K_c, although R is almost the same. However, the crossover scaling function for both choices is precisely identical! Thus, the idea that the crossover scaling functions might be nonuniversal because they depend on
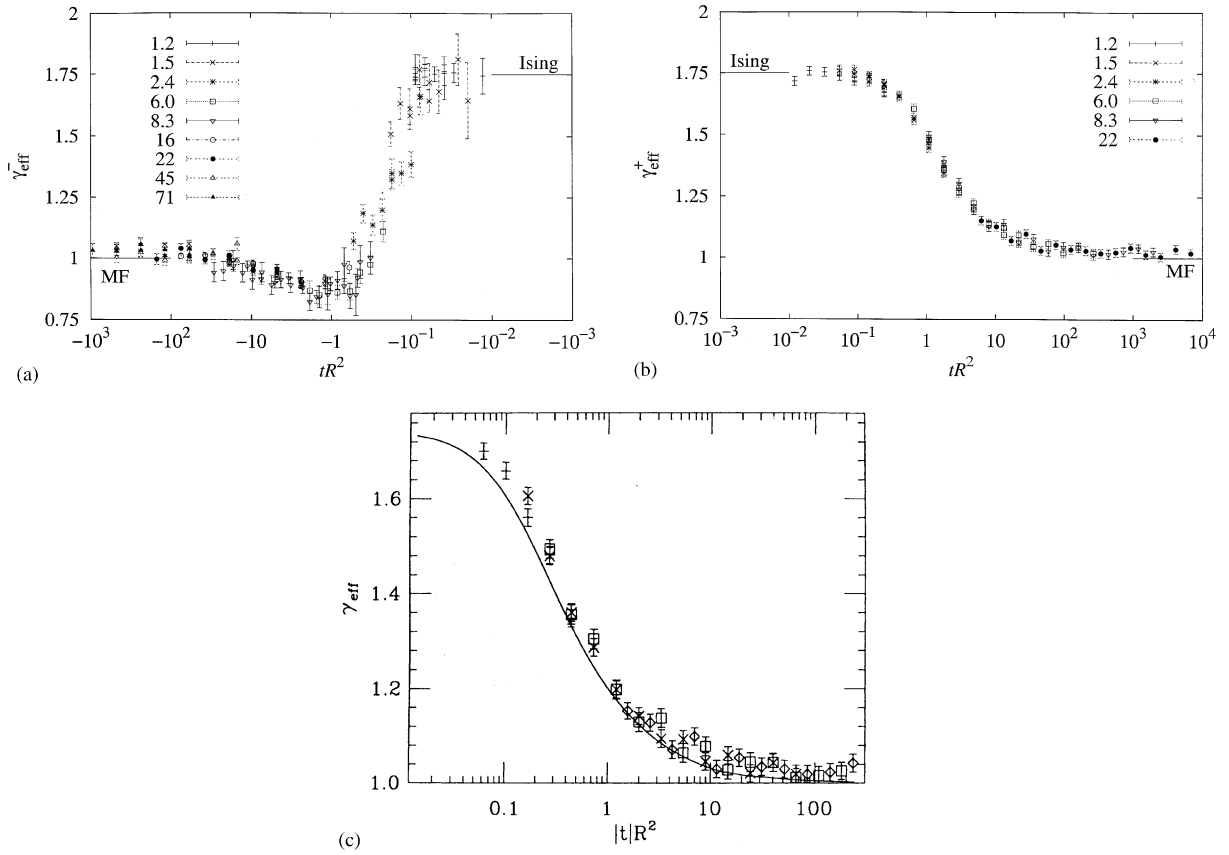
Fig. 14. Effective susceptibility exponents (a) $\gamma_{\mathrm{eff}}^{-}$ and (b) $\gamma_{\mathrm{eff}}^{+}$ for $T < T_c$ and $T > T_c$, respectively, plotted vs. tR^2. The Ising value ($\gamma = 7/4$) and the mean-field (MF) limit ($\gamma = 1$) are indicated. The symbols indicate different values of R. From Luijten et al. [45]. (c) Effective exponent γ_{eff} for the $d = 2$ Ising model for $T > T_c$, as a function of tR^2, comparing results of Luijten et al. [46] with results from a systematic perturbation expansion around the mean-field limit. Pluses, crosses, squares and diamonds correspond to data for $R_m^2 = 10, 72, 140$ and 1000, respectively. From Pelissetto et al. [124].

the detailed shape of $K(r)$ can be refuted – although this finding clearly cannot rule out that other parameters that induce nonuniversal variations of the scaling functions might exist.

5.3. Numerical results in $d = 3$ dimensions and comparison with theoretical predictions

The analysis of Luijten and Binder [48,49] in the case $d = 3$ closely followed the procedures that already had been applied earlier in the case of $d = 2$, and thus we keep the description of the results rather brief. The finite-size crossover scaling variable is now $L/R^{4/(4-d)} = L/R^4$ [cf. Eqs. (5.16)–(5.18)]. Thus one has to reach the regime where $L/R^4 \gg 1$ and at the same time fulfill the requirement $R \gg 1$ in order to span the full crossover region, and these simulations are therefore computationally quite demanding. In fact, simulations have been carried out for linear dimensions up to $L = 200$, i.e., 8 million lattice sites, attempting to nevertheless obtain $Q_L(K_c)$ with a precision of one part in a thousand.
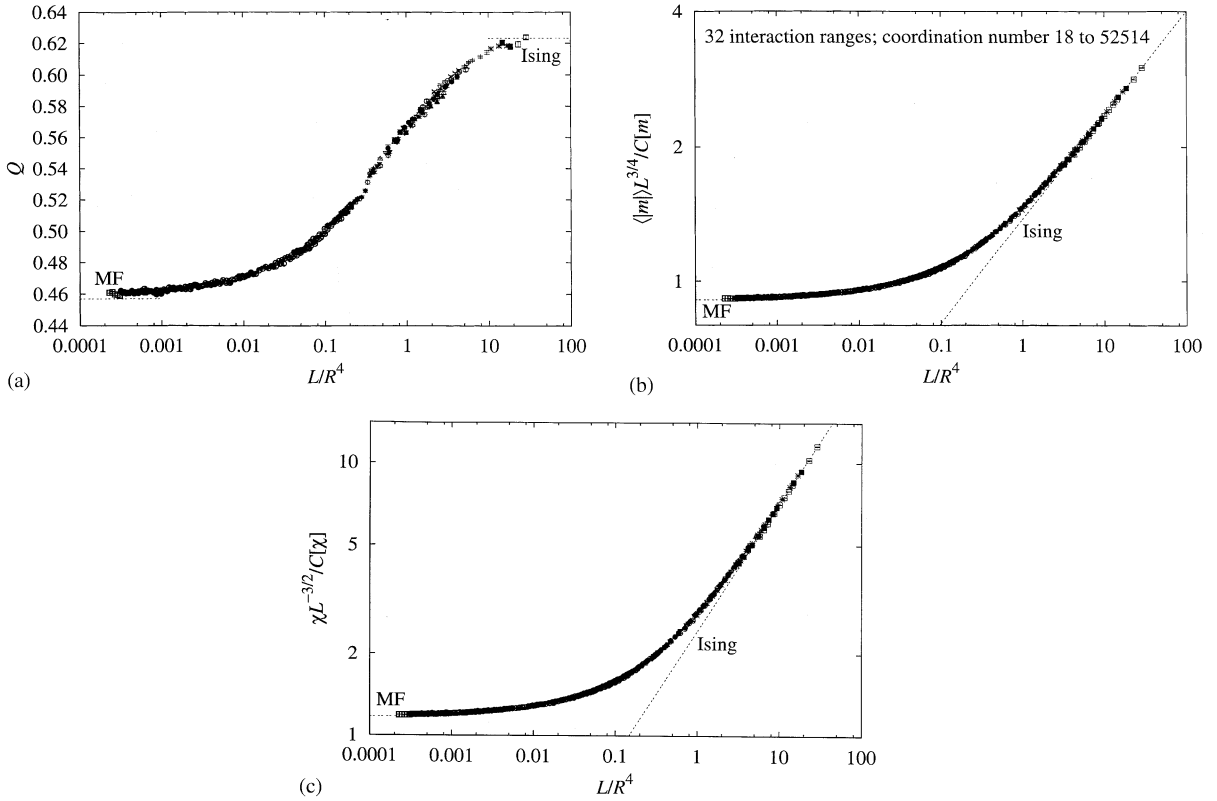
Fig. 15. Finite-size crossover scaling curves for $d = 3$ dimensions at $T = T_c(R)$ vs. L/R^4 for (a) Q, (b) $\langle m \rangle L^{3/4}/C[m]$ and (c) $\chi L^{-3/2}/C[\chi]$. Systems with up to $q = 52\,514$ interacting neighbors have been included. From Luijten [49].

Again $Q_L(K)$ was fitted to Eq. (2.63), using now the value $Q = 0.6233$ (4) as an input (see Section 3), as well as the exponents $1/v = 1.587$ (2) and $\omega = 0.82(6)$, as obtained from a similar data analysis for the nearest-neighbor model. The resulting values for $K_c(R)$ are compatible with an expression expected from renormalization-group arguments,

$$qK_c = 1 + \frac{c_0}{R^3} + \frac{c_1}{R^5} + \frac{c_2 + c_3 \ln R}{R^6} + \cdots \qquad (5.26)$$

In comparison with the corresponding result for $d = 2$, Eq. (5.20), the logarithmic correction appears in rather high order only, and hence the resulting coefficient c_3 (as well as the coefficients of the neighboring orders c_1 and c_2) are difficult to determine. Only $c_0 = 0.498$ (2) is known to a high precision [49].

Fig. 15 shows the analog of the plots in Fig. 10 for the finite-size crossover scaling. One observes that the crossover spans at least four decades in the variable L/R^4. Correction terms of the form $C[m] = 1 + aR^{-2}$, $C[\chi] = 1 + bR^{-2} + cR^{-4}$ were applied to correct for residual finite-range
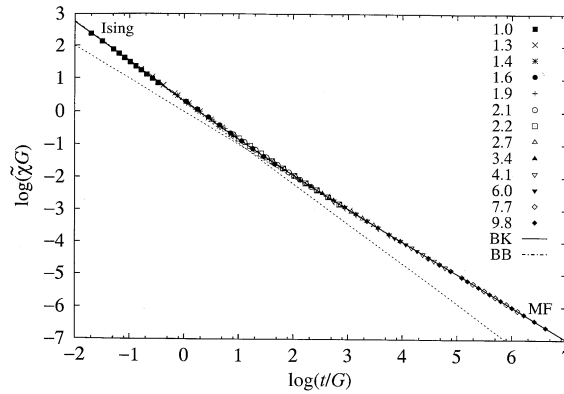
Fig. 16. Log–log plot of the scaled susceptibility, $\tilde{\chi}G$, vs. the scaled temperature distance from criticality, t/G, for the three-dimensional equivalent-neighbor model and temperatures $T > T_c$. Different symbols show different interaction ranges R, as indicated in the key of the figure. The "Ginzburg number" G is defined in Eq. (5.28). The crossover functions due to Belyakov and Kiselev (BK) [119] and Bagnuls and Bervillier (BB) [112] are also included, but are indistinguishable from each other (and from the numerical data) on the scale of this graph. The asymptotic power laws in the mean-field limit ($\tilde{\chi} = 1/t$) and in the Ising limit ($\tilde{\chi} = \Gamma^+ t^{-\gamma}$, with $\gamma = 1.237$ and $\Gamma^+ = 1.1025$, cf. text) are included as well (dotted straight lines). From Luijten and Binder [48].

effects. Coordination numbers from $q = 18$ to $q = 52\,514$ were included in Fig. 15. The straight lines marked "Ising" in parts (b) and (c) have the theoretical slopes $y_h - 9/4 = 0.2315$ and $2y_h - 9/2$, respectively. The amplitudes of the horizontal mean-field asymptotes in these plots are known exactly. For $R \to \infty$ one has

$$\langle |m| \rangle L^{3/4} = 12^{1/4} \frac{\Gamma(1/2)}{\Gamma(1/4)} \approx 0.909891 \; ,$$

$$\chi L^{-3/2} = \sqrt{12} \frac{\Gamma(3/4)}{\Gamma(1/4)} \approx 1.170829 \; , \tag{5.27}$$

which agrees well with the data.

Fig. 16 presents the thermal crossover for the susceptibility χ for $T > T_c$. In this figure, the reduced susceptibility $\tilde{\chi}$ was defined as $(T_c(R)/T)L^3 \langle m^2 \rangle$, so that in the mean-field limit one simply has $\tilde{\chi} = t^{-1}$, while for the nearest-neighbor Ising model $\tilde{\chi} = \Gamma^+ t^{-\gamma}$ where $\gamma = 1.237$ [42] and $\Gamma^+ = 1.1025$ [58] have been taken. From Eq. (5.22) we notice that the crossover scaling variable is tR^6 in $d = 3$ dimensions. When discussing the universality of the crossover scaling description, a suitable amplitude factor for this crossover scaling variable must be taken into account. In order to make contact with experimental analyses of crossover phenomena, we introduce the notion of the "Ginzburg number" G [19,109]. Writing the phenomenological Ginzburg criterion in terms of the mean-field power laws for the order parameter ($\langle |m| \rangle = B_{\mathrm{MF}}(-t)^{1/2}$), the susceptibility ($\tilde{\chi} = \Gamma^+_{\mathrm{MF}} t^{-1}$) and the correlation length ($\xi = \xi^+_{0,\mathrm{MF}} t^{-1/2}$), mean-field theory is valid for $|t| \gg G$, with

$$G = \left(\frac{3}{4\pi}\right)^2 \frac{(\Gamma^+_{\mathrm{MF}})^2}{(B_{\mathrm{MF}})^4} [v_0/(\xi^+_{0,\mathrm{MF}})^3]^2 = G_0 R^{-6} \; . \tag{5.28}$$
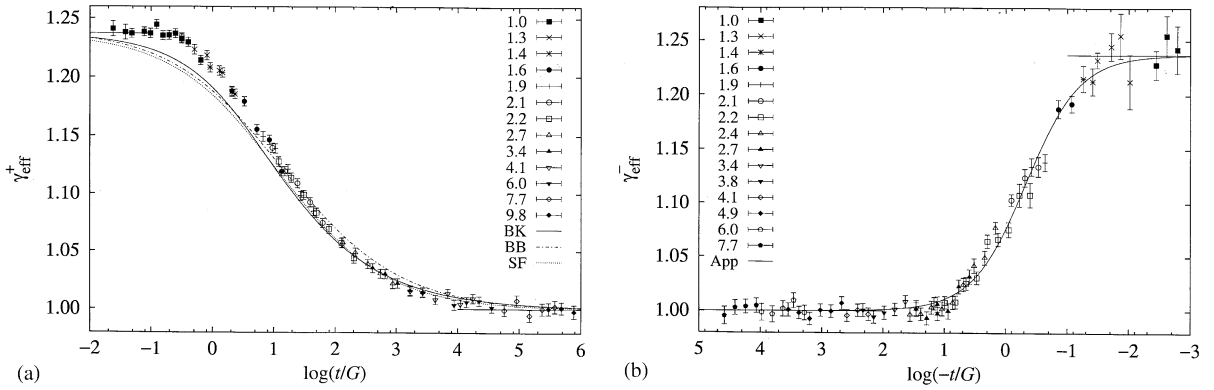
Fig. 17. (a) Effective exponent γ_{eff}^+ of the susceptibility of the three-dimensional equivalent-neighbor Ising model above T_c plotted vs. the logarithm of the crossover scaling variable t/G, along with three theoretical calculations, obtained from the work of Seglar and Fisher (SF) [110], Bagnuls and Bervillier (BB) [112] and Belyakov and Kiselev (BK) [119], as described in the text. (b) Same as (a) but for the exponent γ_{eff}^- for $T < T_c$. "App" denotes the approximation discussed in the text. From Luijten and Binder [48].

Here v_0 is the unit of volume ($v_0 = 1$ in the Ising model, if length is measured in units of the lattice spacing). For the gas–liquid transition or for unmixing transitions in mixtures of small molecules, v_0 is the volume per molecule and in the case of polymer mixtures v_0 is interpreted as the volume per monomer [132–141]. Since in the mean-field theory of an equivalent-neighbor Ising model $\xi_{0,\text{MF}}^+ \propto R$ and the other amplitudes occurring in Eq. (5.28) do not depend on R, the simple power law $G = G_0 R^{-6}$ is obtained. In many experimental studies one actually does not attempt to extract all the amplitudes in Eq. (5.28) from experimental data, but often simply takes G as an adjustable constant [141].

In principle, the crossover scaling description of Eqs. (5.21) and (5.22) is only expected to hold in the limit $|t| \to 0$, $R \to \infty$, with $|tR^{2d/(4-d)}| = |tR^6|$ finite. However, Fig. 16 shows that it is even possible to approximately represent data for all R down to $R = 1$ by a single master curve. This is possible because the amplitude $G_0 \approx 0.1027$ in Eq. (5.28) was chosen such that the scaling function of Ref. [119] precisely reproduces the amplitude $\Gamma^+ = 1.1025$ for $R = 1$ [48]. Also a scale parameter in the theory [112] included in Fig. 16 was adjusted such that the prefactors of the two asymptotic power laws are reproduced. One should not be misled by the apparently perfect agreement between these theories and the simulation results, however: Since the ordinate scale spans 10 decades, systematic deviations in the crossover regime cannot be detected here. Therefore it is again important to also consider the variation of the effective exponents γ_{eff}^+ and γ_{eff}^-, as was done already in the case $d = 2$ (Fig. 17). While in the direct representation of the susceptibility data (Fig. 16) the crossover seems to be rather sharp, the plot of the effective exponent shows that also in $d = 3$ dimensions the crossover is actually spread out over many decades in the scaling variable t/G.

Several theoretical descriptions have been included in Fig. 17a. The first one is based on an extrapolation of a first-order ε-expansion [110], which we write as

$$\gamma_{\text{eff}}^+ = 1 + (\gamma - 1)/\{1 + \exp[\tfrac{1}{2}\ln(ct/G)]\} \,, \tag{5.29}$$

where the constant c is an ad hoc fit parameter introduced in [48] to fit the initial rise of γ_{eff}^{+} with decreasing $\log_{10}(t/G)$. The second curve (labeled as BB) results from a renormalization treatment [112] and also involves a single adjustable parameter for the abscissa scale. Given the great success of this technique in accurately predicting the Ising critical exponents (see Table 3, Section 3), one expects that this theory provides the most accurate description in the limit where $G \to 0$ but t/G remains finite. The third description is another phenomenological generalization of first-order ε-expansions [119], which is now very popular with experimentalists (e.g., it has been used to analyze crossover scaling phenomena in polymer mixtures [140,141]), and hence we describe it here in some detail. The susceptibility is written as the solution of the following implicit equation

$$t/G = [1 + \kappa(\tilde{\chi}G)^{\theta/\gamma}]^{(\gamma-1)/\theta}\{(\tilde{\chi}G)^{-1} + [1 + \kappa(\tilde{\chi}G)^{\theta/\gamma}]^{-\gamma/\theta}\} \,, \tag{5.30}$$

where $\kappa \approx 2.333$ is a universal constant, and $\theta = \omega\nu \approx 0.508\,(25)$ [43] is the critical exponent of the leading correction to scaling. As mentioned above, $G_0 = 0.1027$ must be chosen in order to describe the Ising asymptote in Fig. 16, while the theoretical value [119] for G_0 in our model would be $G_0 = 27/\pi^4 \approx 0.27718$. We shall return to this problem below. Here we only emphasize that all three theoretical formulas as well as the Monte Carlo data imply that in the symmetric phase ($T > T_c$) the variation of the effective exponent with t/G is monotonic, in contrast to a conjecture of Fisher [115] who suggested that a nonmonotonic variation of γ_{eff}^{+} might be a property of the universal scaling function. However, the data in the phase of broken symmetry ($T < T_c$, Fig. 17b) show that here γ_{eff}^{-} stays close to the mean-field value $\gamma_{\text{MF}} = 1$ over a much more extended region of $\log_{10}(-t/G)$, namely from large values of $\log_{10}(-t/G)$ down to about $\log_{10}(-t/G) \approx 1$, followed by a rather sharp rise of γ_{eff}^{-}, similar to the situation for $T < T_c$ in $d = 2$ (Fig. 14a). In fact, a very small underswing ($\gamma_{\text{eff}}^{-} < \gamma_{\text{MF}} = 1$) cannot be ruled out for the data near $\log_{10}(-t/G) = 1$. This would then be a precursor of the pronounced underswing found in $d = 2$ (Fig. 14a). Later systematic expansions around mean-field theory [124] have in fact predicted such a slight underswing (Fig. 18).

Unfortunately, the theoretical predictions for γ_{eff}^{-} are rather scarce: The field-theoretical calculations [298] have only been formulated for relatively small values of t/G and hence do not cover the entire crossover region. Motivated by the success of Eq. (5.29) for $T > T_c$, Luijten and Binder [48] used a similar, but now purely phenomenological, expression for $T < T_c$,

$$\gamma_{\text{eff}}^{-} = 1 + (\gamma - 1)/[1 + \exp(\ln c't/G)] \,, \tag{5.31}$$

where c' is another adjustable constant. This approximation happens to fit the numerical results fairly well (Fig. 17b), although it does not yield the above-mentioned "underswing" predicted by Pelissetto et al. [124].

We now turn to the interpretation of the systematic deviations between the numerical data for γ_{eff}^{+} (Fig. 17a) and all the theories, occurring near the Ising limit: Does this systematic deviation mean that the theories fail to predict the universal crossover scaling limit ($t \to 0$, $G \to 0$, t/G finite) for small t/G (small tR^6)? Actually we believe that this is not the case, but that the discrepancies are caused by the inclusion of too small values of R (such as models with interactions between only nearest ($R = 1$) or nearest and next-nearest ($R = 1.3$) neighbors, for instance). In fact, in Figs. 10, 12 and 15 it was already emphasized that corrections due to the finite range R are required in order to obtain valid data in the crossover scaling limit. Of course, the quantitatively accurate estimation of
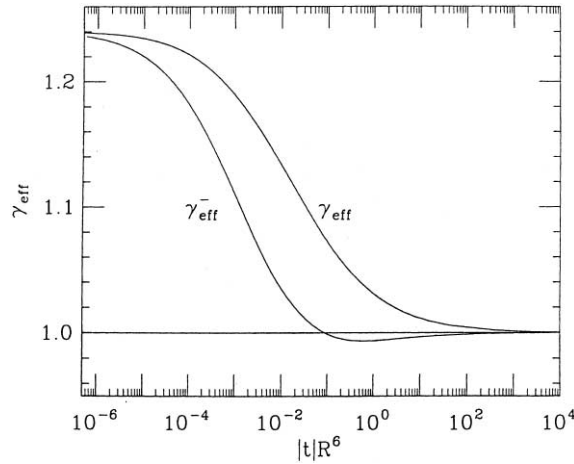
Fig. 18. Effective susceptibility exponent as a function of $|t|R^6$ for the high and low-temperature phase of the three-dimensional Ising model. The curves are the result of a systematic perturbative expansion around the mean-field limit. From Pelissetto et al. [124].

such correction terms is a delicate matter, and hence residual systematic errors must be anticipated for too small R.

This conclusion is also corroborated by the systematic perturbation expansions around the mean-field limit (which is exact for $R \to \infty$ at fixed $t \neq 0$) [124]. This work shows that correction terms to the crossover scaling limit appear in various quantities and scale to leading order like $R^{-2} \ln R$ for $d = 2$ and R^{-3} for $d = 3$, respectively. Hence, these corrections have the same form as the deviations from the mean-field result for the critical temperature [cf. Eq. (5.20) and (5.26), respectively], as found from renormalization-group arguments [49,92].

Further evidence that the Monte Carlo data for small t/G in Fig. 17a do not reflect the behavior of the universal crossover scaling limit comes from analysis of these data [299] in terms of a recent phenomenological two-parameter description of crossover scaling [120,121] that has proven very useful to account for various experimental data of fluids and binary fluid mixtures [142,145,146,300,301]. This description was derived from a renormalization-group matching for the free-energy density, and although it is based on a first-order $\varepsilon = 4 - d$ expansion, using the correct exponents of the $d = 3$ Ising model instead of their values in first order in ε makes this description a flexible and useful interpolation scheme. It contains two crossover parameters, a parameter $\bar{u}$ related to the coefficient u of the quartic term in Eq. (5.5) and a parameter Λ which is essentially a large-momentum cutoff, both of which are system dependent. Then there exist nonuniversal scale factors c_t, c_ρ in the inverse square correlation length ξ^{-2} and the inverse susceptibility χ^{-1}, which are both written in terms of a crossover function $Y(\bar{u}, \Lambda)$:

$$\xi^{-2} = c_t t Y^{(2\nu - 1)/\theta} , \tag{5.32}$$

$$1 - (1 - \bar{u})Y = \bar{u}[1 + (\Lambda\xi)^2]^{1/2} Y^{\nu/\theta} , \tag{5.33}$$

$$\chi^{-1} = c_\rho^2 c_t \frac{T_c}{T} t Y^{(\gamma-1)/\theta} \left\{ 1 + \frac{v u^*}{2\theta} \left\{ 2[(\Lambda\xi)^{-2} + 1] \left[v/\theta + \frac{(1-\bar{u})Y}{1-(1-\bar{u})Y} \right] - (2v-1)/\theta \right\} \right\}^{-1}.$$

(5.34)

Here $u^* = 0.472$ is the universal coupling constant at the RG fixed point [302]. In the approximation of an infinite cutoff $\Lambda \to \infty$, which physically corresponds to neglecting the discrete structure of matter, $\bar{u} \to 0$ and the two crossover parameters $\bar{u}$, Λ in Eqs. (5.32)–(5.34) collapse into a single one, $\bar{u}\Lambda$, which is related to the Ginzburg number G by $G = g_0(\bar{u}\Lambda)^2/c_t$ where $g_0 \approx 0.028$ is a universal constant [120]. In this limit Eqs. (5.32)–(5.34) reduce to Eq. (5.30). This single-parameter crossover is universal, and has been calculated by powerful field-theoretic methods by Bagnuls and Bervillier [112], as noted above. Pelissetto et al. [124] have investigated the numerical accuracy of Eqs. (5.32)–(5.34) [299]. The single-parameter scaling ($\bar{u} = 0$ reduces to the curve labeled BK in Fig. 17a) does not fit the data for small R_m, and one rather needs $\bar{u} = 1.22$ to fit the data for $R_m = 1$. As an interpolation, we have used $\bar{u} = \bar{u}_0 R^{-4}$ with $\bar{u}_0 = 1.22$, and $\Lambda = \pi$ for a three-dimensional Ising lattice. Since the effective exponent $\gamma_{\text{eff}}^+(\bar{u}, \Lambda, t)$ is a nontrivial function of three parameters [121] the different choices of R_m (or R) corresponding to different choices of $\bar{u}$ do not lead to a single function $\gamma_{\text{eff}}^+(tR^6)$ but to a whole family of functions (see Fig. 19). The choice of $\bar{u}_0 = 1.22$ implies a variation of the Ginzburg number $G = G_0^+ R^{-6}$ with $G_0^+ \approx 0.24$, qualitatively consistent with Eq. (5.28). However, a similar fit of γ_{eff}^- implies that for $T < T_c$ $G = G_0^-/G_0^+ = 2.58$, which appears at variance with the theoretical result $G_0^-/G_0^+ = 3.125$ [303].

While it is gratifying that the same crossover scaling model [Eqs. (5.32)–(5.34)] can describe both the equivalent-neighbor Ising model and various experimental systems (although we note that this model is essentially of a phenomenological nature!), it is clear that some problems regarding the quantitative accuracy of both the model [Eqs. (5.32)–(5.34)] and the Monte Carlo results [48] still need to be resolved. Of course, the problem that the simulations cannot easily reach the crossover scaling limit ($t \to 0$, $G \to 0$, t/G fixed) for small t/G is also shared by many experiments, where typically G cannot be varied at all. Thus, it is of interest to compare the Monte Carlo results directly to the experiments. This has recently been performed for both Xe and ^{3}He [304], and for small t/G very good agreement between experiment and the Ising model simulations has been found. Using data for the compressibility above the gas–liquid transition and for the coexistence curve below it, the Ginzburg parameter G_+ (or G_-, respectively) was used as a single adjustable parameter, resulting in $G_-(\text{Xe}) = 0.07\,(2)$, $G_-(\text{He}) = 0.070\,(8)$, $G_+(\text{Xe}) = 0.018\,(2)$, $G_+(\text{He}) = 0.0025\,(10)$. The compressibility data for ^{3}He strongly deviate from the crossover scaling function for $t/G^+ \gtrsim 10$, unlike the Xe data. This distinction was tentatively attributed to quantum effects [304].

Further problems with the theoretical interpretation of experimental crossover scaling data occur for polymer mixtures [140,141], where one does not find the theoretically predicted [125–131] behavior $G \propto N^{-1}$ where N is the degree of polymerization of the polymers. In this case, the discrepancy is attributed to a pressure dependence of the effective interaction parameter not taken into account in the theories. This problem also deserves further investigation. In any case, it is clear that quantitative studies of crossover phenomena from the Ising universality class to mean-field behavior by means of either simulations or experiments have only started a few years ago, and much more work remains to be done.
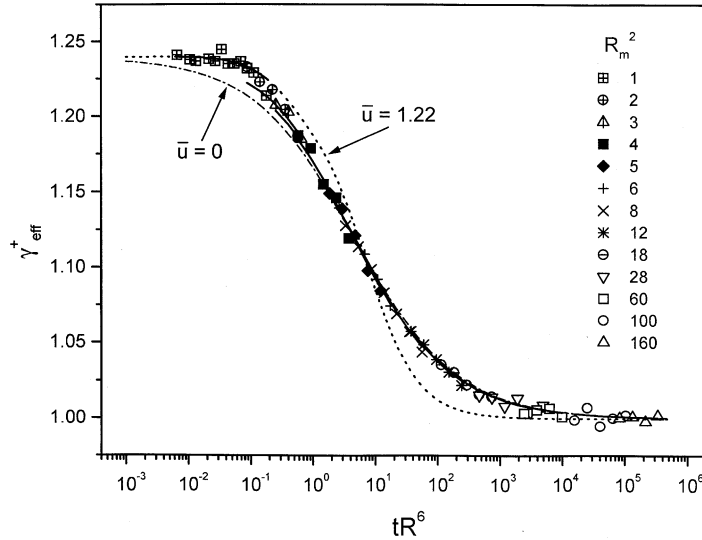
Fig. 19. The effective susceptibility exponent γ_{eff}^{+} for the three-dimensional variable-range Ising model and $T > T_c$. The symbols indicate numerical simulation data for various choices of R_m^2, as indicated (for clarity, the error bars have been omitted; they are all of the order of 0.004). The solid curves were calculated from Eqs. (5.32)–(5.34), using $\bar{u} = \bar{u}R_0^{-4}$ with $\bar{u}_0 = 1.22$. The dotted curve corresponds to the alternative choice $\bar{u} = 1.22$, while the dash-dotted curve refers to the crossover scaling limit. Note that fitting the data for the different choices of R_m^2 separately yields different cuts of a two-dimensional surface and thus one does not find a unique solid curve but a whole family of curves, which merge on the curve for $\bar{u} = 0$ for large enough R_m. From Anisimov et al. [299].

6. Algebraically decaying interactions

6.1. Overview

In addition to the dimensionality, the range of the interactions is one of the few parameters that influence the universal critical properties of Ising spin models. A natural extension of the finite-ranged interactions considered hitherto are interactions that decay as a power of the distance between the spins. Following first calculations for the spherical model by Joyce [305] and a number of rigorous results for the one-dimensional Ising model [306–308] in the 1960s, this case was considered within the framework of the renormalization-group (RG) theory in the seminal work by Fisher et al. [105]. As one of their central results emerged an explicit dependence of the upper critical dimension on the decay power of the interactions. In the following decades, a limited amount of numerical work was performed, almost exclusively restricted to the case $d = 1$ and mainly concerned with the calculation of the (nonuniversal) critical temperature as a function of the power-law decay (cf. the references cited in Ref. [47]). Also on the analytical side progress focused on the one-dimensional case, in particular on the pivotal case with inverse-square interactions [309,310]. Obviously, the study of these systems is greatly complicated by the long-ranged nature of the interactions. As far as numerical approaches are concerned, this leads to prohibitively large computational requirements, restricting practical calculations to very small systems. Fortunately,

for the case of arbitrary ferromagnetic interactions this bottleneck could be resolved by the construction of a novel Monte Carlo algorithm which has an efficiency that is independent of the number of interactions per spin [250]. Indeed, this algorithm has allowed a major step forward in the numerical treatment of several outstanding problems in the field of long-range interactions. For a detailed description of the algorithm the reader is referred to Refs. [250,251].

6.2. Renormalization-group predictions

Let us first give a brief summary of the RG predictions as obtained in Ref. [105]. We employ here the standard notation $J(r) = r^{-(d+\sigma)}$ for the spin–spin interactions. The corresponding Landau–Ginzburg–Wilson (LGW) Hamiltonian in momentum space then takes its standard ϕ^4 form, except that the k^2 term resulting from the Fourier transform of the $(\nabla\phi)^2$ term (representing the short-range interactions) is replaced by a term k^σ (we ignore here additional logarithmic factors appearing for integer σ). It follows then that the upper critical dimension is given by $d_{uc} = 2\sigma$. For smaller values of σ (more slowly decaying interactions), the critical behavior is mean-field-like and the critical exponents take their standard classical values. An exception to this are the correlation-function exponent $\eta = 2 - \sigma$ and the correlation-length exponent $v = 1/\sigma$. For $\sigma > d/2$, the exponents become continuous functions of σ and can be calculated by means of an ε' expansion, where $\varepsilon' = 2\sigma - d$ [105]. There are strong indications, however, that for the exponent η all correction terms vanish identically, such that also in the nonclassical regime η is given by $2 - \sigma$. This places us in the particular situation that we can study the critical properties of systems for which (a) one of the two independent exponents is (presumably) known exactly and in addition (b) the RG predictions can be verified by numerical means for arbitrarily small ε', since ε' is a continuous parameter even if the dimensionality has to take integer values. So we can speak of a truly ideal testing ground here! At some border-line value of σ, the critical behavior changes to the standard short-range universality class. Originally, it was concluded from the RG calculations that this occurred at $\sigma = 2$, where the k^σ term in the LGW Hamiltonian coincides with the short-range k^2 term. This conclusion entails two remarkable implications. First, it would imply a jump discontinuity in the exponent η as a function of σ, since $\lim_{\sigma\uparrow 2} \eta = 0$ and $\lim_{\sigma\downarrow 2} \eta = \eta_{sr} \neq 0$, where η_{sr} is the exponent belonging to the corresponding short-range system. Secondly, the one-dimensional case would not comply with this classification, as rigorous results have shown that a phase transition is absent here already for $\sigma > 1$ [306]. Subsequent work by Sak [106] appeared to have resolved this point, with a smooth crossover at $\sigma = 2 - \eta_{sr}$, but later studies [311–313] have casted some new doubts upon this issue.

Another area where RG predictions can be tested by means of numerical methods is the perturbative calculation of finite-size scaling functions. For systems with short-range interactions, it was shown by Brézin and Zinn-Justin [74] that an RG calculation of such functions is indeed possible below the upper critical dimension, although the resulting expansion in powers of $\varepsilon = 4 - d$ is a singular one. More specifically, the amplitude ratio $Q \equiv \langle m^2 \rangle^2 / \langle m^4 \rangle$, where m is the order parameter or magnetization density, is given by a Taylor series in $\sqrt{\varepsilon}$. A verification of this rather striking result has not been possible to date, as the calculation has been carried out only to second order in $\sqrt{\varepsilon}$, i.e., corrections are of $\mathcal{O}(\varepsilon^{3/2})$, and the numerical results are obviously restricted to $\varepsilon = 1, 2, 3$. It is thus interesting to note that very recently the calculation of Ref. [74] has been

generalized to periodic systems with an n-component order parameter and algebraically decaying interactions [314,315]. It could be shown that, upon replacement of the original expansion parameter $(4 - d)$ by $(2\sigma - d)$, the singular nature of the expansion is preserved, i.e., Q is again given by a power series in $\sqrt{\varepsilon'}$. Explicit expressions for the coefficients of the first two correction terms have been obtained, enabling a comparison to numerical results for small ε'. At criticality, the amplitude ratio is given by

$$Q = \frac{4\Gamma^2(\tfrac{3}{4})}{\Gamma^2(\tfrac{1}{4})}\left[1 + \left(4\frac{\Gamma(\tfrac{3}{4})}{\Gamma(\tfrac{1}{4})} - \frac{1}{2}\frac{\Gamma(\tfrac{1}{4})}{\Gamma(\tfrac{3}{4})}\right)\sqrt{6}x + \left(13\frac{\Gamma^2(\tfrac{3}{4})}{\Gamma^2(\tfrac{1}{4})} + \frac{1}{16}\frac{\Gamma^2(\tfrac{1}{4})}{\Gamma^2(\tfrac{3}{4})} - 2\right)6x^2 + \mathcal{O}(x^3)\right], \qquad (6.1)$$

with

$$x_0 = \sqrt{\varepsilon'}\left\{\frac{1}{2}\frac{n+2}{\sqrt{3(n+8)}}\sqrt{\frac{\Gamma(\sigma)}{\pi^\sigma}}I_1(2\sigma,\sigma,0) + \mathcal{O}(\varepsilon')\right\}. \qquad (6.2)$$

The integral $I_1(d, d/2, 0)$, which has been indicated only symbolically here, can be evaluated numerically, yielding $-2.920709\ldots$, $-3.900264\ldots$ and $-4.822719\ldots$, for $d = 1, 2, 3$, respectively [314].

6.3. Numerical results for the critical exponents

Since there exist very few systematic, precise comparisons between RG predictions for long-range systems and corresponding numerical results beyond those obtained by means of the Monte Carlo method introduced in Ref. [250], we will in this section exclusively concentrate on the latter. The numerical results can be divided into two regimes: (i) $0 < \sigma \leq d/2$, where (up to logarithmic corrections) classical critical behavior is expected and (ii) $\sigma > d/2$, where one expects *non*classical behavior.

Regime (i) has been investigated in Ref. [47], where accurate results have been presented for systems containing up to 300 000 spins, with $d = 1, 2$ and 3. The finite-size analysis concentrated on the magnetization density, the magnetic susceptibility and Q. From the former two quantities, the renormalization exponents y_t^* and y_h^* were determined, where the asterisk indicates that these exponents are modified due to the so-called dangerous-irrelevant-variable mechanism. Within the numerical accuracy, the exponents agreed, over the entire σ regime and for all three lattice dimensionalities, with the predicted values $y_t^* = d/2$ and $y_h^* = 3d/4$. Even at the upper critical dimension, these values could be confirmed to within 1–2 parts in a thousand after imposing the predicted logarithmic factors in the analysis. Obviously, these systems also provide an excellent way to study the behavior of Q above the upper critical dimension. Indeed, the so-called zero-mode value predicted in Ref. [74] could be confirmed with considerable accuracy over a wide range of values for σ and d [99], thus lending strong support to the expectation that the cumulant takes this value over the entire classical regime. Finally, Ref. [47] also demonstrated that essentially two types of behavior can be distinguished for the spin–spin correlation function $g(r)$ in finite systems: at short distances $(r/L \ll 1)$ it decays according to the predicted value for η, i.e., like $r^{-(d-\sigma)}$, to be compared to a decay $r^{-(d+\sigma)}$ for the spin–spin interactions. If one, however, considers $g(r)$ at $r = L/2$, one essentially studies the $\mathbf{k} = \mathbf{0}$ mode and $g(r) \propto L^{-d/2}$ for all $0 < \sigma < d/2$.
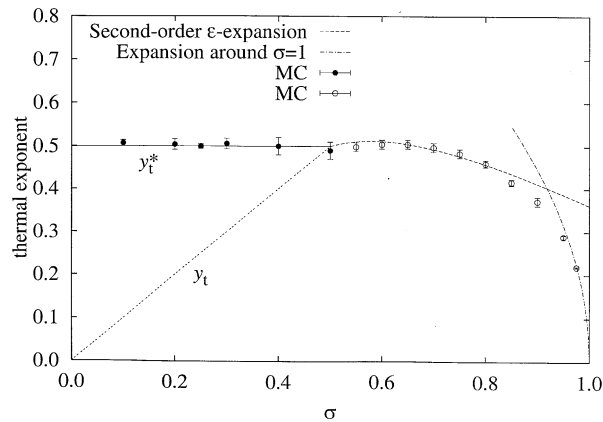
Fig. 20. Thermal exponent for the one-dimensional Ising model with algebraically decaying interactions, as a function of the decay power. From Ref. [289]. Both the agreement with the second-order ε' expansion and the approach of the Kosterlitz–Thouless transition at $\sigma = 1$ can be clearly observed.

The findings for regime (ii), which are at least as interesting, are unfortunately almost exclusively available in Ref. [289, Chapter 5]. Here, we concentrate on the cases $d = 1$ and $d = 2$. Fig. 20 shows the Monte Carlo results for the thermal exponent as a function of σ, together with ε' expansion of Ref. [105]. Up to $\sigma = 0.75$ ($\varepsilon' = 0.5$) the agreement is most satisfactory, where it is stressed that the RG curve contains only terms up to second order in ε', without the application of any series resummation. For higher values of σ, the numerical values exhibit a rapid decay toward zero, in agreement with the presence of a Kosterlitz–Thouless transition at $\sigma = 1$ [316–318] and the consequential absence of an algebraic temperature dependence of the correlation length. We have also included an expansion for y_t around $\sigma = 1$ [318] in Fig. 20 and the numerical data indeed appear to approach this curve for sufficiently large σ. An interesting implication of the displayed behavior of the thermal exponent has been pointed out in Ref. [319]: since $y_t > \frac{1}{2}$ only for $\frac{1}{2} < \sigma \lesssim 0.65$, the specific heat will consequentially only diverge for this part of the nonclassical regime and display a cusp singularity for larger values of σ. (In the classical regime, the specific heat also exhibits a cusp singularity, but of a different nature, cf. Ref. [319].) The corresponding graph for the magnetic exponent (as obtained from a finite-size scaling analysis of the magnetic susceptibility) is displayed in Fig. 21. As can be seen, the Monte Carlo data follow the predicted dependence $y_h = (d + \sigma)/2$ (corresponding to $\eta = 2 - \sigma$) very closely: for $\sigma = 0.95$, the relative deviation lies below one part in a thousand. The analysis of the two-dimensional system is more involved, due to the crossover to short-range critical behavior and the unknown nature of the corrections to scaling. Both at the upper critical dimension ($\sigma = 1$) and in the short-range regime, the thermal exponent is equal to unity. In the intermediate long-range regime, the ε' expansion suggests (like for $d = 1$) an initial increase of y_t as a function of σ, which is consistent with the trend exhibited by the numerical results, although these mostly lie within one standard deviation from unity. The behavior of the magnetic exponent offers the opportunity to determine the location of the transition between the intermediate long-range critical regime and the short-range critical regime. Postponing a detailed
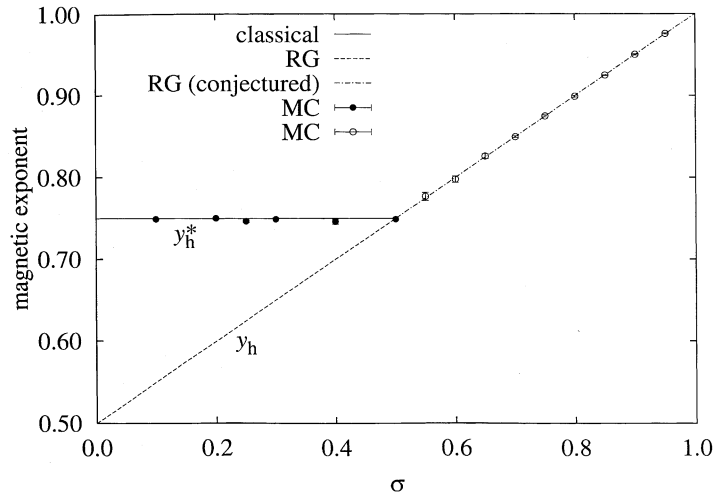
Fig. 21. Magnetic exponent for the one-dimensional Ising model with algebraically decaying interactions, as a function of the decay power. From Ref. [289]. The linear behavior of the numerical data in the nonclassical regime $\frac{1}{2} < \sigma \leq 1$ lends strong support to the conjectured exactness of the zeroth-order RG result.

discussion to a later work [320], we only mention here that the numerical results strongly suggest a crossover at $\sigma = 2 - \eta_{sr}$, i.e., at $\sigma = \frac{7}{4}$ for $d = 2$.

6.4. Finite-size scaling functions

The Monte Carlo simulations in regime (ii) also permit an accurate determination of the amplitude ratio Q as a function of σ. In order to provide a reference frame, Fig. 22 shows known results for Q in periodic linear, square and cubic Ising systems, along with the finite-size scaling function calculated in Ref. [74]. Clearly, it is impossible to draw any conclusion on the singular nature of the ε expansion from this graph. Figs. 23 and 24 then show Q as a function of σ for $d = 1$ and $d = 2$, respectively, where also the corresponding values of ε' have been indicated along the upper horizontal axis. While a very close approach of the upper critical dimension is hampered by the corresponding strong corrections to scaling, the numerical results clearly deeply penetrate into the regime where the convergence of the ε' expansion does not have to be doubted. In the same figures, the second-order $\sqrt{\varepsilon'}$ expansion of Eqs. (1) and (2) has been included. The agreement is obviously extremely poor: the numerical results rather fall strikingly well onto a straight line, with a weak deviation upon increasing ε'. Let us point out two important indications for the consistency of the numerical data: for $d = 1$ the order-parameter jump implied by the Kosterlitz–Thouless transition at $\sigma = 1$ leads to $Q = 1$, in full agreement with the trend exhibited in Fig. 23. For $d = 2$, $Q \approx 0.856$ in the short-range regime, in good agreement with the observed value at the transition point $\sigma = 1.75$. The source of this discrepancy has not been identified yet. While a slow convergence of the ε' expansion appears as a natural suggestion, it is pointed out that marked deviations already occur for values of ε' as low as 0.2 and that the relative size of the coefficients appearing in
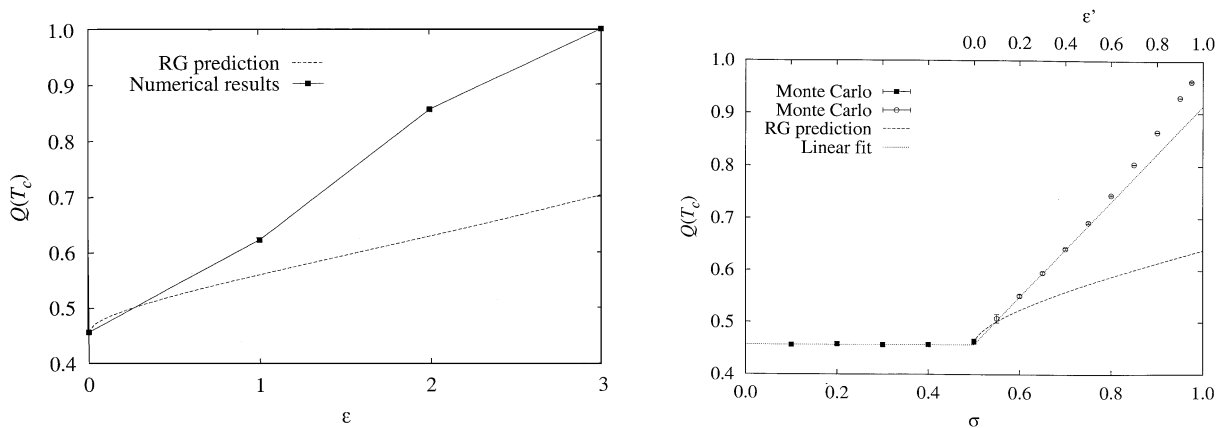
Fig. 22. The amplitude ratio $Q = \langle m^2 \rangle^2 / \langle m^4 \rangle$ at criticality for periodic, short-range Ising models in $d = 1, 2, 3$, along with the singular finite-size scaling function obtained by means of the ε expansion. For the numerical results, the symbol size by far exceeds the uncertainty.

Fig. 23. The critical amplitude ratio $Q(T_c)$ for the one-dimensional Ising model with algebraically decaying interactions together with its second-order $\sqrt{\varepsilon'}$ expansion, as a function of the decay power. The corresponding values for ε' are indicated along the upper horizontal axis. From Ref. [314].
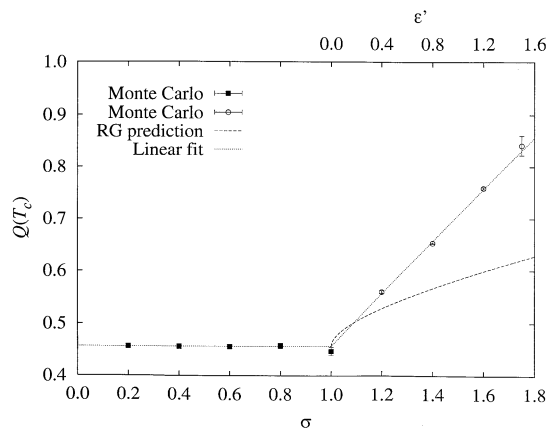
Fig. 24. The analog of Fig. 23 for the two-dimensional long-range Ising model. From Ref. [314].

Eq. (1) does not hint at unusually strong higher-order corrections. In addition, it is not obvious how such correction terms would largely compensate the singular contribution of the first-order term. In any case, an explicit calculation of the correction terms to $\mathcal{O}(\varepsilon^2)$ and $\mathcal{O}(\varepsilon'^2)$, respectively, seems highly desirable in order to shed some light onto this unexplained discrepancy.

7. The interface localization transition in Ising films with competing walls

7.1. A finite-size scaling study

In the previous sections, ferromagnetic Ising systems in various dimensionalities have been considered, and different choices for the interaction range were treated, but bulk homogeneous systems were studied exclusively. Although also in these cases there are some open questions, we feel that the basic aspects of critical phenomena in these systems are well understood. The situation is rather different, however, when we consider inhomogeneous systems confined by walls. Many new phenomena can arise because surface magnetic fields may act at the walls, exchange constants near walls may have values different from those in the bulk, etc. Here we are not at all aiming at an exhaustive review of such phenomena, but only treat one case which provides a good example of the wealth of new physics that is involved. This case concerns a nearest-neighbor Ising ferromagnet on the simple cubic lattice in an $L \times L \times D$ geometry, where periodic boundary conditions act in the x and y direction, while one chooses two free $L \times L$ surfaces in the z-direction, where surface fields H_1, act in the layer $n = 1$ and $H_D = -H_1$ in the layer $n = D$ [148–159],

$$\mathscr{H} = -J \sum_{\langle i,j \rangle} S_i S_j - H_1 \sum_{\substack{i \in \text{surface} \\ n=1}} S_i - H_D \sum_{\substack{i \in \text{surface} \\ n=D}} S_i . \tag{7.1}$$

In the limit $L \to \infty$, for any finite D the transition from the disordered phase for temperatures T above the bulk critical temperature T_{cb} to the ordered phase at $T < T_{\text{cb}}$ is a gradual, rounded transition without any singular behavior, although the system is already infinite in two spatial directions. This smearing of the transition happens because for $T \lesssim T_{\text{cb}}$ the state of the system is characterized by the presence of an interface which runs parallel to the wall and has an average position in the center of the film (Fig. 25). For $T \gg T_{\text{cb}}$ due to the action of the surface fields there is already a region of thickness ξ_b (the correlation length in the bulk) adjacent to the left wall where the local magnetization $m(z)$ is positive, and similarly in the region $D - \xi_b$ we have $m(z) < 0$. Near T_{cb}, when D becomes comparable to $2\xi_b$, these two regions start to interact, and a profile $m(z)$ develops, which decays smoothly from $m(z = 0)$ near the bulk magnetization m_b toward $m(z = D)$ near $-m_b$. Although $m(z) = 0$ only for $z = D/2$, in the center of the film, and we have (for $T \lesssim T_{\text{cb}}$ and large D) a coexistence of two oppositely oriented domains with magnetizations $\pm m_b$ separated by an interface, the thin film as a whole still has zero magnetization, since $\int_0^D m(z)\mathrm{d}z = 0$ when $H_D = -H_1$.

However, at some lower temperature $T_{\text{c}}(D)$, which does not converge to T_{cb} when $D \to \infty$, a phase transition does occur where the interface is either bound to the left wall (then $\langle m \rangle_{\text{film}} < 0$) or the right wall (then $\langle m \rangle_{\text{film}} > 0$), cf. Fig. 25. The spontaneous symmetry breaking that occurs here involves an one-component order parameter, and if a continuous transition occurs it should fall in the universality class of the two-dimensional Ising model. If one studies this transition with a finite-size scaling analysis of Monte Carlo data, applying the most straightforward version of the techniques described in Section 2.4, where one attempts to first locate T_{c} by looking for cumulant crossings (analogous to Fig. 2), one experiences a bad surprise (Fig. 26): Even on a very coarse scale of inverse temperature, there is a distinct spread of cumulant crossings, and thus the extrapolation of these crossing points toward $L \to \infty$ can yield only a rather crude estimate of $J/k_{\text{B}}T_{\text{c}}$ in a plot vs.
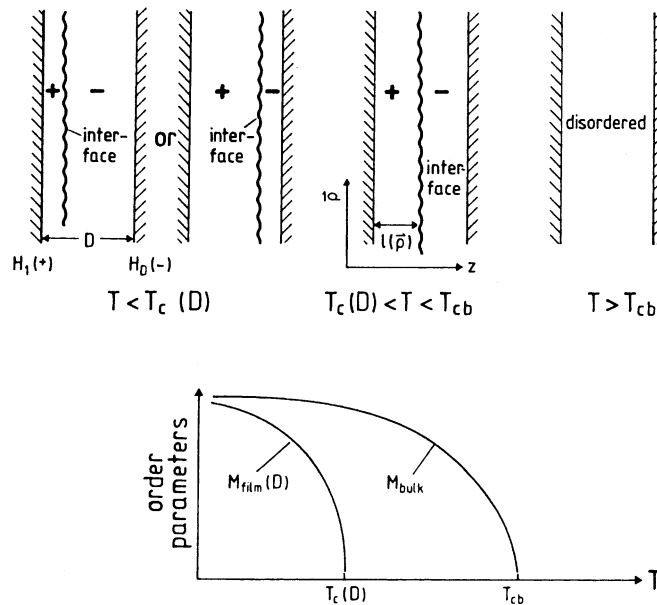
Fig. 25. Schematic description of the interface localization–delocalization transition of an Ising model confined between two walls a distance D apart, where at one wall (left side) a positive field H_1 acts, while on the other wall (right side) a negative field H_D acts. For $T < T_c(D)$ the interface is bound either to the left or the right wall, and then the average magnetization $\langle m \rangle_{film}$ of the film is nonzero. For $T_c(D) < T < T_{cb}$, however, the interface fluctuates in the center of the film, and thus $\langle m \rangle_{film} = 0$, although there is still a nonzero bulk magnetization $\pm m_{bulk}$ in an infinite system, as well as locally in the film away from the interface. For $T > T_{cb}$, however, the film is disordered (apart from the regions near the walls, where due to the response of the system to the surface fields there occurs a local nonzero magnetization). The description of the interface in terms of a coordinate $z = \ell(\rho)$ with ρ being the x, y coordinates in the plane formed by the left wall is also indicated. From Binder et al. [157].

$1/L$ (Fig. 27). The alternative method (shown in the same figure) of extrapolating the locations $K_{max}(L)$ of the maxima of specific heat (C_{max}), susceptibility (χ_{max}), etc. is not at all better. It is also very disturbing that the ordinates of these cumulant crossings (U_{cross}) are far off the theoretical value ($U^* = 0.6107$ in the $d = 2$ Ising model [296], although they possibly converge to the correct value as $L \to \infty$ (at least for $D = 6$ and $D = 8$ this seems plausible). Problems are also encountered for the critical exponents: testing for the law $\chi'(K_{max}(L)) \equiv \chi'_{max} \propto L^{\gamma/\nu} = L^{1.75}$ (Fig. 28) we find rough agreement with the predicted power law for $D = 6$, while systematically smaller effective exponents occur for $D = 8$ and $D = 12$; note that this analysis is not affected by the uncertainty in finding the correct $K_c(D)$. And the thermal finite-size scaling, as predicted in Eq. (2.40), $\langle |m| \rangle L^{\beta/\nu} = M_1(L^{1/\nu}t)$ [$\langle |m| \rangle L^{1/8} = M_1(Lt)$ in our case] works only roughly for $D = 6$ and if we restrict ourselves to $L \geq 128$ (Fig. 29). In fact, despite considerable effort (for $L = 256$, $D = 6$ we have in total $393\,216$ spins in the system, and the relaxation time at criticality is expected to be of the order $\tau \propto L^{2.16} \approx 1.6 \times 10^5$ Monte Carlo steps/site) a data collapse is obtained (Fig. 29) which only has a quality comparable to that of $L \times L$ square lattices with $L = 20$ to 40, which would be a student's exercise for a small personal computer.
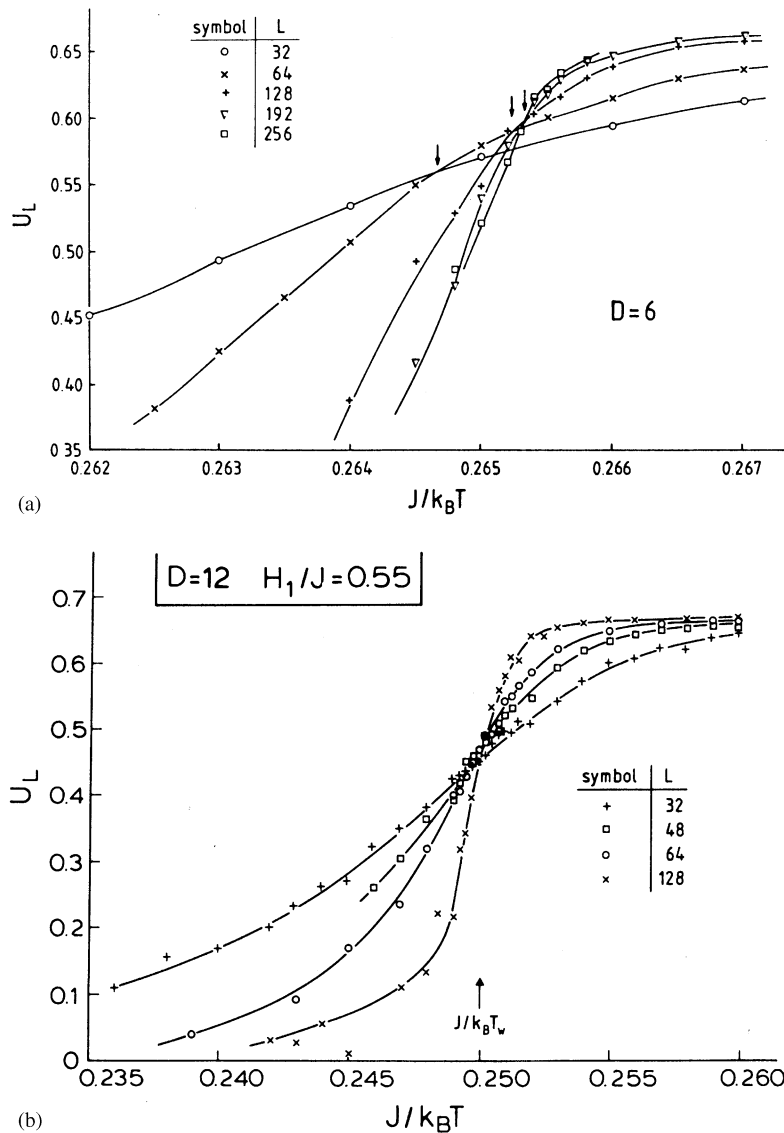
Fig. 26. Cumulant U_L plotted vs. $J/k_B T$, for the case $H_1/J = 0.55$ and film thickness $D = 6$ (a) and $D = 12$ (b), and several choices of L, as indicated. Arrows in (a) indicate the locations of cumulant crossings of two neighboring lattice sizes L, L', while the arrow in part (b) indicates the location of the transition temperature of the wetting transition T_w at the surface of a semi-infinite system. From Binder et al. [156].

7.2. Phenomenological mean-field theory and Ginzburg criteria

The data shown in Figs. 26–29 already point to the fact that the critical region is very narrow due to crossover phenomena. The theoretical interpretation of these crossover phenomena can in fact be provided by the concept of the effective interface Hamiltonian $\mathscr{H}_{\mathrm{eff}}(\ell)$ [160–162,164–167],
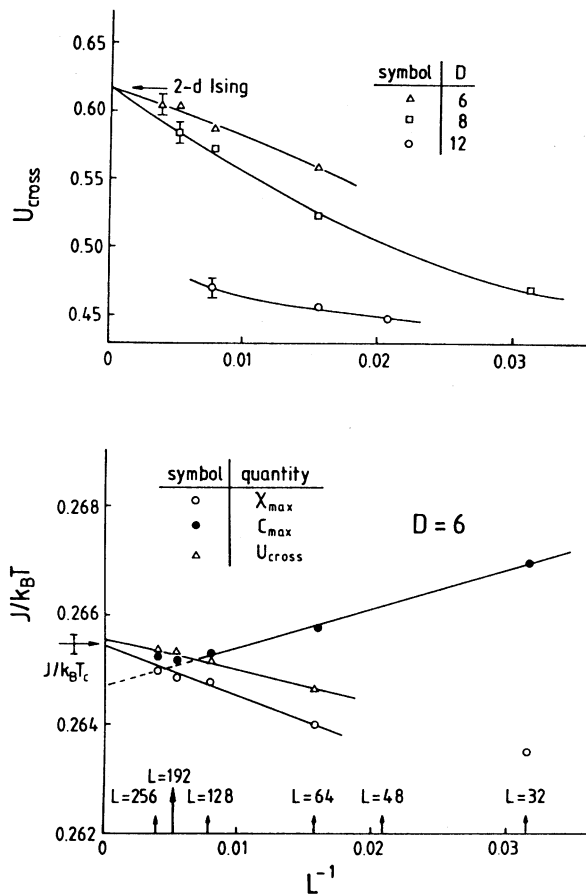
Fig. 27. Cumulant crossing values U_{cross} vs. L^{-1} for $D = 6, 8$ and 12 (upper part). The arrow shows the value of the two-dimensional Ising universality class, and the curves are only guides to the eye. The lower part shows, for $D = 6$ only, the extrapolations of inverse temperatures $K_{cross}(L)$ of cumulant crossings as well as the inverse temperatures $K_{max}(L)$ where susceptibility (χ_{max}) and specific heat (C_{max}) have their maxima. The arrow with the error bar marks the final estimate of $J/k_B T(D = 6)$, while straight lines indicate possible extrapolations. From Binder et al. [156].

a concept which is a very popular starting point for the description of wetting phenomena, surface-induced disordering, surface melting, and related phenomena [167]. In its simplest version, $\mathscr{H}_{eff}(\ell)$ is written in terms of a single collective coordinate $\ell(\rho)$, the local distance of the interface from the left wall at position ρ in the xy plane (Fig. 25),

$$\mathscr{H}_{eff}(\ell) = \int d\rho \left[\frac{\sigma}{2}(\nabla \ell)^2 + \Sigma\{\ell(\rho)\} \right]. \tag{7.2}$$

Here a factor of $(k_B T)^{-1}$ is absorbed in the Hamiltonian throughout, and we have assumed that the interfacial stiffness σ is a constant (rather than considering a dependence of σ on the distance ℓ of the interface from the wall, $\sigma(\ell)$ [171,172,179,180]). For short-range forces due to the walls, such as
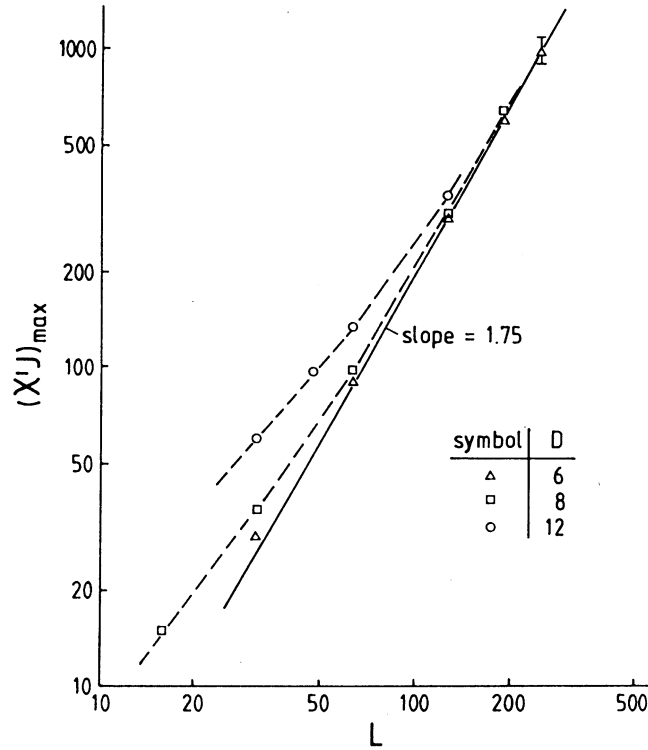
Fig. 28. Log–log plot of $(\chi'J)_{max} = J\chi'(K_{max}(L))$ vs. L for $D = 6, 8$ and 12. Straight line shows the theoretically predicted slope $\gamma/\nu = 1.75$, while broken curves are guides to the eye only. From Binder et al. [156].

the surface fields H_1, H_D [Eq. (7.1)], the effective potential is phenomenologically assumed as follows [152]:

$$\Sigma(\ell) = -\delta\varepsilon a_0 [e^{-\kappa\ell} + e^{-\kappa(D-\ell)}] + b_0 [e^{-2\kappa\ell} + e^{-2\kappa(D-\ell)}] - h(\ell - D/2), \quad h \equiv 2m_b H \, ,$$

$$\delta\varepsilon \equiv (T_w - T)/T_w \, . \tag{7.3}$$

Here a_0, b_0 are constants, $\delta\varepsilon$ is the normalized distance from a second-order wetting transition which would occur at the temperature T_w in a semi-infinite system, and κ^{-1} is a transverse length scale associated with the interface (if one derives Eq. (7.3) approximately from a Ginzburg–Landau theory for the magnetization profile $m(z)$ across the film, $\kappa^{-1} = \xi_b$ is obtained [152,171,172]). The last term on the right-hand side of Eq. (7.3) accounts for the effect of a bulk magnetic field H, which is included here for convenience.

Apart from the questionable approximations that yield the explicit form (7.3) of the interface potential $\Sigma(\ell)$, Eq. (7.2) has also been questioned on more general grounds, suggesting that one needs (at least) a second collective coordinate $\ell_1(\rho)$, which is related to fluctuations of the local magnetization $m(z)$ very close to the wall [181–184]. It is argued that the coupling between $\ell(\rho)$ and
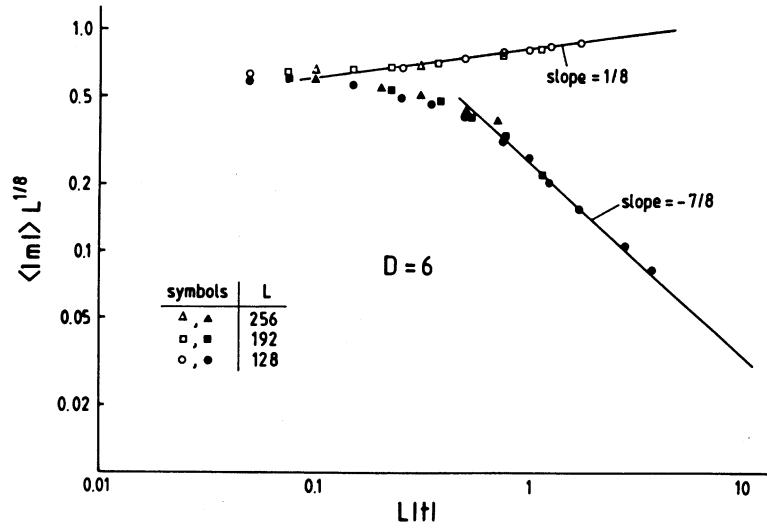
Fig. 29. Log–log plot of $\langle|m|\rangle L^{1/8}$ vs. $L|t|$ for $D = 6$. Three choices of L are included. Data for $T < T_c(D)$ are shown by open symbols, data for $T > T_c(D)$ by full symbols. The straight lines through the data were fitted using the correct exponents for order parameter ($\beta = 1/8$) and susceptibility ($\gamma = 7/4$) [recall that for $T > T_c(D)$ we have [31] $\langle|m|\rangle \propto \sqrt{\langle m^2 \rangle} \propto (k_B T \chi / L^2)^{1/2}$ in $d = 2$ dimensions, and hence $L^{1/8}\langle|m|\rangle \propto (tL)^{-7/8}$]. From Binder et al. [157].

$\ell_1(\rho)$ has important effects, and when one approximately integrates out $\ell_1(\rho)$, one effectively obtains Eqs. (7.2) and (7.3), but $\kappa^{-1} = \xi_b$ is no longer true and one has instead [181–184]

$$\kappa^{-1} = \xi_b(1 + \omega/2) ,$$ (7.4)

where $\omega = [4\pi\xi_b^2\sigma]^{-1}$ is the universal constant entering the theory of critical wetting [160–162,164–167].

At this point, we only aim at a description of the interface localization transition in terms of the most simple mean-field theory. In this spirit, fluctuations of the interface position, included in Eq. (7.2) via the $(\nabla\ell)^2$ term, are neglected altogether. Hence $\Sigma(\ell)$ is treated as an effective free energy function, which simply needs to be minimized in order to find the average position of the interface ℓ_{eq} in thermal equilibrium. For zero field $h = 0$ and $T > T_w$ all terms in Eq. (7.3) are positive, and hence $\Sigma(\ell)$ assumes its minimum for $\ell_{eq} = D/2$, i.e., we are in the "delocalized phase". For $T < T_w$, however, $\delta\varepsilon > 0$ in Eq. (7.3), so that the terms within the first pair of square brackets compete with those within the second pair and a solution $\ell_{eq} \neq D/2$ is expected, i.e., a nonzero order parameter. For $h = 0$ the equilibrium condition hence yields

$$0 = \left.\frac{\partial\Sigma(\ell)}{\partial\ell}\right|_{\ell=\ell_{eq}} = \delta\varepsilon\, a_0\kappa[e^{-\kappa\ell} - e^{-\kappa(D-\ell)}] - 2b_0\kappa[e^{-2\kappa\ell} - e^{-2\kappa(D-\ell)}]$$ (7.5)

and setting $\ell_{eq} = D/2 + \Delta$ one obtains an equation for the order parameter Δ,

$$\cosh(\kappa\Delta) = \delta\varepsilon\, a_0 \exp(\kappa D/2)/4b_0 .$$ (7.6)

For $X = \kappa\Delta \ll 1$, the expansion $\cosh x \approx 1 + x^2/2$ yields

$$X = \pm \frac{\exp(\kappa D/4)}{\sqrt{2b_0/a_0}}(-t)^{1/2}\,, \quad -t \equiv \delta\varepsilon - \frac{4b_0}{a_0}\exp(-\kappa D/2)\,. \tag{7.7}$$

Here $t \equiv [T_c(D) - T]/T_w$ is nothing but the reduced distance from the transition temperature in the thin film. It is seen that $T_c(D)$ differs from T_w only by terms exponentially small in $\kappa D/2$ [152]. The order parameter $\langle m \rangle_{\text{film}}$ (i.e., the magnetization) is then given by this mean-field (MF) theory as follows:

$$\langle m \rangle_{\text{film}}^{\text{MF}} = 2_{m_b}\Delta/D = \pm\sqrt{2a_0/b_0}\,m_b \exp(\kappa D/4)(-t)^{1/2}/(\kappa D)\,. \tag{7.8}$$

Thus one sees that the order parameter satisfies the standard mean-field power law, $\langle m \rangle_{\text{film}}^{\text{MF}} = B_{\text{MF}}(-t)^{1/2}$, but the amplitude is not $B_{\text{MF}} = \sqrt{3}$ as in the molecular-field approximation of a ferromagnet, but scales exponentially with the film thickness:

$$B_{\text{MF}} \propto \exp(\kappa D/4)/(\kappa D)\,. \tag{7.9}$$

Defining the response function for nonzero h as $\bar{\chi} \equiv (\partial\ell_{\text{eq}}/\partial h)_{T,D}$ and noting that Eq. (7.3) also implies $\bar{\chi} = 1/(\partial^2\Sigma(\ell)/\partial\ell^2)_{\ell=\ell_{\text{eq}}}$, we obtain from Eq. (7.3) for $t > 0$

$$\left.\frac{\partial^2\Sigma}{\partial\ell^2}\right|_{\ell_{\text{eq}}} = 2\exp(-\kappa D/2)\kappa^2[-a_0\,\delta\varepsilon + 4b_0\exp(-\kappa D/2)]\,, \tag{7.10}$$

where on the right-hand side $\ell_{\text{eq}} = D/2$ has already been inserted. From Eq. (7.7) we see that $\partial^2\Sigma/\partial\ell^2_{\ell_{\text{eq}}}$ vanishes at $t = 0$, as expected. Thus

$$\bar{\chi} = \exp(\kappa D/2)t^{-1}/(2\kappa^2 a_0)\,, \tag{7.11}$$

and noting that $\chi = \partial\langle m \rangle_{\text{film}}/\partial H = 4m_b^2\bar{\chi}/D$ one gets

$$\chi_{\text{MF}} = \Gamma_{\text{MF}}^+ t^{-1}\,, \quad \Gamma_{\text{MF}}^+ = (2m_b^2/\kappa a_0)\exp(\kappa D/2)/(\kappa D)\,. \tag{7.12}$$

Finally, the correlation length $\xi_\parallel$ for fluctuations of the order parameter is computed. In the framework of Eqs. (7.2) and (7.3), these fluctuations arise from fluctuations of the local interface position around its mean value, $\delta\ell(\rho) = \ell(\rho) - \ell_{\text{eq}}$. From a quadratic expansion of Eq. (7.2) around $\ell = \ell_{\text{eq}}$ it follows that the problem is formally analogous to the treatment of correlations in the standard Ginzburg–Landau theory. Thus the correlation function $G_\parallel(\rho - \rho') = \langle\delta\ell(\rho)\delta\ell(\rho')\rangle$ has the standard Ornstein–Zernike form, with a correlation length $\xi_\parallel$ related to the coefficient $\sigma/2$ of the $(\nabla\ell)^2$ term in Eq. (7.2) and the second derivative $\partial^2\Sigma/\partial\ell^2|_{\ell_{\text{eq}}}$ in the standard way, $\xi_\parallel^{-2} = (\partial^2\Sigma/\partial\ell^2|_{\ell_{\text{eq}}})/\sigma$, and hence

$$\xi_{\parallel,\text{MF}} = \xi_{0,\text{MF}}^+ t^{-1/2}\,, \quad \xi_{0,\text{MF}}^+ = (\sigma/2a_0)^{1/2}\exp(\kappa D/4)/\kappa\,. \tag{7.13}$$

The most interesting aspect of this mean-field theory is the unusual behavior of the critical amplitudes, which has the consequence that the regime where two-dimensional Ising critical behavior occurs is unusually narrow and hence mean-field theory is unusually good. This is seen when we work out the Ginzburg criterion, which states that mean-field theory is good if

$$G \ll |t| \ll 1 \tag{7.14}$$

where the Ginzburg number G for d-dimensional critical behavior is (suppressing prefactors of order unity) [321]

$$G = (\Gamma_{\text{MF}}^{+})^{2/(4-d)} B_{\text{MF}}^{-4/(4-d)} \left[\frac{v_0}{(\xi_{0,\text{MF}}^{+})^d} \right]^{2/(4-d)} . \tag{7.15}$$

Here the dimensionality of the problem is $d = 2$, and so we have instead of Eq. (5.28)

$$G = \Gamma_{\text{MF}}^{+} B_{\text{MF}}^{-2} [v_0/(\xi_{0,\text{MF}}^{+})^2] \propto \exp(-\kappa D/2) . \tag{7.16}$$

As a result, we predict that there is a crossover scaling similar to that described in Section 5.1, except that the parameter $R^{2d/(4-d)} \propto G^{-1}$ has to be replaced using Eq. (7.16). As an example,

$$\langle m_{\text{film}} \rangle = D^{-1} \exp(\kappa D/4) t^{1/2} \tilde{M}[t \exp(\kappa D/2)] \tag{7.17}$$

is the analog of Eq. (5.21) and the cumulant ratio at $t = 0$ is

$$U_L = \check{U}[\exp(\kappa D/2)/L] , \tag{7.18}$$

analogous to Eq. (5.18).

7.3. Monte Carlo test of the theory

First, the prediction that the critical amplitudes in the mean-field regime vary exponentially with film thickness D is considered. This is most easily studied for the susceptibility χ at temperatures $T > T_c(D)$, Eq. (7.12). Noting that $T_c(D)$ differs from T_w only by small terms proportional to $\exp(-\kappa D/2)$, cf. Eq. (7.7), one can check Eq. (7.12) by simply studying χ (or related quantities referring to the layer magnetization m_n in the nth layer, such as $\chi_n = (\partial m_n/\partial H)_T$ or $\chi_{nn} = (\partial m_n/\partial H_n)_T$, the response function to a field acting in the nth layer) at fixed temperature as function of D (Fig. 30). The theory outlined above implies $\chi \propto \chi_n^{\text{max}} \propto \chi_{nn}^{\text{max}} \propto \exp(\kappa D/2)$, and such a behavior seems indeed more or less compatible with the data. There is clearly some curvature present in these plots, and it would have been desirable to try to estimate these susceptibilities not only for the systematically investigated range $6 \le D \le 20$, but for still larger thicknesses as well. This task would be very difficult, however, because then also the lateral dimension L must be substantially larger than the choice $L = 128$ used in Fig. 30, and also much larger sampling times are necessary to avoid the bias shown in Fig. 1b. Thus the points for $D = 28$ included in Fig. 30 may already be subject to rather large systematic errors.

Nevertheless one can try to estimate κ by considering $\ln(\chi_{nn}^{\text{max}})/D$ as function of D (Fig. 31). Rather clear evidence is obtained that the identification $\kappa = \xi_b^{-1}$ proposed by Parry and Evans [152] is not correct; however, the idea of Parry and Boulter [181–184] that κ effectively gets renormalized [Eq. (7.4)] is better compatible with the data (Fig. 32). This choice of κ [from Eq. (7.4)] then also needs to be used in the crossover scaling relations Eqs. (7.17) and (7.18). The analysis shows (Fig. 33) that the surprising behavior of the cumulant U_L (Figs. 26 and 27) and the maximum value of the susceptibility χ'_{max} (Fig. 27) can indeed be interpreted in terms of the predicted crossover scaling effects. However, unlike the data in Section 5 – which have benefited from a very efficient novel Monte Carlo algorithm – here only data of a much poorer statistical quality are available, and systematic errors (e.g., due to the smallness of D) are clearly still present. In addition, only a small part of the crossover regime could be explored [the mean-field limit $U^* = 0.2704$, cf.
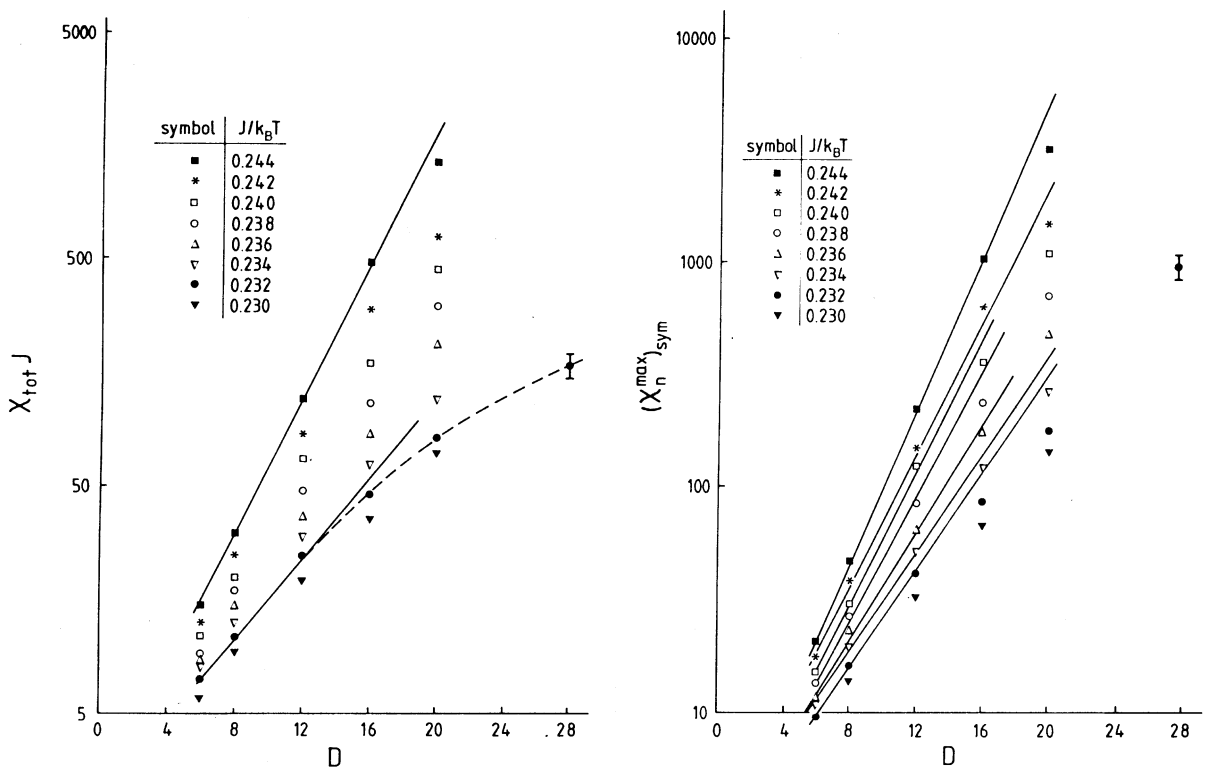
Fig. 30. Semilog plot of (a) the total susceptibility $\chi_{\text{tot}} = \partial \langle m \rangle_{\text{film}} / \partial H$ and (b) the maximum value of the (symmetrized) layer susceptibility χ_n vs. film thickness. Different symbols show various inverse temperatures $J/k_B T$, as indicated in the figure. Straight lines indicate the predicted exponential variation with thickness, while the broken curve is only a guide to the eye. Linear dimension $L = 128$ was used throughout. From Binder et al. [156].

Eq. (4.16), is beyond the scale of Fig. 33]. While the qualitative understanding of the interface localization transition in thin Ising films as provided by the simulations reviewed here and the pertinent theory is certainly encouraging, a quantitative understanding of the critical behavior of this transition and the associated crossover phenomena remains a challenge for the future. Note that the theoretical understanding of this transition is also rather rudimentary – it is just in the stage of mean-field theory and phenomenological Ginzburg criteria, while a renormalization approach only exists for critical wetting: for the interface localization transition between competing walls it remains to be developed!

8. Summary and outlook

   In this review we have summarized results on the static critical behavior of ferromagnetic Ising models as obtained from Monte Carlo simulations by various groups, and have contrasted them to pertinent theoretical predictions. Our emphasis has been on bulk properties; the critical behavior of
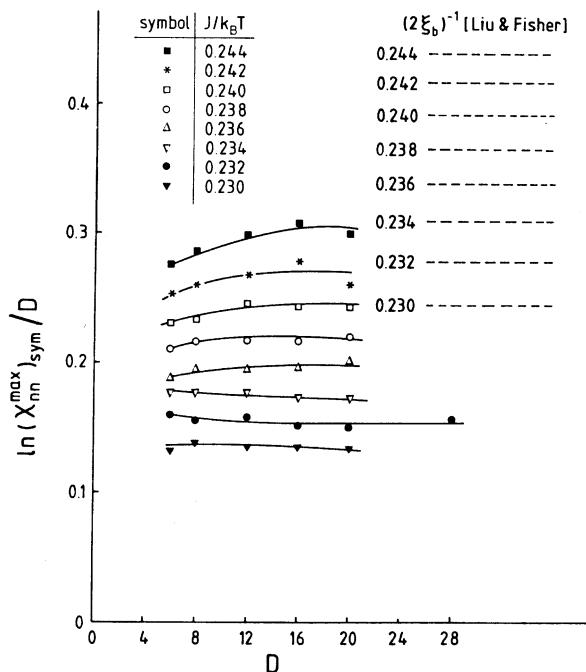
Fig. 31. Plot of the logarithm of the maximum value of the symmetrized layer susceptibility $[(\chi_{nn})_{\mathrm{sym}} = (\chi_{nn} + \chi_{n'n'})/2,$ where $n' = D - n + 1]$, divided by the film thickness, as a function of D. Different symbols show various temperatures, as indicated in the key. Curves are guides to the eye only, to illustrate that $\ln(\chi_{nn}^{\max})_{\mathrm{sym}}/D$ actually approaches plateau values for each temperature, which can be interpreted as $\kappa(T)/2$ according to the theory [Eq. (7.12)]. However, the identification $\kappa(T)/2 = (2\xi_b)^{-1}$ does not hold, as shown by the corresponding broken horizontal straight lines, that were calculated from the series expansions of Liu and Fisher [58]. From Binder et al. [156].

the interfacial tension has only been mentioned in connection with pertinent universal amplitude ratios, and the effects of free surfaces have not been analyzed here at all. Both the critical behavior of free surfaces and the problem of critical wetting with short-range forces have been outside the scope of this review, although these topics still involve many fascinating and partially unsolved questions.

We have also emphasized the approach of finite-size scaling analysis of Monte Carlo data calculated in the (grand)-canonical ensemble as the appropriate technique to study critical phenomena by means of simulations. Other approaches exist in the literature (e.g., the analysis of critical phenomena in the micro-canonical ensemble, or the use of the initial behavior of critical relaxation to extract static critical exponents as well, etc.), but have been deliberately left out here. Despite the interest of having several different approaches, we felt that these "off-mainstream" approaches are not as thoroughly explored and have not yielded as accurate results as the methods described here.

From the simulation data reviewed here, it is clear that with respect to bulk properties of Ising models with short-range interactions in various dimensionalities, accurate numerical data can be obtained by means of the single-cluster Wolff algorithm, allowing the extraction of estimates for the critical temperature, critical exponents and critical amplitudes with an accuracy that is already
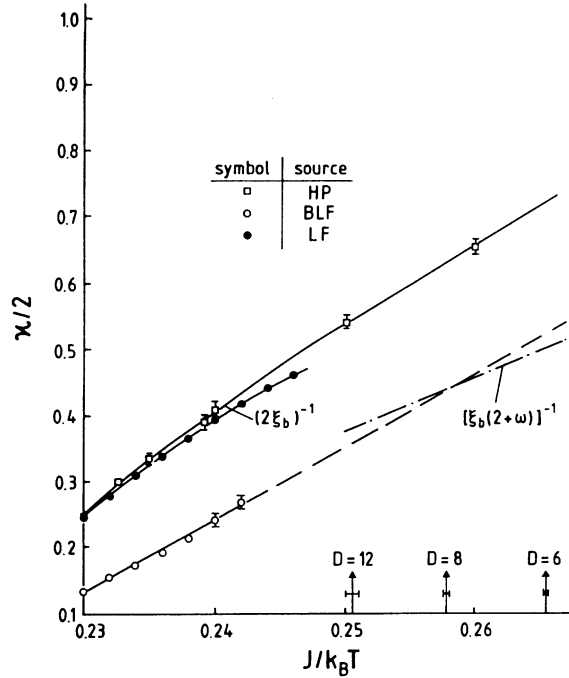
Fig. 32. Plot of the inverse length scale $\kappa/2$ vs. $J/k_B T$. Here full dots represent estimates of $(2\xi_b)^{-1}$, ξ_b being the true correlation range in a lattice direction, obtained from the leading term of the Padé approximant to the low-temperature series analysis of Liu and Fisher (LF) [58]. Open squares are corresponding Monte Carlo estimates of Hasenbusch and Pinn (HP) [278]. Open circles are the direct estimates of $\kappa/2$ extracted by Binder, Landau and Ferrenberg (BLF) [156], as shown in Fig. 31. The dash-dotted curve shows the suggestion of Parry and coworkers [181–184] that $\kappa/2 = [\xi_b(2 + \omega)]^{-1}$, Eq. (7.4), using $\omega \approx 0.86$ [173] in the temperature region of interest. Arrows (with error bars) at the abscissa show the location of $T_c(D)$ for $D = 12$, 8 and 6, respectively. From Binder et al. [157].

better than the analysis of systematic high- and low-temperature series expansions. Universal properties (critical exponents, universal amplitude ratios) can be obtained by field-theoretic renormalization-group methods with a competitive accuracy: this method, however, does not yield the nonuniversal characteristics of the critical behavior at the same time. Furthermore, some properties that field-theoretic renormalization may yield in principle, like the crossover scaling function for the universal crossover limit ($R \to \infty$, $t \to 0$, $tR^{2d/(4-d)}$ finite), are so far only available for $T > T_c$, but not for $T < T_c$. In contrast, Monte Carlo simulations yield such results for $T > T_c$ and for $T < T_c$ equally well. Thus, utilizing a novel extension of the cluster algorithm to Ising models with interaction of arbitrary long range, the crossover in the critical behavior from the Ising universality class in $d = 2$ and $d = 3$ dimensions to mean-field behavior, with increasing range R of the interaction, has been thoroughly investigated, and we have reviewed these recent studies here in detail. Results such as the nonmonotonic variation of the effective exponent γ_{eff} of the susceptibility below T_c so far could not be obtained with any other method than Monte Carlo simulation.

For the nearest-neighbor Ising model on the simple cubic lattice, there now exist numerous high-precision Monte Carlo studies, and the value of T_c as well as the critical exponents are known
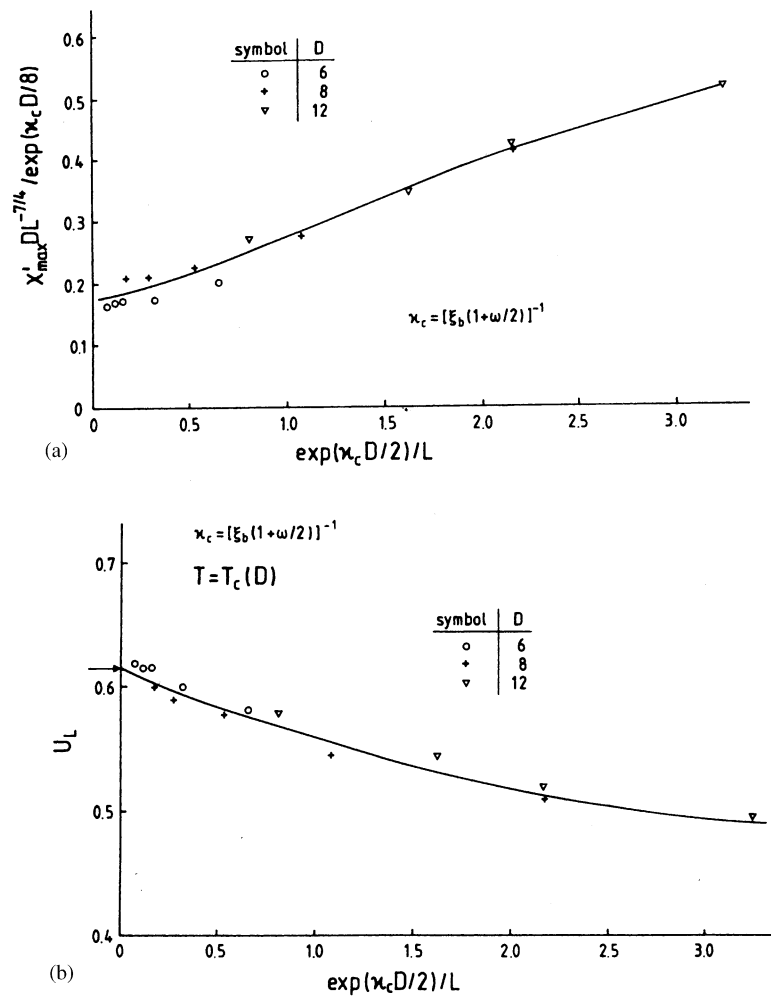
Fig. 33. Plot of the scaled susceptibility maximum $\chi'_{\max}$ (a) and of the cumulant (b) [Eq. (7.18)] vs. the crossover scaling variable $\exp(\kappa_c D/2)/L$, using Eq. (7.4) and all values of L that were available. Curves are guides to the eye only. The arrow on the ordinate in (b) shows U^*. From Binder et al. [157].

very accurately. However, much less effort has been devoted to critical amplitude ratios, and a matter which has been particularly neglected is the equation of state as a function of magnetic field near the critical point. Thus, even for the $d = 3$ nearest-neighbor Ising model still interesting and important studies need to be made!

Another problem which we have emphasized in this article are short-range Ising models at high dimensionality (such as $d = 5$) and Ising models with a long-range interaction, described by a power-law decay. Both cases are convenient testing grounds for our understanding of the theory of phase transitions. In the former problem, the critical behavior is mean-field like: not only the critical exponents are known, but it is also possible to systematically compute all quantities of

interest by means of perturbation expansions. However, it is somewhat disturbing that there still occur deviations between the theoretical description of finite-size behavior and the simulational results and our main hope is that the theoretical description will be extended to included higher-order corrections. The case of long-range interactions is particularly rewarding, since here the distance to the marginal dimension d^* where mean-field behavior becomes valid is a parameter that can be varied continuously. Also for this problem it appears that some properties are incompletely understood, such as the variation of the invariant $Q(K_c)$ with $d - d^*$ in the non-mean-field regime.

As a final case study reviewed here, we have taken the interface localization transition in Ising films confined between competing walls. We have argued that the theoretical understanding of this problem remains on a qualitative rather than a quantitative level: already the starting point of the theory – the effective interface Hamiltonian – involves fundamental questions, which hamper other problems (such as critical wetting) as well and theories beyond the mean-field level remain to be developed. Unfortunately, also the quality of the available Monte Carlo data is much lower than for the other problems described in the present article – available studies are based on the use of simple Metropolis algorithms and hence severely suffer from the problem of critical slowing down.

In conclusion we draw attention to extensions that were not dealt with here at all. One such extension is to allow for antiferromagnetic interactions to more distant neighbors competing with the nearest-neighbor exchange: this yields the possibility of different types of ordering beyond the Ising universality class, and nontrivial phase diagrams occur [321]. A particularly fascinating topic is the ANNNI (axial next-nearest-neighbor Ising model) [322], where the competing antiferromagnetic exchange occurs in one lattice direction only. Beyond a certain critical strength of this exchange, a transition to a modulated phase rather than to ferromagnetic order occurs. The critical properties of the multicritical point that separates these different types of order (the "Lifshitz point" [322]) are known only very roughly. Another fascinating extension of the Ising ferromagnet is to re-interpret it as a lattice gas model and assign charges to the particles, adding an electric field acting on these charges in order to maintain an electrical current through the system. Beyond a critical interaction strength, this model undergoes a phase separation into a lattice gas of high density coexisting with a low-density lattice gas, analogous to the transition of the standard Ising-lattice gas model, but in a different universality class. The critical exponents of this model have been controversial for a long time, and only recent work applying an anisotropic extension of finite-size scaling seems to settle the issue [323].

Particularly interesting problems occur when we generalize the Ising model by introducing quenched disorder, such as random bonds or random fields [324]. The problem becomes much harder now, because quantities such as the susceptibility χ have to be obtained by a double average, $k_B T \chi = L^d [\langle m^2 \rangle_T]_{av}$, where $\langle \ldots \rangle_T$ can still be obtained by the Monte Carlo methods as described in the present article, but an additional average $[\ldots]_{av}$ has to be carried out (via a simple random sampling) over the distribution over the random bonds or random fields, respectively. The simplest case is that in which one has only random-bond disorder with bonds that still are all ferromagnetic (i.e., a random mixture of stronger and weaker bonds). This problem has been studied extensively by Monte Carlo simulations [325] and high-temperature series extrapolations [326], but many problems remain. Much harder, however, is the problem of the random-field Ising model (RFIM) [327] or the Ising spin glass [328–331]. In the RFIM, it is still controversial whether one has a second-order transition from the paramagnetic to the ferromagnetic phase in $d = 3$, or

a weak first-order transition, or whether one has a glass-like phase intervening between the para- and ferromagnetic phase. Ising spin glasses, on the other hand, where one has exchange constants of random sign $\pm J$, have already been studied since about twenty-five years by Monte Carlo methods [328]: still it seems controversial whether in $d = 3$ the transition occurs at $T_c \approx 1.1J$ [329] or $T_c \approx 1.3J$ [330], and the nature of the ordered phase is also a point of debate [330–332]. Thus, much still remains to be done in the field of simulation studies of Ising models in the next decades!

Acknowledgements

References

[1] E. Ising, Z. Phys. 31 (1925) 253.
[2] B.M. McCoy, T.T. Wu, The Two-Dimensional Ising Model, Harvard University Press, Cambridge, MA, 1973.
[3] R.J. Baxter, Exactly Solved Models in Statistical Mechanics, Academic Press, London, 1982.
[4] C. Domb, M.S. Green (Eds.), Phase Transitions and Critical Phenomena, Vol. 3, Academic Press, London, 1974.
[5] L.P. Kadanoff et al., Rev. Mod. Phys. 39 (1967) 395.
[6] M.E. Fisher, Rep. Prog. Phys. 30 (1967) 615.
[7] L.P. Kadanoff, Physics 2 (1966) 263.
[8] L.P. Kadanoff, in: M.S. Green (Ed.), Critical Phenomena, Proceedings of 51st Enrico Fermi Summer School, Varenna, Italy, Academic, New York, 1971, p. 99.
[9] H.E. Stanley, An Introduction to Phase Transitions and Critical Phenomena, Oxford University Press, Oxford, 1971.
[10] K.G. Wilson, Phys. Rev. B 4 (1971) 3174, 3184.
[11] K.G. Wilson, M.E. Fisher, Phys. Rev. Lett. 28 (1972) 248.
[12] K.G. Wilson, J. Kogut, J. Rep. 12C (1974) 75.
[13] M.E. Fisher, Rev. Mod. Phys. 46 (1974) 597.
[14] C. Domb, M.S. Green (Eds.), Phase Transitions and Critical Phenomena, Vol. 6, Academic Press, London, 1976.
[15] S.-k. Ma, Modern Theory of Critical Phenomena, Addison-Wesley, Redwood, CA, 1976.
[16] P. Pfeuty, G. Toulouse, Introduction to the Renormalization Group and to Critical Phenomena, Wiley, London, 1977.
[17] T.W. Burkhardt, J.M.J. van Leeuwen (Eds.), Real-Space Renormalization, Springer, Berlin, 1982.
[18] K.G. Wilson, Rev. Mod. Phys. 55 (1983) 583.
[19] D.J. Amit, Field Theory, the Renormalization Group and Critical Phenomena, World Scientific, Singapore, 1984.
[20] J. Zinn-Justin, Quantum Field Theory and Critical Phenomena, Oxford University Press, Oxford, 1996.
[21] J. Cardy, Scaling and Renormalization in Statistical Physics, Cambridge University Press, Cambridge, 1996.
[22] M.E. Fisher, Rev. Mod. Phys. 70 (1998) 653.
[23] K. Binder, H. Rauch, Z. Phys. 219 (1969) 201.
[24] K. Binder, Physica 62 (1972) 508.
[25] K. Binder, Adv. Phys. 23 (1974) 917.

[26] K. Binder, Thin Solid Films 20 (1974) 367.
[27] D.P. Landau, Phys. Rev. B 13 (1976) 2997.
[28] D.P. Landau, Phys. Rev. B 14 (1976) 255.
[29] K. Binder, in: C. Domb, M.S. Green (Eds.), Phase Transitions and Critical Phenomena, Vol. 5b, Academic Press, London, 1976, p. 1.
[30] K. Binder (Ed.), Monte Carlo Methods in Statistical Physics, Springer, Berlin, 1979.
[31] K. Binder, Z. Phys. B 43 (1981) 119.
[32] K. Binder, D.W. Heermann, Monte Carlo Simulation in Statistical Physics – An Introduction, Springer, Berlin, 1988.
[33] D.P. Landau, in: K. Binder (Ed.), The Monte Carlo Method in Condensed Matter Physics, Springer, Berlin, 1992, p. 23.
[34] B. Dünweg, in: K. Binder, G. Ciccotti (Eds.), Monte Carlo and Molecular Dynamics of Condensed Matter Systems, Italian Physical Society, Bologna, 1996, p. 215.
[35] W. Janke, in: K.H. Hoffmann, M. Schreiber (Eds.), Computational Physics. Selected Methods, Simple Exercises, Serious Applications, Springer, Berlin, 1996, p. 10.
[36] K. Binder, Rep. Prog. Phys. 60 (1997) 487.
[37] D.P. Landau, K. Binder, A Guide to Monte Carlo Simulation in Statistical Physics, Cambridge University Press, Cambridge, 2000.
[38] F. Livet, Europhys. Lett. 16 (1991) 139.
[39] A.M. Ferrenberg, D.P. Landau, Phys. Rev. B 44 (1991) 5081.
[40] H.W.J. Blöte, G. Kamieniarz, Physica A 196 (1993) 455.
[41] D.P. Landau, Physica A 205 (1994) 41.
[42] H.W.J. Blöte, E. Luijten, J.R. Heringa, J. Phys. A: Math. Gen. 28 (1995) 6289.
[43] A.L. Talapov, H.W.J. Blöte, J. Phys. A: Math. Gen. 29 (1996) 5727.
[44] M. Hasenbusch, K. Pinn, J. Phys. A: Math. Gen. 30 (1997) 63.
[45] E. Luijten, H.W.J. Blöte, K. Binder, Phys. Rev. Lett. 79 (1997) 561.
[46] E. Luijten, H.W.J. Blöte, K. Binder, Phys. Rev. E 56 (1997) 6540.
[47] E. Luijten, H.W.J. Blöte, Phys. Rev. B 56 (1997) 8945.
[48] E. Luijten, K. Binder, Phys. Rev. E 58 (1998) R4060; ibid. 59 (1999) 7254 (E).
[49] E. Luijten, Phys. Rev. E 59 (1999) 4997.
[50] E. Luijten, K. Binder, Europhys. Lett. 47 (1999) 311.
[51] K. Binder, E. Luijten, Computer Phys. Commun. 127 (2000) 126.
[52] J.C. Le Guillou, J. Zinn-Justin, Phys. Rev. Lett. 39 (1977) 95.
[53] J.C. Le Guillou, J. Zinn-Justin, Phys. Rev. B 21 (1980) 3976.
[54] J.C. Le Guillou, J. Zinn-Justin, J. Phys. Lett. (Paris) 46 (1985) L137.
[55] R. Guida, J. Zinn-Justin, J. Phys. A: Math. Gen. 31 (1998) 8103.
[56] J. Adler, J. Phys. A 16 (1983) 3585.
[57] B.G. Nickel, Physica A 177 (1991) 189.
[58] A.J. Liu, M.E. Fisher, Physica A 156 (1989) 35.
[59] A.J. Guttmann, I.G. Enting, J. Phys. A 27 (1994) 8007.
[60] G.S. Pawley, R.H. Swendsen, D.J. Wallace, K.G. Wilson, Phys. Rev. B 29 (1984) 4030.
[61] C.F. Baillie, R. Gupta, K.A. Hawick, G.S. Pawley, Phys. Rev. B 45 (1992) 10438.
[62] R. Gupta, P. Tamayo, Int. J. Mod. Phys. C 7 (1996) 305.
[63] H.W.J. Blöte, J.R. Heringa, A. Hoogland, E.W. Meyer, T.S. Smit, Phys. Rev. Lett. 76 (1996) 2613.
[64] M. Kolesik, M. Suzuki, Physica A 215 (1995) 138.
[65] M.E. Fisher, in: M.S. Green (Ed.), Critical Phenomena, Academic Press, London, 1971, p. 1.
[66] M.E. Fisher, M.N. Barber, Phys. Rev. Lett 28 (1972) 1516.
[67] E. Brézin, J. Phys. (Paris) 43 (1982) 15.
[68] R. Botet, R. Jullien, P. Pfeuty, Phys. Rev. Lett. 49 (1982) 478.
[69] R. Botet, R. Jullien, Phys. Rev. B 28 (1983) 3955.
[70] M.N. Barber, in: C. Domb, J.L. Lebowitz (Eds.), Phase Transitions and Critical Phenomena, Vol. 8, Academic Press, New York, 1983, p. 145.

[71] V. Privman, M.E. Fisher, J. Stat. Phys. 33 (1983) 385.
[72] K. Binder, M. Nauenberg, V. Privman, A.P. Young, Phys. Rev. B 31 (1985) 1498.
[73] K. Binder, Z. Phys. B 61 (1985) 13.
[74] E. Brézin, J. Zinn-Justin, Nucl. Phys. B 257 [FS14] (1985) 867.
[75] J. Rudnick, H. Guo, D. Jasnow, J. Stat. Phys. 41 (1985) 353.
[76] J. Rudnick, G. Gaspari, V. Privman, Phys. Rev. B 32 (1985) 7594.
[77] J. Shapiro, J. Rudnick, J. Stat. Phys. 43 (1986) 51.
[78] Y.Y. Goldschmidt, Nucl. Phys. B 280 (1987) 340; ibid. 285 (1987) 519.
[79] K. Binder, Ferroelectrics 73 (1987) 43.
[80] J.L. Cardy (Ed.), Finite Size Scaling, North-Holland, Amsterdam, 1988.
[81] W. Huhn, V. Dohm, Phys. Rev. Lett. 61 (1988) 1368.
[82] K. Binder, J.S. Wang, J. Stat. Phys. 55 (1989) 87.
[83] V. Privman (Ed.), Finite Size Scaling and Numerical Simulation of Statistical Systems, World Scientific, Singapore, 1990.
[84] K. Binder, in: H. Gausterer, C.B. Lang (Eds.), Computational Methods in Field Theory, Springer, Berlin, 1992.
[85] K. Binder, H.-P. Deutsch, Europhys. Lett. 18 (1992) 667.
[86] V. Dohm, Phys. Scr. T 49 (1993) 46.
[87] K.K. Mon, K. Binder, Phys. Rev. E 48 (1993) 2498.
[88] P.A. Rikvold, B.M. German, M.A. Novotny, Phys. Rev. E 47 (1993) 1474.
[89] A. Esser, V. Dohm, X.S. Chen, Physica A 222 (1995) 355.
[90] A. Esser, V. Dohm, M. Hermes, J.S. Wang, Z. Phys. B 97 (1995) 205.
[91] W. Koch, V. Dohm, D. Stauffer, Phys. Rev. Lett. 77 (1996) 1789.
[92] E. Luijten, H.W.J. Blöte, K. Binder, Phys. Rev. E 54 (1996) 4626.
[93] X.S. Chen, V. Dohm, Physica A 251 (1998) 439.
[94] X.S. Chen, V. Dohm, Int. J. Mod. Phys. C 9 (1998) 1007.
[95] X.S. Chen, V. Dohm, Int. J. Mod. Phys. C 9 (1998) 1105.
[96] X.S. Chen, V. Dohm, Eur. Phys. J. B 5 (1998) 529.
[97] X.S. Chen, V. Dohm, Eur. Phys. J. B 7 (1999) 183; ibid 15 (2000) 283.
[98] Ch. Rickwardt, P. Nielaba, K. Binder, Ann. Phys. (Leipzig) 3 (1994) 483.
[99] E. Luijten, H.W.J. Blöte, Phys. Rev. Lett. 76, 1557, 3662(E) (1996).
[100] K.K. Mon, Europhys. Lett. 34 (1996) 399.
[101] G. Parisi, J.J. Ruiz-Lorenzo, Phys. Rev. B 54 (1996) R 3698; ibid. 55 (1997) 6082 (E).
[102] E. Luijten, Europhys. Lett. 37 (1997) 489; K.K. Mon, Europhys. Lett. 37 (1997) 493.
[103] H.W.J. Blöte, E. Luijten, Europhys. Lett. 38 (1997) 565.
[104] E. Luijten, K. Binder, H.W.J. Blöte, Eur. Phys. J. B 9 (1999) 289.
[105] M.E. Fisher, S.-k. Ma, B.G. Nickel, Phys. Rev. Lett. 29 (1972) 917.
[106] J. Sak, Phys. Rev. B 8 (1973) 281.
[107] M. Suzuki, Y. Yamazaki, G. Igarashi, Phys. Lett. A 42 (1972) 313.
[108] A. Aharony, in: C. Domb, M.S. Green (Eds.), Phase Transitions and Critical Phenomena, Vol. 6, Academic Press, London, 1976, p. 357.
[109] V.L. Ginzburg, Fiz. Tverd. Tela 2 (1960) 2031 [Sov. Phys. Solid State 2 (1960) 1824].
[110] P. Seglar, M.E. Fisher, J. Phys. C 13 (1980) 6613.
[111] S.F. Nicoll, J.K. Bhattacharjee, Phys. Rev. B 23 (1981) 389.
[112] C. Bagnuls, C. Bervillier, J. Phys. (Paris) Lett. 45 (1984) L-95.
[113] J.F. Nicoll, P.C. Albright, Phys. Rev. B 31 (1985) 4576.
[114] C. Bagnuls, C. Bervillier, Phys. Rev. B 32 (1985) 7209.
[115] M.E. Fisher, Phys. Rev. Lett. 57 (1986) 1911.
[116] C. Bagnuls, C. Bervillier, Phys. Rev. Lett. 58 (1987) 435.
[117] R. Schloms, V. Dohm, Nucl. Phys. B 328 (1989) 639.
[118] Z.Y. Chen, P.C. Albright, J.V. Sengers, Phys. Rev. A 41 (1990).
[119] M.Y. Belyakov, S.B. Kiselev, Physica A 190 (1992) 75.

[120] M.A. Anisimov, S.B. Kiselev, J.V. Sengers, S. Tang, Physica A 188 (1992) 487.
[121] M.A. Anisimov, A.A. Povodyrev, V.D. Kulikov, J.V. Sengers, Phys. Rev. Lett. 75 (1995) 3146.
[122] C. Bagnuls, C. Bervillier, Phys. Rev. Lett. 76 (1996) 4095.
[123] A. Pelissetto, P. Rossi, E. Vicari, Phys. Rev. E 58 (1998) 7146.
[124] A. Pelissetto, P. Rossi, E. Vicari, Nucl. Phys. B 554 (1999) 552.
[125] P.G. de Gennes, J. Phys. Lett. (Paris) 38 (1977) L44.
[126] J.F. Joanny, J. Phys. A 11 (1978) L117.
[127] P.G. de Gennes, Scaling Concepts in Polymer Physics, Cornell University Press, Ithaca, New York, 1979.
[128] K. Binder, J. Chem. Phys. 79 (1983) 6387.
[129] K. Binder, Phys. Rev. A 29 (1984) 341.
[130] A. Sariban, K. Binder, J. Chem. Phys. 86 (1987) 5859.
[131] H.-P. Deutsch, K. Binder, Macromolecules 25 (1992) 6214.
[132] H.-P. Deutsch, K. Binder, J. Phys. (Paris) II 3 (1993) 1049.
[133] K. Binder, Adv. Polym. Sci. 112 (1994) 181.
[134] D. Schwahn, K. Mortensen, Y. Yee-Madeira, Phys. Rev. Lett. 58 (1987) 1544.
[135] F.S. Bates, J.H. Rosedale, P. Stepanek, T.P. Lodge, P. Wiltzius, G.H. Fredrickson, P.P. Hjelm Jr., Phys. Rev. Lett. 65 (1990) 1893.
[136] P. Stepanek, T.P. Lodge, C. Kdrowski, S.F. Bates, J. Chem. Phys. 94 (1991) 8289.
[137] S. Janssen, D. Schwahn, T. Springer, Phys. Rev. Lett. 68 (1992) 3180.
[138] G. Meier, B. Momper, E.W. Fischer, J. Chem. Phys. 97 (1992) 5884.
[139] E.K. Hobbie, L. Reed, C.C. Huang, C.C. Han, Phys. Rev. E 48 (1993) 1579.
[140] G. Meier, D. Schwahn, K. Mortensen, S. Janssen, Europhys. Lett. 22 (1993) 577.
[141] D. Schwahn, G. Meier, K. Mortensen, S. Janssen, J. Phys. II (Paris) 4 (1994) 837.
[142] Y.B. Melnichenko, M.A. Anisimov, A.A. Povodyrev, G.D. Wignall, J.V. Sengers, W.A. Van Hook, Phys. Rev. Lett. 79 (1997) 5266.
[143] H. Seto, D. Schwahn, M. Nagao, E. Yokoi, S. Komura, M. Imai, K. Mortensen, Phys. Rev. E 54 (1996) 629.
[144] T. Narayanan, K.S. Pitzer, J. Chem. Phys. 102 (1995) 8118.
[145] J. Jacob, A. Kumar, M.A. Anisimov, A.A. Povodyrev, J.V. Sengers, Phys. Rev. E 58 (1998) 2188.
[146] M.A. Anisimov, A.A. Povodyrev, J.V. Sengers, Fluid Phase Equilibria 158–160 (1999) 537.
[147] M.E. Fisher, J. Stat. Phys. 75 (1994) 1.
[148] E.V. Albano, K. Binder, D.W. Heermann, W. Paul, Surf. Sci. 223 (1989) 15.
[149] A.O. Parry, R. Evans, Phys. Rev. Lett. 64 (1990) 523.
[150] M.R. Swift, A.L. Owczarek, J.O. Indekeu, Europhys. Lett. 14 (1991) 475.
[151] J.O. Indekeu, A.L. Owczarek, M.R. Swift, Phys. Rev. Lett. 66 (1991) 2174; A.O. Parry, R. Evans, Phys. Rev. Lett. 66 (1991) 2175.
[152] A.O. Parry, R. Evans, Physica A 181 (1992) 250.
[153] J. Rogiers, J.O. Indekeu, Europhys. Lett. 24 (1993) 21.
[154] K. Binder, A.M. Ferrenberg, D.P. Landau, Ber. Bunsenges. Phys. Chem. 98 (1994) 340.
[155] K. Binder, D.P. Landau, A.M. Ferrenberg, Phys. Rev. Lett. 74 (1995) 298.
[156] K. Binder, D.P. Landau, A.M. Ferrenberg, Phys. Rev. E 51 (1995) 2823.
[157] K. Binder, R. Evans, D.P. Landau, A.M. Ferrenberg, Phys. Rev. E 53 (1996) 5023.
[158] A.M. Ferrenberg, D.P. Landau, K. Binder, Phys. Rev. E 58 (1998) 3353.
[159] M. Müller, E.V. Albano, K. Binder, Physica A 279 (2000) 188.
[160] E. Brézin, B.I. Halperin, S. Leibler, Phys. Rev. Lett. 50 (1983) 1387; J. Phys. (Paris) 44 (1983) 775.
[161] R. Lipowsky, D.M. Kroll, R.K.P. Zia, Phys. Rev. B 27 (1983) 4499.
[162] D.S. Fisher, D.A. Huse, Phys. Rev. B 32 (1985) 247.
[163] K. Binder, D.P. Landau, D.M. Kroll, Phys. Rev. Lett. 56 (1986) 2276.
[164] R. Lipowsky, M.E. Fisher, Phys. Rev. B 36 (1987) 2126; Phys. Rev. Lett. 57 (1986) 2411.
[165] E. Brézin, T. Halpin-Healey, Phys. Rev. Lett. 58 (1987) 1220.
[166] E. Brézin, T. Halpin-Healey, J. Phys. (Paris) 48 (1987) 757.
[167] S. Dietrich, in: C. Domb, J.L. Lebowitz (Eds.), Phase Transitions and Critical Phenomena, Vol. 12, Academic Press, London, 1988, p. 1.

[168] K. Binder, D.P. Landau, Phys. Rev. B 37 (1988) 1745.
[169] K. Binder, D.P. Landau, S. Wansleben, Phys. Rev. B 40 (1989) 6971.
[170] A.O. Parry, R. Evans, K. Binder, Phys. Rev. B 34 (1991) 11535.
[171] M.E. Fisher, A.J. Jin, Phys. Rev. B 44 (1991) 1430.
[172] M.E. Fisher, A.J. Jin, Phys. Rev. Lett. 69 (1992) 792.
[173] M.E. Fisher, H. Wen, Phys. Rev. Lett. 68 (1992) 3654.
[174] K. Binder, D.P. Landau, D.M. Kroll, Phys. Rev. Lett. 68 (1992) 3655.
[175] R. Evans, D.C. Hoyle, A.O. Parry, Phys. Rev. A 45 (1992) 3823.
[176] C.J. Boulter, Phys. Rev. Lett. 79 (1997) 1897.
[177] D. Ross, D. Bonn, J. Meunier, Nature 400 (1999) 737.
[178] A.O. Parry, R. Evans, Phys. Rev. B 39 (1989) 12336.
[179] A.J. Jin, M.E. Fisher, Phys. Rev. B 47 (1993) 7365.
[180] M.E. Fisher, A.J. Jin, A.O. Parry, Ber. Bunsenges. Phys. Chem. 98 (1994) 357.
[181] C.J. Boulter, A.O. Parry, Phys. Rev. Lett. 74 (1995) 3403.
[182] A.O. Parry, C.J. Boulter, Physica A 218 (1995) 77.
[183] C.J. Boulter, A.O. Parry, Physica A 218 (1995) 109.
[184] A.O. Parry, C.J. Boulter, P.S. Swain, Phys. Rev. E 52 (1995) 5768.
[185] C.J. Boulter, J.O. Indekeu, Phys. Rev. E 56 (1997) 5734.
[186] P.J. Upton, Phys. Rev. E 60 (1999) R3475.
[187] H. Müller-Krumbhaar, K. Binder, J. Stat. Phys. 8 (1973) 1.
[188] P.C. Hohenberg, B.I. Halperin, Rev. Mod. Phys. 49 (1977) 435.
[189] E. Stoll, K. Binder, T. Schneider, Phys. Rev. B 8 (1973) 3266.
[190] Z. Racz, Phys. Rev. B 13 (1976) 263; M.E. Fisher, Z. Racz, Phys. Rev. B 13 (1976) 5039.
[191] R. Kretschner, K. Binder, D. Stauffer, J. Stat. Phys. 15 (1976) 267.
[192] G. Marsaglia, Proc. Nat. Acad. Sci. 61 (1968) 25.
[193] D. Knuth, The Art of Computer Programming, Vol. 2, Addison-Wesley, Reading, MA, 1979.
[194] S. Kirkpatrick, E. Stoll, J. Comput. Phys. 40 (1981) 517.
[195] G.A. Marsaglia, in: L. Billard (Ed.), Computer Science and Statistics: The Interface, Elsevier, Amsterdam, 1985, p. 1.
[196] F. James, Comput. Phys. Commun. 60 (1990) 329.
[197] G. Marsaglia, B. Narasimhan, A. Zaman, Comput. Phys. Commun. 60 (1990) 345.
[198] P.D. Coddington, Int. J. Mod. Phys. C 5 (1994) 547; ibid. C 7 (1996) 295.
[199] M. Lüscher, Comput. Phys. Commun. 79 (1994) 100.
[200] F. James, Comput. Phys. Commun. 79 (1994) 111.
[201] A. Compagner, Phys. Rev. E 52 (1995) 5634.
[202] L.N. Shchur, P. Butera, Int. J. Mod. Phys. C 9 (1998) 607.
[203] M.N. Barber, R.B. Pearson, D. Toussaint, J.L. Richardson, Phys. Rev. B 32 (1985) 1720.
[204] A.M. Ferrenberg, D.P. Landau, Y.J. Wong, Phys. Rev. Lett. 69 (1992) 3382.
[205] W. Selke, A.L. Talapov, L.N. Shchur, JETP Lett. 58 (1993) 665.
[206] K. Kankaala, T. Ala-Nissilä, I. Vattulainen, Phys. Rev. E 48 (1993) R4211.
[207] P. Grassberger, Phys. Lett. A 181 (1993) 43; F. Schmid, N.B. Wilding, Int. J. Mod. Phys. C6 (1996) 781; F. Gutbrod, Int. J. Mod. Phys. C 7 (1996) 909.
[208] L.N. Shchur, H.W.J. Blöte, Phys. Rev. E 55 (1997) R4905; D. Stauffer, Int. J. Mod. Phys. C 10 (1999) 807.
[209] P. Heller, Rep. Prog. Phys. 30 (1967) 731.
[210] M. Vicentini-Missoni, in: M.S. Green (Ed.), Critical Phenomena, Academic, New York, 1971, p. 157.
[211] D. Beysens, in: M. Lévy, J.-C. Le Guillou, J. Zinn-Justin (Eds.), Proceedings of the 1980 Cargèse Summer Institute on Phase Transitions, Plenum Press, New York, 1982, p. 25; G. Ahlers, ibid, p. 1; J.V. Sengers, ibid., p. 95.
[212] J.V. Sengers, J.M.H. Levelt Sengers, Annu. Rev. Phys. Chem. 37 (1986) 189.
[213] V. Privman, P.C. Hohenberg, A. Aharony, in: C. Domb, J.L. Lebowitz (Eds.), Phase Transitions and Critical Phenomena, Vol. 14, Academic, London, 1991, p. 1.
[214] G. Orkoulas, A.Z. Panagiotopoulos, M.E. Fisher, Phys. Rev. E 61 (2000) 5930.
[215] J.K. Kim, Phys. Rev. Lett. 70 (1993) 1735.

[216] A. Patrascioiu, E. Seiler, Phys. Rev. Lett. 73 (1994) 3325.
[217] J.K. Kim, Europhys. Lett. 28 (1994) 11; Phys. Rev. D 50 (1994) 4663.
[218] S. Caracciolo, R.G. Edwards, S.J. Ferreira, A. Pelisseto, A.D. Sokal, Phys. Rev. Lett. 74 (1995) 2969.
[219] G.A. Baker, N. Kawashima, Phys. Rev. Lett. 75 (1995) 994; ibid. 76 (1996) 2403.
[220] J.K. Kim, A.J. de Souza, D.P. Landau, Phys. Rev. E 54 (1996) 2291.
[221] H.G. Ballesteros, L.A. Fernandez, V. Martin-Mayer, A. Munoz-Sudupe, Phys. Lett. B 441 (1998) 330.
[222] M. Hasenbusch, K. Pinn, S. Vinti, Phys. Rev. B 59 (1999) 1147.
[223] M. Hasenbusch, J. Phys. A: Math. Gen. 32 (1999) 4851.
[224] A.M. Ferrenberg, R.H. Swendsen, Phys. Rev. Lett. 61 (1988) 2635; ibid. 63 (1989) 1195.
[225] R.H. Swendsen, J.S. Wang, A.M. Ferrenberg, in: K. Binder (Ed.), The Monte Carlo Method in Condensed Matter Physics, Springer, Berlin, 1992, p. 75.
[226] B.A. Berg, T. Neuhaus, Phys. Lett. B 267 (1991) 249; Phys. Rev. Lett. 68 (1992) 9.
[227] W. Janke, Int. J. Mod. Phys. C 3 (1992) 1137; Physica A 254 (1988) 164.
[228] B.A. Berg, Int. J. Mod. Phys. C 3 (1992) 1083; and in: F. Karsch, B. Monien, H. Satz (Eds.), Multiscale Phenomena and Their Simulation, World Scientific, Singapore, 1997, p. 137.
[229] B.A. Berg, U. Hansmann, T. Neuhaus, Phys. Rev. B 47 (1993) 47; Z. Physik B 90 (1993) 229.
[230] G. Besold, J. Risbo, O.G. Mouritsen, Comp. Mat. Sci. 15 (1999) 311.
[231] N. Metropolis, A.W. Rosenbluth, M.N. Rosenbluth, A.H. Teller, E. Teller, J. Chem. Phys. 21 (1953) 1087.
[232] H.W. Alexander, Elements of Mathematical Statistics, Wiley, New York, 1961.
[233] A.M. Ferrenberg, D.P. Landau, K. Binder, J. Stat. Phys. 63 (1991) 867.
[234] S. Wansleben, D.P. Landau, Phys. Rev. B 43 (1991) 6006.
[235] A. Milchev, K. Binder, D.W. Heermann, Z. Phys. B 63 (1986) 521.
[236] R.H. Swendsen, J.S. Wang, Phys. Rev. Lett. 58 (1987) 86.
[237] U. Wolff, Phys. Rev. Lett. 62 (1989) 361.
[238] U. Wolff, Phys. Lett. A 228 (1989) 379.
[239] U. Wolff, Nucl. Phys. B 322 (1989) 759.
[240] J.S. Wang, Physica A 161 (1989) 249.
[241] X.-L. Li, A.D. Sokal, Phys. Rev. Lett. 63 (1989) 827.
[242] P.G. Lauwers, V. Rittenberg, Phys. Lett. B 233 (1990) 210.
[243] D.W. Heermann, A.N. Burkitt, Physica A 162 (1990) 55.
[244] V.S. Dotsenko, W. Selke, A.L. Talapov, Physica A 170 (1991) 278.
[245] A.D. Sokal, Nucl. Phys. B (Proc. Suppl.) 20 (1991) 55.
[246] E. Marinari, R. Marra, Nucl. Phys. B 342 (1990) 737.
[247] X.-L. Li, A.D. Sokal, Phys. Rev. Lett. 67 (1991) 1482.
[248] P. Tamayo, Physica A 201 (1993) 543.
[249] N. Ito, G.A. Kohring, Physica A 201 (1993) 543.
[250] E. Luijten, H.W.J. Blöte, Int. J. Mod. Phys. C 6 (1995) 359.
[251] W. Janke, Math. Comput. Simulation 47 (1998) 329.
[252] P.W. Kasteleyn, C.M. Fortuin, J. Phys. Soc. Jpn. 26 (Suppl.) (1969) 11; C.M. Fortuin, P.W. Kasteleyn, Physica 57 (1972) 536.
[253] D. Stauffer, A. Aharony, Introduction to Percolation Theory, Taylor & Francis, London, 1994.
[254] J. Hoshen, R. Kopelman, Phys. Rev. B 14 (1976) 3438.
[255] K. Binder, Ann. Phys. (N.Y.) 98 (1976) 390.
[256] N. Ito, Physica A196 (1993) 591; M. Kikuchi, N. Ito, J. Phys. Soc. Jpn 62 (1993) 3052.
[257] E. Luijten, in: D.P. Landau, S.P. Lewis, H.B. Schüttler (Eds.), Computer Simulation Studies in Condensed-Matter Physics, Vol. XII, Springer, Heidelberg, 2000, p. 86.
[258] D. Stauffer, R. Knecht, Int. J. Mod. Phys. C 7 (1996) 893.
[259] D. Stauffer, Physica A 244 (1997) 344.
[260] M. Suzuki, Prog. Theor. Phys. 58 (1977) 1142.
[261] P. Butera, M. Comi, Phys. Rev. B 56 (1997) 8212.
[262] P. Butera, M. Comi, Phys. Rev. B 56 (1998) 11552.
[263] Z. Salman, J. Adler, Int. J. Mod. Phys. C 9 (1998) 195.

[264] H.W.J. Blöte, J. DeBruin, A. Compagner, J.H. Croockewit, Y.T.J.C. Fonck, J.R. Heringa, A. Hoogland, A.L. van Willigen, Europhys. Lett. A 161 (1989) 105; H.W.J. Blöte, A. Compagner, J.H. Crookewit, Y.T.J.C. Fonck, J.R. Heringa, A. Hoogland, T.S. Smit, A.L. van Willigen, Physica A 161 (1989) 1.
[265] N. Ito, M. Suzuki, J. Phys. Soc. Jpn. 60 (1991) 1978.
[266] H.W.J. Blöte, L.N. Shchur, A.L. Talapov, Int. J. Mod. Phys. C 10 (1999) 1137.
[267] A. Rosengren, J. Phys. A 28 (1986) 1709.
[268] M.E. Fisher, J. Phys. A 28 (1995) 6323.
[269] M.E. Fisher, J.H. Chen, J. Phys. (Paris) 46 (1985) 1645; J.H. Chen, M.E. Fisher, B.G. Nickel, Phys. Rev. Lett. 48 (1982) 630.
[270] A.J. Guttmann, J. Phys. A: Math. Gen. 20 (1987) 1855.
[271] B.G. Nickel, J.J. Rehr, J. Stat. Phys. 61 (1990) 1.
[272] H.G. Ballesteros, L.A. Fernandez, V. Martin-Mayor, A. Munez Suolupe, G. Parisi, J.J. Ruiz-Lorenzo, J. Phys. A 32 (1999) 1.
[273] P. Butera, M. Comi, Phys. Rev. E 55 (1997) 6391.
[274] A. Pelissetto, E. Vicari, Nucl. Phys. B 519 (1998) 626.
[275] G.A. Baker Jr., Quantitative Theory of Critical Phenomena, Academic, Boston, 1990.
[276] M. Hasenbusch, K. Pinn, J. Phys. A 31 (1998) 6157.
[277] M. Caselle, M. Hasenbusch, J. Phys. A: Math. Gen. 30 (1997) 4963; Nucl. Phys. Proc. 63 (Suppl.) (1998) 613.
[278] M. Hasenbusch, K. Pinn, Physica A 192 (1993) 342.
[279] D. Stauffer, M. Ferer, M. Wortis, Phys. Rev. Lett. 29 (1972) 345.
[280] C. Bagnuls, C. Bervillier, D.I. Meiron, B.G. Nickel, Phys. Rev. B 35 (1987) 3585; C. Bervillier, Phys. Rev. B 34 (1986) 8141.
[281] A. Aharony, P.C. Hohenberg, Phys. Rev. B 13 (1976) 3081.
[282] C. Gutsfeld, J. Küster, K. Münster, Nucl. Phys. B 479 (1996) 654.
[283] C. Ruge, P. Zhu, F. Wagner, Physica A 226 (1994) 431.
[284] E. Brézin, S. Feng, Phys. Rev. B 29 (1984) 472.
[285] G. Münster, Nucl. Phys. B 340 (1990) 559.
[286] L.J. Shaw, M.E. Fisher, Phys. Rev. A 39 (1989) 2189.
[287] K.K. Mon, D. Jasnow, Phys. Rev. A 30 (1984) 670.
[288] M.E. Fisher, H. Wen, Phys. Rev. Lett. 68 (1992) 3654.
[289] E. Luijten, Interaction Range, Universality and the Upper Critical Dimension, Delft University Press, Delft, 1997.
[290] E. Luijten, A.M. Ferrenberg, K. Binder, in preparation, but shall not be reviewed here.
[291] H.J.F. Knops, J.M.J. van Leeuwen, P.C. Hemmer, J. Stat. Phys. 17 (1977) 197.
[292] M.E. Fisher, in: F.J.W. Hahne (Ed.), Critical Phenomena, Springer, Berlin, 1983, p. 1.
[293] V. Privman, in: V. Privman (Ed.), Finite Size Scaling and Numerical Simulation of Statistical Systems, World Scientific, Singapore, 1990, p. 1.
[294] A.J. Guttmann, J. Phys. A 14 (1981) 233.
[295] E. Riedel, F. Wegner, Z. Phys. 225 (1969) 195.
[296] G. Kamieniarz, H.W.J. Blöte, J. Phys. A 26 (1993) 201.
[297] J.S. Kouvel, M.E. Fisher, Phys. Rev. 136A (1964) 1626.
[298] C. Bagnuls, C. Bervillier, D.I. Meiron, B.G. Nickel, Phys. Rev. B 35 (1987) 3585.
[299] M.A. Anisimov, E. Luijten, V.A. Agayan, J.V. Sengers, K. Binder, Phys. Lett. A 264 (1999) 63.
[300] A. Kastrowicka Wyczalkowska, M.A. Anisimov, J.V. Sengers, Fluid Phase Equilibria 158–160 (1999) 523.
[301] T.A. Edison, J.V. Sengers, Int. J. Refrigeration 22 (1999) 365.
[302] J.C. Le Guillou, J. Zinn-Justin, J. Phys. Paris 48 (1987) 19.
[303] M. Lifshitz, J. Dudowicz, K.F. Freed, J. Chem. Phys. 100 (1994) 3957.
[304] E. Luijten, H. Meyer, Phys. Rev. E 62 (2000) 3257.
[305] G.S. Joyce, Phys. Rev. 146 (1966) 349.
[306] D. Ruelle, Commun. Math. Phys. 9 (1968) 267.
[307] F.J. Dyson, Commun. Math. Phys. 12 (1969) 91.
[308] F.J. Dyson, Commun. Math. Phys. 12 (1969) 212.
[309] J. Fröhlich, T. Spencer, Commun. Math. Phys. 84 (1982) 87.

[310] M. Aizenman, J.T. Chayes, L. Chayes, C.M. Newman, J. Stat. Phys. 50 (1988) 1.
[311] Y. Yamazaki, Phys. Lett. A 61 (207) 1977.
[312] Y. Yamazaki, Physica A 92 (1978) 446.
[313] M.A. Gusmão, W.K. Theumann, Phys. Rev. B 28 (1983) 6545.
[314] E. Luijten, Phys. Rev. E 60 (1999) 7558.
[315] E. Luijten, in preparation.
[316] P.W. Anderson, G. Yuval, D.R. Hamann, Phys. Rev. B 1 (1970) 4464.
[317] P.W. Anderson, G. Yuval, J. Phys. C 4 (1971) 607.
[318] J.M. Kosterlitz, Phys. Rev. Lett. 37 (1976) 1577.
[319] M. Krech, E. Luijten, Phys. Rev. E 61 (2000) 2058.
[320] E. Luijten, H.W.J. Blöte, in preparation.
[321] K. Binder, in: D.G. Pettifor (Ed.), Cohesion and Structure of Surfaces, Elsevier, Amsterdam, 1995, p. 121.
[322] W. Selke, Phys. Rep. 170 (1998) 213.
[323] K.T. Leung, J.-S. Wang, Int. J. Mod. Phys. C 10 (1999) 853.
[324] A.P. Young (Ed.), Spin Glasses and Random Fields, World Scientific, Singapore, 1998.
[325] W. Selke, L.N. Shchur, A.L. Talapov, in: D. Stauffer (Ed.), Annual Reviews of Computational Physics, Vol. 1, World Scientific, Singapore, 1994, p. 17.
[326] A. Roder, J. Adler, W. Janke, Phys. Rev. Lett. 80 (1998) 4697; Physica A 265 (1999) 28.
[327] T. Nattermann, in: Spin Glasses and Random Fields, World Scientific, Singapore, 1998, p. 277.
[328] K. Binder, K. Schröder, Phys. Rev. B 14 (1976) 2142.
[329] N. Kawashima, A.P. Young, Phys. Rev. B 53 (1996) R484.
[330] N. Hatano, J.E. Gubernatis, AIP Conf. Proc. 4 (69) (1999) 565.
[331] E. Marinari, G. Parisi, J.J. Ruiz-Lorenzo, in: Spin Glasses and Random Fields, World Scientific, Singapore, 1998, p. 59.
[332] B.A. Berg, W. Janke, Phys. Rev. Lett 80 (1998) 4771; W. Janke, B.A. Berg, A. Billoire, Ann. Phys. (Leipzig) 7 (1998) 544.
[333] B.G. Nickel, Physica A 106 (1981) 48.
[334] J. Zinn-Justin, J. Phys. (Paris) 42 (1981) 783.
[335] X.S. Chen, V. Dohm, Phys. Rev. E 63 (2001), in press.